Molekulare Effekte von Kohlenstoffnanopartikeln in Lungenepithelzellen: Mechanismen der Aktivierung von Membranrezeptoren und zellulärer Seneszenz

Inaugural-Dissertation

zur Erlangung des Doktorgrades
der Mathematisch-Naturwissenschaftlichen Fakultät
der Heinrich-Heine-Universität Düsseldorf

vorgelegt von

Tim Tobias Spannbrucker
Uelzen

Düsseldorf, Februar 2019

aus dem Leibniz-Institut für umweltmedizinische Forschung
der Heinrich-Heine-Universität Düsseldorf

Gedruckt mit der Genehmigung der
Mathematisch-Naturwissenschaftlichen Fakultät
der Heinrich-Heine-Universität Düsseldorf

Berichterstatter:

1. PD Dr. Klaus Unfried

2. Prof. Dr. Axel Gödecke

Tag der mündlichen Prüfung:

29.05.2019

Erklärung

Ich versichere an Eides statt, dass die Dissertation von mir selbstständig und ohne unzulässige fremde Hilfe unter Beachtung der „Grundsätze zur Sicherung guter wissenschaftlicher Praxis an der Heinrich-Heine-Universität Düsseldorf“ erstellt worden ist.

_____

(Tim Spannbrucker)

Düsseldorf, 26.02.2019

„Wir leben auf einem blauen Planet
der sich um einen Feuerball dreht
mit einem Mond, der die Meere bewegt.
Und du glaubst nicht an Wunder.“

(Marten Laciny)

Inhaltsverzeichnis

Partikuläre Luftverschmutzung

Luftverschmutzung stellt weltweit gegenwärtig das größte Umweltrisiko für die menschliche Gesundheit dar (WHO, 2016). Ungefähr 91 % der Weltbevölkerung atmen verschmutzte Luft; sieben Millionen Menschen sterben jährlich daran. Hierfür werden in erster Linie luftgetragene Partikel verantwortlich gemacht (Dockery et al., 1993). Diese Umweltpartikel (engl.: particulate matter, PM) werden anhand ihres aerodynamischen Durchmessers (d_{ae})[1] klassifiziert. Die Größenklassen PM_{10}, $PM_{2,5}$ und $PM_{0,1}$ enthalten jeweils Partikel mit einem d_{ae} von bis zu 10 µm, 2,5 µm und 0,1 µm. Diese Klassen unterscheiden sich bezüglich ihrer Gesundheitseffekte. Es gibt experimentelle und epidemiologische Hinweise, dass ultrafeine Partikel ($PM_{0,1}$) im Vergleich zu gröberen Partikeln die stärksten Effekte in diesem Zusammenhang aufweisen (Ibald-Mulli et al., 2002; MacNee et al., 2003). Aufgrund ihrer Größe werden ultrafeine Partikel auch oftmals als Umweltnanopartikel bezeichnet. Der Begriff Nanopartikel wurde im Zusammenhang mit der modernen Nanotechnologie definiert. Technologisch erzeugte Nanopartikel sind Partikel, die in mindestens einer Dimension einen Durchmesser zwischen 1 nm und 100 nm aufweisen (European Commission (2011/696/EU)).

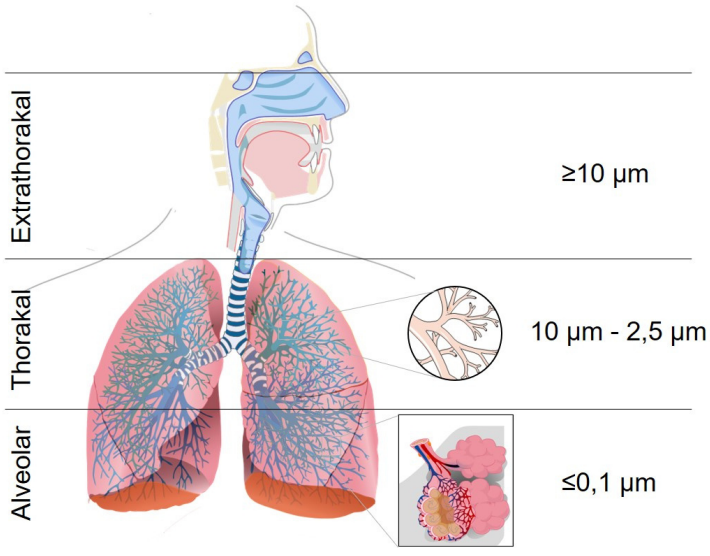

Abbildung 1: Schematische Darstellung der Deposition von luftgetragenen Partikeln in den Atemwegen. Während große Partikel überwiegend in den oberen Atemwegen deponieren, sind Nanopartikel in der Lage bis in die alveolaren Strukturen der Lunge vorzudringen (modifiziert nach Nemmar et al., 2013; BéruBé et al., 2007).

Entsprechend ihrer Größe erreichen inhalierte Partikel unterschiedliche Bereiche der Atemwege (Abbildung 1). Im nasopharyngealen Bereich (obere Atemwege) lagern sich

[1] Der aerodynamische Durchmesser ist definiert als der Durchmesser eines kugelförmigen Partikels mit der Dichte 1 g/cm^3, der dieselbe Sinkgeschwindigkeit aufweist wie der zu betrachtende Partikel (DIN ISO 7708).

überwiegend gröbere Partikel ab. In den mittleren Atemwegen, in denen sich die Trachea mit den Bronchien und Bronchiolen zum trachobronchialen Bereich zusammenschließen, wird ein Großteil der feinen Partikel deponiert. In den unteren Atemwegen, bestehend aus Alveolargängen und den von Blutkapillaren umgebenen Alveolen, lagern sich überwiegend die ultrafeinen Partikel ab (Borm et al., 2004). Die verschiedenen Bereiche der Atemwege verfügen über unterschiedliche Reinigungssysteme, um Fremdkörper zu entfernen. In den oberen und mittleren Atemwegen werden Partikel überwiegend durch die sogenannte „Mukoziliäre Clearance“ entfernt. In den unteren Atemwegen ist dieser Mechanismus nicht vorhanden. Dort werden Fremdkörper von Makrophagen phagozytiert. Die Effizienz dieser Reinigung ist entscheidend von der Größe des jeweiligen Fremdkörpers abhängig. Ultrafeine Partikel werden durch die alveolaren Makrophagen nicht erkannt (Donaldson et al., 2001; Hoet et al., 2004). Erst ab einer Größe von 1 µm können Partikel über Phagozytose aufgenommen werden (Geiser et al., 2005). Folglich verbleiben Nanopartikel in den Alveolarstrukturen und interagieren länger mit den Epithelzellen der Lunge. Neben dem Verbleib in den Atemwegen können Nanopartikel auch die natürliche Lungenbarriere überwinden und in das Gefäßsystem gelangen, um dort zur Entstehung von kardiovaskulären Erkrankungen beizutragen (Nemmar et al., 2004; Ruckerl et al., 2006).

Partikeleigenschaften

Nanopartikel unterscheiden sich in ihren physikalisch-chemischen Eigenschaften von größeren Partikeln. Bei gleicher Masse weisen sie eine erhöhte Partikelanzahl bei geringerem Durchmesser auf, was mit einer größeren spezifischen Oberfläche einhergeht (Oberdorster et al., 2005). Diese vergrößerte Oberfläche spielt vermutlich eine entscheidende Rolle bei den negativen Gesundheitseffekten. So konnte gezeigt werden, dass bei gleicher Massedosierung Nanofasern gegenüber größeren Fasern mehr Tumore in den Lungen von Ratten auslösen konnten (Driscoll, 1996; Greim et al., 2001). Oxidierte Gase, organische Komponenten und Übergangmetalle können mit der relativ großen Oberfläche der ultrafeinen Partikel interagieren und deren chemische Reaktivität beeinflussen (Oberdorster, 2001; Wilson et al., 2002). Des Weiteren können an der Oberfläche von Nanopartikeln katalytische Prozesse stattfinden, die die Bildung von freien Radikalen zur Folge haben können (Unfried et al., 2007). Aufgrund von jeweils spezifischen Oberflächenladungen können in der Gasphase Agglomerate

und Aggregate von Partikeln entstehen. Dadurch verändert sich zwar ihr aerodynamischer Durchmesser, die reaktive Oberfläche bleibt aber weitestgehend unbeeinflusst (Donaldson et al., 2005; Oberdorster et al., 2007).

Kohlenstoffnanopartikel als Modell für Umweltnanopartikel

Der hauptsächliche Bestandteil der partikulären Luftverschmutzung sind verbrennungsgenerierte Kohlenstoffpartikel. So können bei unvollständigen Verbrennungsprozessen Kohlenstoffnanopartikel in Form von z.B. Dieselruß oder Flugasche auftreten (Donaldson et al., 2005). Diese Partikel weisen, in Abhängigkeit ihrer Quelle, eine hohe Kontamination mit organischen und anorganischen Bestandteilen auf (BeruBe et al., 2007). Neben der unbeabsichtigten Entstehung werden Kohlenstoffnanopartikel allerdings auch gezielt für verschiedene Anwendungen produziert. So werden sie als Füllstoff in der Automobilindustrie bei der Produktion von Reifengummierung verwendet. Durch Anwendungen in Konsumartikeln, z.B. als Farbpigment in Druckertonern, ist die Bevölkerung täglich der Exposition mit diesen Kohlenstoffpartikeln ausgesetzt (Pirela et al., 2015). Industriell produzierte Kohlenstoffpartikel bestehen fast ausschließlich aus elementarem Kohlenstoff mit einer geringen Kontamination an organischen Kohlenstoffverbindungen (Borm et al., 2005). Als Gemeinsamkeit haben anwendungsspezifisch produzierte und verbrennungsgenerierte Umweltnanopartikel einen Kohlenstoffkern, dessen primärer aerodynamischer Durchmesser 100 nm nicht überschreitet. Mehrere Untersuchungen belegen den negativen Einfluss dieser Partikel auf den menschlichen Organismus. Dabei zeigte sich, dass diese Effekte durch reine Kohlenstoffnanopartikel ausgelöst werden können (BeruBe et al., 2007; Nikula et al., 1995). Daher eignen sich diese Partikel als Modell für den Kohlenstoffkern aller verbrennungsgenerierten Partikel. Dieses Modellsystem ist etabliert, um zelluläre und molekulare Effekte von verbrennungsgenerierten Kohlenstoffnanopartikeln zu untersuchen.

Biologische Effekte der Nanopartikel-Zell-Interaktion

Inhalierte Nanopartikel werden von phagozytierenden Zellen nicht spezifisch erkannt und deshalb nur passiv aufgenommen (Geiser et al., 2010; Geiser et al., 2005). Akute Reaktionen der Lunge auf Kohlenstoffnanopartikel werden deshalb vor allem durch die Interaktion der Partikel mit Lungenepithelzellen ausgelöst (Stöger, 2016). Die moleku-

laren Ereignisse dieser Nanopartikel-Zell-Interaktion sind Gegenstand aktueller Forschung mit dem Ziel, pathogene Reaktionen, die von inhalierbaren Partikeln ausgehen, zu identifizieren und Strategien der molekularen Prävention zu entwickeln.

Die Interaktion von Lungenepithelzellen mit Kohlenstoffnanopartikeln führt kurzfristig zur Entstehung von intrazellulären reaktiven Sauerstoffspezies (ROS), die eine Veränderung der Lipidzusammensetzung der Zellmembran auslösen (Peuschel et al., 2012). Der Abbau von Sphingolipiden und die damit verbundene Anreicherung von Ceramiden führt zu Veränderungen von in Lipid Rafts organisierten Signalkomplexen und letztendlich zur Aktivierung des epidermalen Wachstumsfaktorrezeptors („epidermal growth factor receptor“, EGFR). Auf diese Weise werden Signalkaskaden aktiviert, an denen die Mitogen-aktivierten Proteinkinasen (MAPK) c-Jun N-terminale Kinasen (Jnk1/2), „extracellular-signal regulated kinases 1/2“ (Erk1/2) und p38-mitogen-aktivierte Proteinkinasen (p38) beteiligt sind (Abbildung 2) (Sydlik et al., 2006; Unfried et al., 2008; Weissenberg et al., 2010). Über diese Signalkaskade werden Proliferation, Apoptose und pro-inflammatorische Prozesse von Epithelzellen nach Exposition mit Kohlenstoffnanopartikeln reguliert (Sydlik et al., 2006). Die Aktivierung von MAPK ist für die Erhöhung der Expression des Chemokins Interleukin-8 (IL-8) verantwortlich, das die Rekrutierung von neutrophilen Granulozyten verursacht und so zur Entstehung der neutrophilen Lungenentzündung beiträgt (Kim et al., 2005; Sydlik et al., 2009). Der molekulare Mechanismus der Aktivierung des EGFR durch reine Kohlenstoffnanopartikel ist dabei noch nicht näher untersucht.

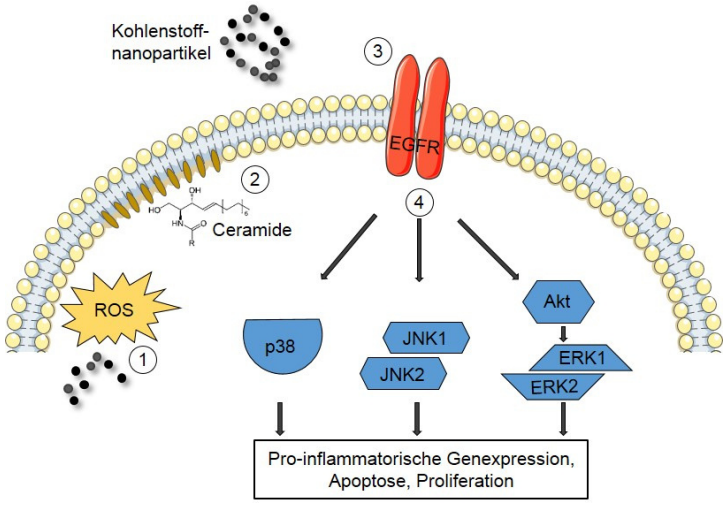

Abbildung 2: Membranabhängige Signalereignisse in Lungenepithelzellen ausgelöst durch Kohlenstoffnanopartikel. 1: Entstehung intrazellulärer reaktiver Sauerstoffspezies (ROS). 2: Anreicherung von Ceramiden in Lipid Rafts. 3: Translokation und Aktivierung des EGFR. 4: Aktivierung der MAPK Signalkaskaden unter Beteiligung von Jnk1/2, Erk1/2 über Akt oder p38.

Neben den beschriebenen Akutreaktionen von Lungenepithelzellen, sind Effekte von langanhaltenden Expositionen mit Konzentrationen von Kohlenstoffnanopartikeln, wie sie in vielen Regionen in westlichen Ländern auftreten, von besonderem Interesse. Typische, durch Umweltpartikel ausgelöste Krankheitsbilder wie die chronisch obstruktive Lungenerkrankung (COPD) und idiopathische pulmonale Fibrose (IPF) werden nach langjähriger Exposition beobachtet (Chilosi et al., 2013; Schikowski et al., 2005) und weisen einen hohen Anteil an seneszenten Zellen in exponierten Geweben auf (Disayabutr et al., 2016; Houssaini et al., 2018). Erste mechanistische Untersuchungen der Arbeitsgruppen Haendeler und Unfried zeigten, dass Kohlenstoffnanopartikel zelluläre Seneszenz in Lungenepithelzellen und Endothelzellen auslösen. In beiden Zelltypen führte die Exposition mit nicht-zytotoxischen Dosen von Kohlenstoffnanopartikeln zu einem Anstieg von reaktiven Sauerstoffspezies. Als typisches Zeichen seneszenter Zellen wurde in beiden Zelltypen die von der Tyrosinkinase Src-abhängige Reduktion der Telomeraseaktivität beobachtet. Zudem zeigte die Studie, dass eine zweiwöchige, repetitive Belastung mit Kohlenstoffnanopartikeln einen Anstieg des Zellzyklusinhibitors CDK-Inhibitor 1 (p21) sowohl in Lungenepithelzellen als auch in Endothelzellen induziert (Buchner et al., 2013). Es wurde weitergehend nachgewiesen, dass es nach dieser Behandlung zum Anstieg der Seneszenz-assoziierten Beta-Galactosidase (SA-β-Gal) und dem Verlust der replikativen Kapazität kam. *In vivo* Versuche zeigten, dass eine Langzeitexposition mit Kohlenstoffnanopartikeln Inflammations-unabhängig einen Verlust der endothelialen NO-Synthase (eNOS) Expression in der thorakalen Aorta bewirkte.

Weitere Untersuchungen haben - wie zuvor beschrieben - gezeigt, dass Kohlenstoffnanopartikel den EGFR in Lungenepithelzellen aktivieren. Allerdings sind die molekularen Mechanismen dieses Aktivierungsprozesses bislang nur unvollständig verstanden. Daher sollte in dieser Arbeit zunächst untersucht werden, ob die Aktivierung des EGFR durch Kohlenstoffnanopartikel über den kanonischen oder den nicht-kanonischen Aktivierungsweg *ex vivo* und *in vivo* erfolgt.

Nicht-kanonische Aktivierung des EGFR durch akute Belastung mit Kohlenstoffnanopartikeln

Der epidermale Wachstumsfaktorrezeptor (EGFR) ist eine ubiquitär vorkommende Rezeptor-Tyrosinkinase, die durch spezifische Liganden, wie beispielsweise dem epidermalen Wachstumsfaktor (EGF) aktiviert werden kann (Lemmon et al., 2014). Diese

Liganden liegen auf der Zelloberfläche in Form von membranverankerten Vorläufermolekülen vor. Die Freisetzung erfolgt durch die Spaltung dieser Vorläufermoleküle durch spezifische Proteasen auf der Zelloberfläche (Adrain et al., 2014). Durch die Bindung der Liganden an membranständige Monomere kommt es zur Ausbildung einer aktiven dimeren Konformation aus zwei EGFR-Molekülen (Lemmon et al., 1997). Nach der Aktivierung des EGFR durch spezifische Liganden wird dieser durch Endozytose von Membranbereichen, die Clathrin enthalten („clathrin-coated pits"), internalisiert.

Wie einleitend beschrieben, führt die Exposition von Lungenepithelzellen mit inhalierbaren Kohlenstoffnanopartikeln kurzfristig zu EGFR-abhängigen Zellreaktionen wie Proliferation, Apoptose oder Ausschüttung pro-inflammatorischer Faktoren (Sydlik et al., 2006; Sydlik et al., 2009). Als zentraler Mechanismus für die Aktivierung dieser Zellreaktionen konnte die Entstehung von intrazellulären reaktiven Sauerstoffspezies in Lungenepithelzellen durch die Exposition mit Kohlenstoffnanopartikeln identifiziert werden (Weissenberg et al., 2010). Die molekularen Mechanismen, die zu einer Nanopartikel-vermittelten Aktivierung des EGFR führen, sind jedoch noch nicht geklärt. Aus der Literatur gibt es Hinweise, dass durch Partikel-spezifische Aktivierung von membranständigen Proteinasen natürliche Liganden freigesetzt werden und es so zu einer Liganden-spezifischen Aktivierung der EGFR kommt. Derartige Beobachtungen wurden in Bronchialepithelzellen gemacht, die mit Umweltpartikeln oder Silika-Nanopartikeln behandelt wurden (Ovrevik et al., 2011; Skuland et al., 2014). Vorbefunde der Arbeitsgruppe weisen jedoch auf einen anderen Weg der EGFR-Aktivierung durch Kohlenstoffnanopartikel in Lungenepithelzellen hin (Peuschel et al., 2012). Reaktive Sauerstoffspezies sind in der Lage, neutrale Sphingomyelinase zu aktivieren, ein Enzym, das Sphingomyeline zu Ceramiden abbaut (Chung et al., 2015). Ein Verlust von Sphingomyelinen und die Anreicherung von Ceramiden in der Zellmembran in Abhängigkeit von durch Kohlenstoffnanopartikel ausgelösten reaktiven Sauerstoffspezies konnte in früheren Studien beobachtet werden (Peuschel et al., 2012). Untersuchungen zur Aktivierung des EGFR durch oxidativen Stress zeigen, dass derartige Veränderungen der Membranzusammensetzung über einen nicht vollständig verstandenen Prozess, zu einer Liganden-unabhängigen EGFR-Aktivierung und einer Caveolin-1-abhängigen Internalisierung des Rezeptors führen (Khan et al., 2006).

In der vorliegenden Arbeit sollte überprüft werden, ob die EGFR-Aktivierung durch Kohlenstoffnanopartikel über einen Liganden-unabhängigen, durch reaktive Sauerstoffspezies verursachten Mechanismus erfolgt. Hierbei wurde die Hypothese zugrunde gelegt, dass sich die nicht-kanonische Aktivierung von der Liganden-abhängigen Aktivierung des EGFR anhand der Caveolin-1-abhängigen Internalisierung unterscheiden läßt. Weiterhin sollte die Relevanz dieses Mechanismus‘ der Rezeptoraktivierung für das Partikel-exponierte Lungenepithel *in vivo* verifiziert werden.

Caveolin-1 (Cav-1) ist ein membranständiges Strukturprotein, das essentiell für die Ausbildung von Caveolae ist. Durch die Oligomerisierung von Caveolin-1 Molekülen werden Membranstrukturen ermöglicht, die zur Ausbildung von Membranvesikeln führen und so die Caveolae-abhängige Endozytose ermöglichen (Hansen et al., 2010).

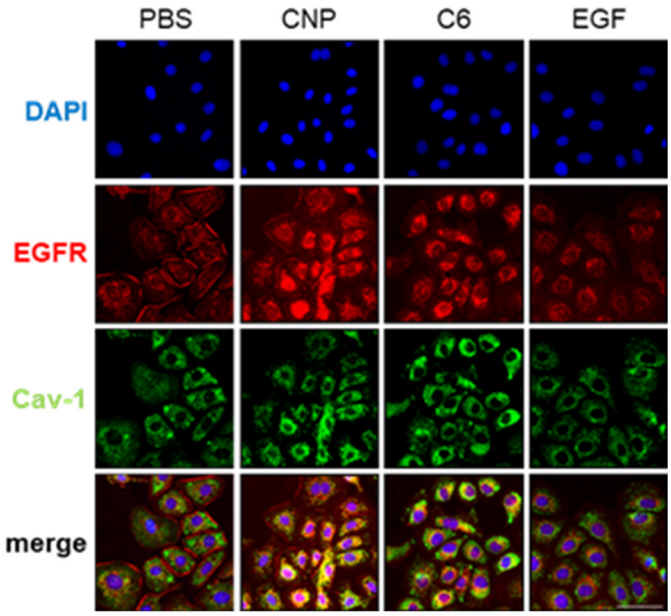

Abbildung 3: Caveolin-1 und EGFR Kolokalisierung als Merkmal für die nicht-kanonische EGFR Aktivierung. Lungenepithelzellen (RLE-6TN) wurden 5 Minuten mit Kohlenstoffnanopartikeln (CNP, 10 µg/cm²), C_6-Ceramid (5 µM) oder EGF (100 ng/ml) inkubiert. Die Abbildung zeigt die subzelluläre Lokalisation von EGFR (rot) und Caveolin-1 (grün). Kolokalisierung ist in den überlagerten Bildern gelb dargestellt. Experiment wurde in drei unabhängigen Wiederholungen durchgeführt. Maßstab beträgt 20 µm. (modifiziert nach Stockmann, **Spannbrucker** et al., 2018)

Zunächst wurde der Prozess der EGFR-Internalisierung, die nach dessen Aktivierung erfolgt, untersucht. Hierbei wurde die subzelluläre Lokalisation des Rezeptors und von Caveolin-1 nach Exposition mit Kohlenstoffnanopartikeln, C_6-Ceramid oder EGF betrachtet. Alle drei Stimuli lösten eine Translokation des EGFR aus der Plasmamembran in das Zytoplasma aus (Abbildung 3). Die Aktivierung wurde zusätzlich auf der Ebene der aktivierenden Phosphorylierung des EGFR nachgewiesen (Stöckmann et al., 2018). Gleichzeitig kam es zu einer intrazellulären Akkumulation von Caveolin-1,

sowohl nach der Belastung mit Nanopartikeln, als auch C_6-Ceramid, nicht jedoch bei der Behandlung mit dem natürlichen Liganden EGF. Die spezifischen Fluoreszenzmarkierungen für Caveolin-1 und EGFR zeigen, dass die Proteine nach Behandlung mit Kohlenstoffnanopartikeln und Ceramid intrazellulär kolokalisieren, also nach Aktivierung und Translokation gemeinsam in der Zelle vorliegen. Die spezifische intrazelluläre Akkumulation von Caveolin-1 und dessen Kolokalisierung mit dem EGFR ist also ein typisches Zeichen für die Liganden-unabhängige Aktivierung des EGFR durch Kohlenstoffnanopartikel und Ceramide (Abbildung 3).

Die Vorgänge, die zur Kolokalisation von EGFR und Caveolin-1 nach der Rezeptoraktivierung durch Kohlenstoffnanopartikel führen, wurden anhand einer Reihe von Interventionsversuchen analysiert (Abbildung 4). Die Ausbildung von Caveolae kann durch das Antibiotikum Filipin III verhindert werden (Schnitzer et al., 1994). Dieses bindet in der Zellmembran an Cholesterin, verhindert die Oligomerisierung von Caveolin-1 und inhibiert so die Endozytose durch Caveolae. Durch die Vorbehandlung der Lungenepithelzellen mit Filipin III wird die Translokation von EGFR und Caveolin-1 nach Behandlung mit Kohlenstoffnanopartikeln oder C_6-Ceramid unterbunden. Sie hat jedoch keinen Einfluss auf die Translokation des Rezeptors nach Aktivierung mit EGF. Die Kolokalisation von EGFR und Caveolin-1 ist also auf die Caveolae-abhängige Endozytose des EGFR nach dessen nicht-kanonischer Aktivierung zurückzuführen.

In einem weiteren Interventionsversuch wurde das kompatible Solut Ectoin verwendet, welches in der Lage ist, Membranstrukturen zu stabilisieren und die Aktivierung und Internalisierung des EGFR zu verhindern (Peuschel et al., 2012; Roychoudhury et al., 2012; Sydlik et al., 2009). Die postulierte Stabilisierung der Membran durch Ectoin reduziert die Effekte von Kohlenstoffnanopartikel und C_6-Ceramid, nicht aber die EGFR-Translokation nach EGF-Behandlung (Abbildung 4A).

In einem dritten Ansatz wurden die Zellen mit α-Tocopherol vorbehandelt. In Vorarbeiten wurde gezeigt, dass durch die Vorbehandlung mit diesem Antioxidans die durch Kohlenstoffnanopartikel ausgelösten intrazellulären reaktiven Sauerstoffspezies reduziert werden (Peuschel et al., 2012). Diese antioxidative Strategie reduziert die Translokation von EGFR und Caveolin-1 nach Behandlung mit Kohlenstoffnanopartikeln. Da Ceramide erst durch den Einfluss reaktiver Sauerstoffspezies auf die neutrale Sphingomyelinase entstehen, lässt sich kein Einfluss von α-Tocopherol auf die durch externe Zugabe von C_6-Ceramid ausgelösten Effekte beobachten (Abbildung 4A). Der

Zusammenhang der Translokation von Caveolin-1 und oxidativem Stress wurde in einem weiteren Experiment durch Zugabe von Wasserstoffperoxid (H_2O_2) untersucht (Abbildung 4B). Die fluoreszenzmikroskopischen Aufnahmen zeigen, dass sowohl die Behandlung mit Kohlenstoffnanopartikel als auch H_2O_2 zu einer Translokation von Caveolin-1 führen. Die Abhängigkeit der Internalisierung von Caveolin-1 von reaktiven Sauerstoffspezies wird durch diese Ergebnisse bestätigt.

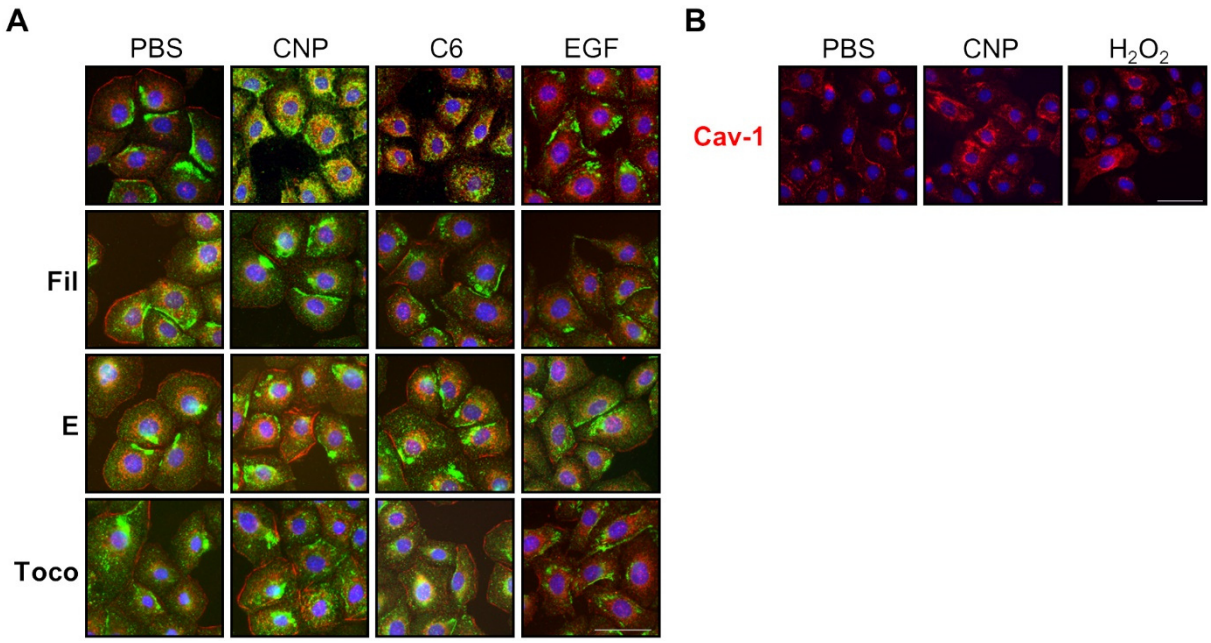

Abbildung 4: Subzelluläre Lokalisation von EGFR und Caveolin-1 in Lungenepithelzellen. Lungenepithelzellen (RLE-6TN) wurden 5 Minuten mit Kohlenstoffnanopartikeln (CNP, 10 µg/cm²), C_6-Ceramid (5 µM) oder EGF (100 ng/ml) belastet. (A) Zuvor wurden die Zellen mit unterschiedlichen Inhibitoren vorinkubiert: Filipin III (Fil, 1 µg/ml), Ectoin (E, 1 mM) oder α-Tocopherol (Toco, 75 µM). EGFR ist in rot, Caveolin-1 in grün dargestellt. Kolokalisierung ist in den überlagerten Bildern gelb dargestellt. (B) Subzelluläre Lokalisation von Caveolin-1 (rot) nach der Belastung mit Kohlenstoffnanopartikeln (CNP, 10 µg/cm²) oder Wasserstoffperoxid (H_2O_2, 5 µM). Experiment wurde in drei unabhängigen Wiederholungen durchgeführt. Maßstab beträgt 20 µm. (modifiziert nach Stockmann, **Spannbrucker** et al., 2018)

Mit diesen Ergebnissen wird demonstriert, dass die Caveolae-abhängige Endozytose des EGFR in Lungenepithelzellen nach Exposition mit Kohlenstoffnanopartikeln durch reaktive Sauerstoffspezies ausgelöst wird. Die Stabilisierung der Membran durch die Applikation von Ectoin wirkt der Liganden-unabhängigen Aktivierung entgegen und stellt möglicherweise eine Option für präventive Ansätze dar (Sydlik et al., 2009).

Die kausale Relevanz einer Caveolin-1-abhängigen, nicht-kanonischen Aktivierung des EGFR für pathogene Mechanismen des Lungenepithels wurde *in vivo* im Modell mit Caveolin-1-defizienten Mäusen untersucht. Es wurde die Hypothese überprüft, ob das Fehlen von Caveolin-1 *in vivo* zur Blockierung der Liganden-unabhängigen Aktivierung dieser Signalwege und nachgeschalteter Endpunkte wie z.B. die Freisetzung

des Chemokins KC (analog zu humanem IL-8) und der daraus resultierenden Rekrutierung von neutrophilen Granulozyten führt. Dazu wurden Caveolin-1 Knockout-Mäusen und ihren wildtypischen Geschwistern einmalig Partikelsuspensionen durch pharyngeale Aspiration in die Lunge appliziert.

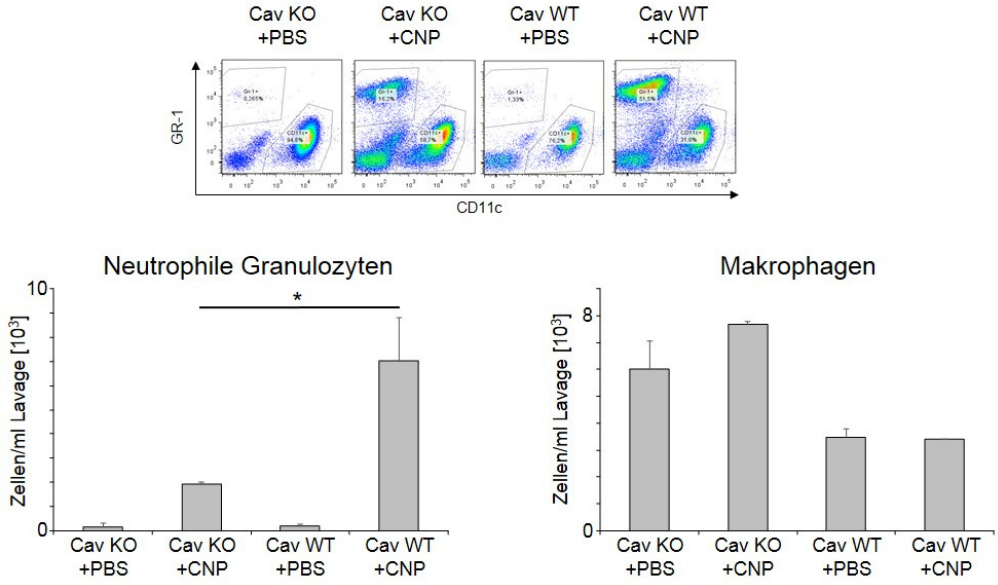

Abbildung 5: Durchflusszytometrische Analyse der inflammatorischen Zellen in Lungenlavagen. Caveolin-1 Knockout (Cav KO) Mäuse und ihre wildtypischen Geschwister (Cav WT) wurden durch pharyngeale Aspiration mit Kohlenstoffnanopartikeln (CNP, 2,5 mg/kg) oder PBS belastet. 6 Stunden nach der Belastung wurden Lungenlavagen entnommen. GR-1 positive Zellen (neutrophile Granulozyten) und CD11c positive Zellen (Makrophagen) wurden pro ml Lungenlavage quantifiziert. Gezeigt sind die Mittelwerte +/- Standardfehler. (PBS n = 3, CNP n = 4, *p<0.05, Mann-Whitney U Test). (modifiziert nach Stockmann, **Spannbrucker** et al., 2018)

Die Anzahl von neutrophilen Granulozyten und Makrophagen in der Lavageflüssigkeit wurde mittels differentieller Zellzählung durchflusszytometrisch bestimmt (Kroker et al., 2015). Es zeigt sich, dass die durch die Exposition ausgelöste Rekrutierung von neutrophilen Granulozyten in Knockout-Tieren im Vergleich zu Wildtyp-Geschwistertieren deutlich reduziert ist (Abbildung 5). Hingegen sind in beiden Genotypen nach Exposition keine signifikanten Erhöhungen der Makrophagenzahlen zu beobachten. Allerdings fällt auf, dass Knockout-Tiere basal und unabhängig von der Exposition eine höhere Makrophagenzahlen in der Lunge aufweisen. Dies könnte eine bislang nicht beschriebene phänotypische Veränderung der Knockout-Tiere sein. Die differentiellen Zellzählungen geben Hinweise darauf, dass durch den Verlust der Caveolin-1-abhängigen Aktivierung der Signalwege eine deutlich geringere Entzündungsreaktion ausgelöst werden kann.

Als spezifische Endpunkte der direkten Interaktion von Kohlenstoffnanopartikeln mit Lungenepithelzellen wurden die pro-inflammatorischen Signalwege über „RAC-alpha

serine/threonine-protein kinase 1“ (Akt) und Erk1/2 im Lungenhomogenat untersucht (Abbildung 6). Semiquantitative Western-Blot-Analysen der phosphorylierten Formen beider Proteine zeigen deutlich die Relevanz von Caveolin-1 für diesen EGFR-abhängigen Signalweg. Durch die Exposition wird in den Wildtyp Tieren ein statistisch signifikanter Anstieg der phosphorylierten Formen von Akt und Erk1/2 hervorgerufen. In den Caveolin-1 Knockout-Tieren hingegen konnten Kohlenstoffnanopartikel diese pro-inflammatorischen Signalwege nicht auslösen.

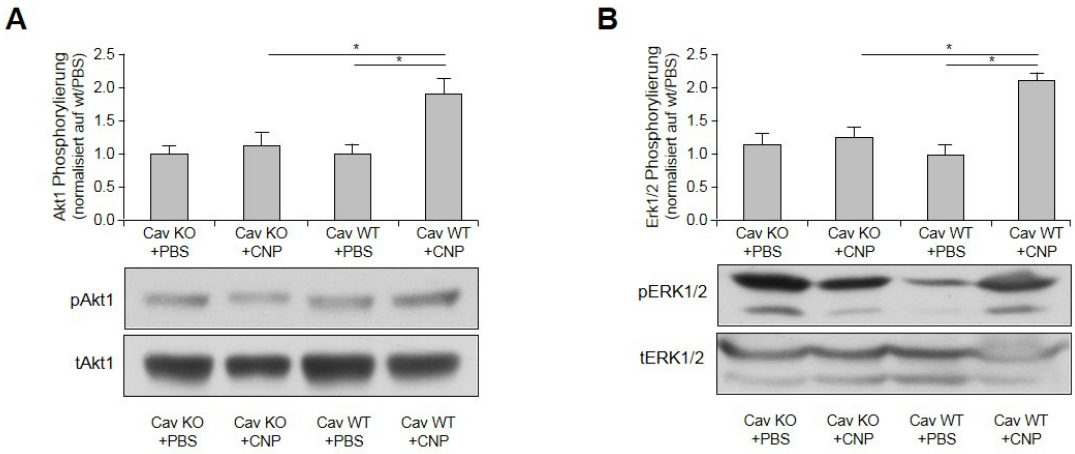

Abbildung 6: Nicht-kanonische Aktivierung des MAPK Signalwegs durch EGFR *in vivo*. Caveolin-1 Knockout Mäuse (Cav KO) und ihre wildtypischen Geschwister (Cav WT) wurden durch pharyngale Aspiration mit Kohlenstoffnanopartikeln (CNP, 2,5 mg/kg) oder PBS belastet. 6 Stunden nach der Belastung wurden Lungenlysate erzeugt. (A) Relative Phosphorylierung von Akt1 in Lungenhomogenaten relativ zu totalem Akt1. Proteinlevel wurden durch Immunoblot bestimmt. Gezeigt sind die Mittelwerte +/- Standardfehler (semiquantitative Auswertung von Western-Blots). (B) Relative Phosphorylierung von Erk1/2 in Lungenhomogenaten relativ zu totalem Erk1/2. Proteinlevel wurden durch Immunoblot bestimmt. Gezeigt sind die Mittelwerte +/- Standardfehler (PBS n = 4–5, CNP n = 7–8, *p<0.05, Mann-Whitney U Test). (modifiziert nach Stockmann, **Spannbrucker** et al., 2018)

Zur Verifizierung dieser Befunde hinsichtlich ihres Auftretens im Lungenepithel wurden immunhistologische Untersuchungen an Kryopräparaten der Lungen durchgeführt (Abbildung 7). Die Färbung von Gewebeschnitten mit Hämatoxilin und Eosin (HE) zeigte eine bereits in der Literatur beschriebene leichte Verdickung der Lungensepten (Drab et al., 2001). Wie zu erwarten, war im Lungengewebe der Knockout-Mäuse kein Caveolin-1 nachweisbar, während das Protein in den Lungenschnitten der Wildtyp-Mäuse vorhanden ist. Aufgrund der Morphologie der Zellen konnten im Alveolarbereich Typ I Epithelzellen von Typ II Epithelzellen unterschieden werden. In beiden Zelltypen der Wildtyp-Tiere wird Caveolin-1 exprimiert. Die immunhistologische Färbung des EGFR zeigt deutlich, dass dieses Protein sowohl in Knockout-Tieren wie auch in Wildtyp-Geschwistertieren in Alveolarzellen gleichermaßen vorhanden ist. Das Vorliegen der phosphorylierten Formen von Akt und Erk1/2 im Alveolarbereich in Typ I und Typ II

Epithelzellen nach Behandlung der Tiere mit Kohlenstoffnanopartikeln hingegen unterscheidet sich deutlich abhängig vom Genotyp.

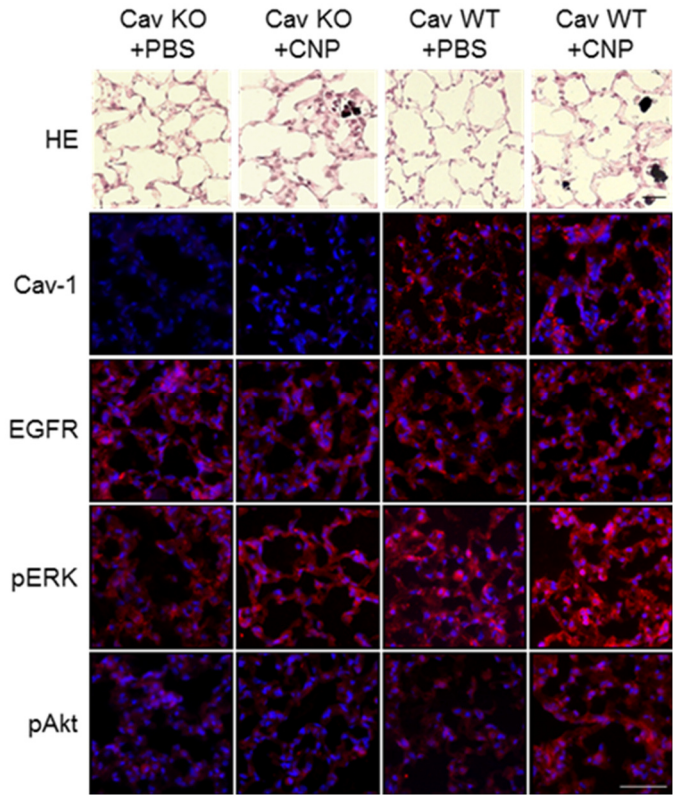

Abbildung 7: Nicht-kanonische Aktivierung des EGFR *in vivo*. Caveolin-1 defiziente Mäuse (Cav KO) und ihre wildtypischen Geschwister (Cav WT) wurden mittels pharyngealer Aspiration mit Kohlenstoffnanopartikeln (CNP, 2,5 mg/kg) oder PBS belastet. 6 Stunden nach der Belastung wurden die Lungen entnommen. Immunhistochemische Analyse von Kryoschnitten der Lungen (PBS n = 3, CNP n = 4). Die Lungen wurden entweder mit Hämatoxilin/Eosin (HE) oder mittels Immunfärbung (rot) gegen Caveolin-1 (Cav-1), EGFR, phosphoErk1/2 (pErk) oder phosphoAkt (pAkt) gefärbt. Zellkerne wurden mittels DAPI (blau) angefärbt. Dargestellt sind repräsentative Immunfärbungen. Messbalken zeigt 50 µm. (modifiziert nach Stockmann, **Spannbrucker** et al., 2018)

Analog zu den Befunden der Western-Blot-Analysen lässt sich in Wildtyp-Tieren durch die Partikelbehandlung ein deutlich verstärktes Vorkommen der phosphorylierten Formen (pAkt, pErk1/2) beobachten, die in den Knockout-Tieren nicht auftritt. Die Daten aus den *in vivo*-Versuchen belegen die Relevanz der nicht kanonischen EGFR-Aktivierung für die Aktivierung pro-inflammatorischer Signalwege in Lungenepithelzellen und der Auslösung einer neutrophilen Lungenentzündung durch Kohlenstoffnanopartikel.

Die Untersuchungen der akuten Wirkung von Kohlenstoffnanopartikeln auf Lungenepithelzellen zeigen erstmalig, dass diese durch direkte Partikel-Zell-Interaktion zur Liganden-unabhängigen Aktivierung des EGFR führen. Diese nicht-kanonische Aktivierung ist gekennzeichnet durch die Caveolin-1-vermittelte Internalisierung des

Rezeptors und kann so von der Liganden-abhängigen Rezeptoraktivierung unterschieden werden. Diese spezifische Aktivierungsreaktion bietet die Möglichkeit einer präventiven Intervention für exponierte Personen, die nicht mit der physiologisch relevanten Aktivierung durch natürliche Liganden interferiert. Die Stabilisierung der Zellmembran durch kompatible Solute wie Ectoin, die vom Menschen gut vertragen werden (K. Unfried et al., 2016), bietet die Möglichkeit einer molekularen Prävention in Situationen, in denen eine Exposition des Menschen nicht vermieden werden kann.

Einfluss einer chronischen Belastung mit Kohlenstoffpartikel auf zelluläre Alterung in der Lunge

Wie in der Einleitung beschrieben, führt die chronische Belastung der Atemwege mit inhalierten Partikeln zur Entstehung von altersassoziierten Erkrankungen wie beispielsweise chronisch obstruktiver Lungenerkrankung (COPD) und idiopathischer pulmonaler Fibrose (IPF) (Conti et al., 2018; Schikowski et al., 2005). Beide Erkrankungen zeigen Anzeichen von vorzeitiger Lungenalterung und zellulärer Seneszenz (Aasen et al., 2018; Chilosi et al., 2013; Faner et al., 2012). Reine Kohlenstoffnanopartikel induzieren zelluläre Seneszenz in Lungenepithelzellen (Buchner et al., 2013). Jedoch sind die zugrundeliegenden Mechanismen nicht vollständig aufgeklärt. Der Verlust von interzellulärer Kommunikation scheint wesentlich zur Organdysfunktion bis hin zum Organversagen beizutragen (Lopez-Otin et al., 2013). So wurde bereits gezeigt, dass es während des Alterungsprozesses zu einer Reduktion der Gap Junction-vermittelten Zellkommunikation zwischen Kardiomyozyten kommt (Nagibin et al., 2016). Des Weiteren kann eine gestörte Zell-Zellkommunikation im Endothel zu arterieller Hypertonie und Atherosklerose führen (Okamoto et al., 2017). Für eine funktionale Gewebshomöostase ist eine intakte interzelluläre Kommunikation notwendig. Seneszenz führt in dysfunktionalen Organen zu einer reduzierten proliferativen Kapazität. Dies hat zur Folge, dass Schädigungen des Gewebes nicht mehr vollständig repariert werden können; es liegt also eine reduzierte regenerative Kapazität vor. Es stellt sich daher die Frage, ob die langfristige Exposition von Lungenepithelzellen mit Kohlenstoffnanopartikeln mit einer Abnahme der interzellulären Kommunikation verbunden ist, was in Folge zu einer Dysfunktion der Lunge beitragen kann. Da Partikel unterschiedlicher Größenordnung auch in den alveolaren Lungenbereich vordringen können, ist zudem

zu ergründen, ob sich Partikel unterschiedlicher Größenklassen in ihrer Wirkweise unterscheiden.

Um diese Fragen zu beantworten, wurde das zuvor verwendete Modell eingesetzt (Buchner et al., 2013), in dem die alveolaren Typ II Zellen jeden zweiten Tag mit Kohlenstoffnanopartikeln oder größeren Vergleichspartikeln (Kohlenstoffpartikel >0,1 µm) behandelt wurden (Abbildung 8). Wie bereits in der vorherigen Studie mit akuter Belastung durch Kohlenstoffnanopartikel wurde auch hier eine Dosierung von 10 µg/cm^2 verwendet, da dies einer langjährigen kumulativen Partikellast des menschlichen Lungenepithels in belasteten Großstädten entspricht. Zusätzlich wurde eine 10-fach geringere Dosis (1 µg/cm^2) appliziert, um Dosiseffekte beobachten zu können. In früheren Studien wurde gezeigt, dass die Dosierung von 10 µg/cm² keine zytotoxischen Effekte auslöste (Buchner et al., 2013; Sydlik et al., 2006).

Zelluläre Seneszenz ist gekennzeichnet durch einen Zellzyklus-Arrest (Lopez-Otin et al., 2013). Um zu untersuchen, ob dieser Prozess auch bei der Langzeitbelastung mit Kohlenstoffnanopartikeln eintritt, wurde die proliferative Kapazität der Zellen mittels Bromdesoxyuridin (BrdU) bestimmt. BrdU wird analog zu Thymidin während der Synthese in die DNA eingebaut. So ist es möglich, über die BrdU-Inkorporation Rückschlüsse auf die DNA-Syntheserate und somit der proliferativen Aktivität zu ziehen. Die über zwei Wochen repetitiv exponierten konfluenten Epithelzellen wurden geerntet und mit einer Zelldichte ausplattiert, die eine erneute Proliferation nicht-seneszenter Zellen erlaubt. Es zeigte sich, dass die zuvor mit Kohlenstoffnanopartikeln behandelten Zellen in beiden Konzentrationen nicht mehr in der Lage waren, die DNA-Syntheserate der Kontrollzellen zu erreichen. Die Exposition mit nicht-Nanopartikeln zeigte hingegen keinen signifikanten Effekt im Vergleich zur Kontrolle (Abbildung 8).

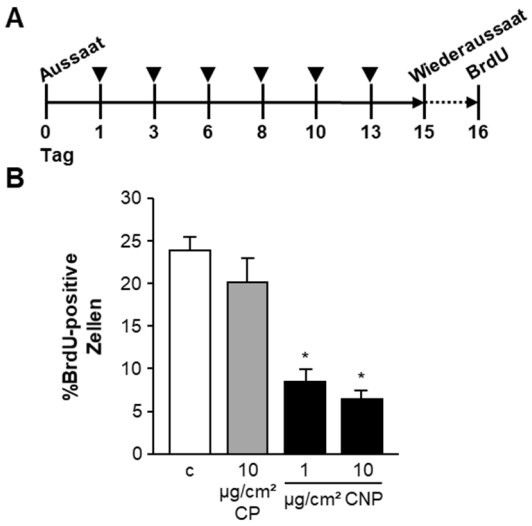

Abbildung 8: Kohlenstoffnanopartikel verursachen eine Reduktion der replikativen Kapazität. (A) Exposition der Lungenepithelzellen. ▼ symbolisieren die Belastungszeitpunkte mit Kohlenstoffpartikeln (CP) und Kohlenstoffnanopartikeln (CNP). (B) Exponierte Lungenepithelzellen wurden trypsiniert und neu ausgesät. Die Proliferation wurde mittels BrdU-Inkoporation zytometrisch bestimmt. c bezeichnet die unbehandelte Kontrolle. Gezeigt sind die Mittelwerte +/- Standardfehler (n=3, *p<0.05 vs Kontrolle, zweiseitiger, ungepaarter t-Test). (modifiziert nach **Spannbrucker** et al., 2018)

Der Verlust der Replikationsfähigkeit im Rahmen der zellulären Seneszenz kann mit der Erhöhung der Zellzyklus inhibierenden Proteine CDK-Inhibitor 2A (p16) und p21 einhergehen (Campisi, 2013). Die Akkumulation dieser Zellzyklusinhibitoren wurde in semi-quantitativen Western-Blot-Analysen repetitiv exponierter Zellen untersucht. Für p21 zeigte sich, wie auch schon zuvor beschrieben (Buchner et al., 2013), dass die Nanopartikel in beiden Dosierungen einen stärkeren Anstieg von p21 im Vergleich zu den nicht-Nanopartikeln auslösten (Abbildung 9A). Der geringe signifikante Anstieg von p21 bei den nicht-Nanopartikeln ist möglicherweise auf die in der Einleitung erläuterte Oberflächenreaktivität zurückzuführen. Die Akkumulation von p16 ließ sich anhand der signifikanten, offensichtlich dosisabhängigen Erhöhung der Proteinlevel in den mit Kohlenstoffnanopartikeln behandelten Zellen beobachten (Abbildung 9B). Die mit größeren Partikeln behandelten Zellen wiesen hingegen keine Veränderung auf.

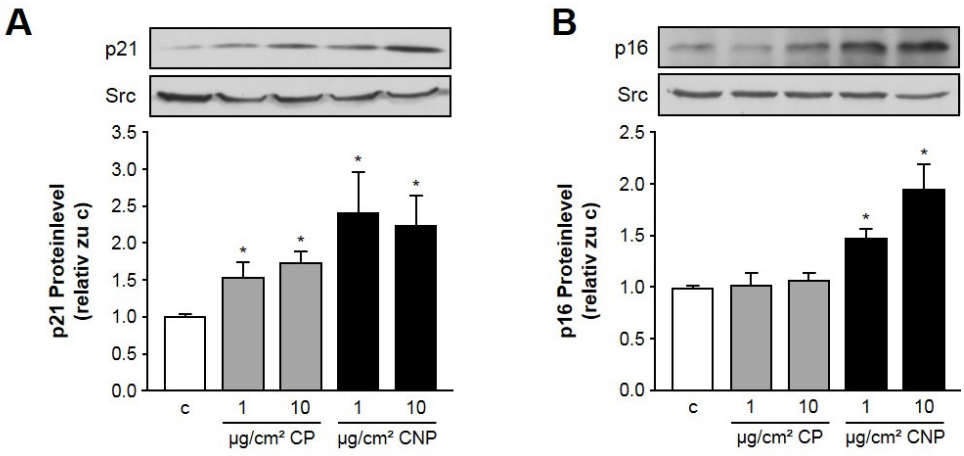

Abbildung 9: Langzeitbelastung mit Kohlenstoffnanopartikeln verursacht einen Anstieg von Zellzyklus Inhibitoren. RLE-6TN Zellen wurden jeden zweiten Tag über eine Periode von 14 Tagen mit Kohlenstoffpartikeln (CP) oder Kohlenstoffnanopartikeln (CNP) belastet. c bezeichnet die unbehandelte Kontrolle. (A) p21 Proteinlevel wurden durch Immunoblot bestimmt, Src diente als Ladungskontrolle. Gezeigt sind repräsentative Immunoblots und eine semiquantitative Analyse von p21 normiert auf Src. (Mittelwerte +/- Standardfehler n=4-5, *p<0.05 vs Kontrolle, zweiseitiger, ungepaarter t-test). (B) p16 Proteinlevel wurden durch Immunoblot bestimmt, Src diente als Ladungskontrolle. Gezeigt sind repräsentative Immunoblots und eine semiquantitative Analyse von p16 normiert auf Src. (Mittelwerte +/- Standardfehler n=4, *p<0.05 vs Kontrolle, zweiseitiger, ungepaarter t-test). (modifiziert nach **Spannbrucker** et al., 2018)

Die meisten Erkenntnisse, die darauf hindeuten, dass inhalierte Schadstoffe zelluläre Seneszenz im Lungenepithel auslösen können, stammen aus Untersuchungen mit Tabakrauch, der als Hauptursache für COPD gilt (Mercado et al., 2015). Tabakrauch ist allerdings eine hochkomplexe Mischung aus festen aber auch flüchtigen Stoffen. So wurde in den Lungen von COPD Patienten, sowie Rauchern, ein Verlust der Histondeacetylase Sirtuin-1 (SIRT1) beobachtet (Rajendrasozhan et al., 2008). Dieses redox-sensitive Enzym reguliert u.a. metabolische Signalwege und kann das Überleben von Zellen beeinflussen (Poulose et al., 2015). Durch Überexpression oder pharmakologische Aktivierung von SIRT1 konnte die Entstehung von Emphysemen experimentell verhindert werden (Yao et al., 2012). Als Ursache für den Verlust von SIRT1 und frühzeitiger Seneszenz wird oxidativer Stress diskutiert, welcher durch Tabakrauch entsteht. Durch die entstehenden reaktiven Sauerstoffspezies wird SIRT1 posttranslational modifiziert, was zu seiner proteasomalen Degradation führt (Caito et al., 2010). So führt der oxidative Stress, entweder direkt durch Partikel oder durch den von neutrophilen Granulozyten induzierten inflammatorischen, oxidativen Burst welcher, zur zellulären Seneszenz des Lungenepithels. Eine SIRT1 Reduktion kann einen Anstieg der Zellzyklusinhibitoren p16 und p21 zur Folge haben (Yao et al., 2012). Es stellt sich die Frage, ob es auch nach einer chronischen Belastung mit Kohlenstoffnanopartikeln in

Lungenepithelzellen zu einer Verringerung von SIRT1 kommt. Dies wäre anzunehmen, da die Akkumulation von p16 und p21 beobachtet wurde (Abbildung 9). Daher wurde nun überprüft, ob dies ebenfalls bei einer chronischen Belastung zutrifft. Nach einer 14-tägigen Belastung zeigte sich keine Verminderung von SIRT1 in den mit nicht-Nanopartikeln belasteten Zellen (Abbildung 10). Bei den mit Kohlenstoffnanopartikeln behandelten Zellen zeigte sich hingegen eine dramatische, signifikante Abnahme bei einer Konzentration von 10 µg/cm².

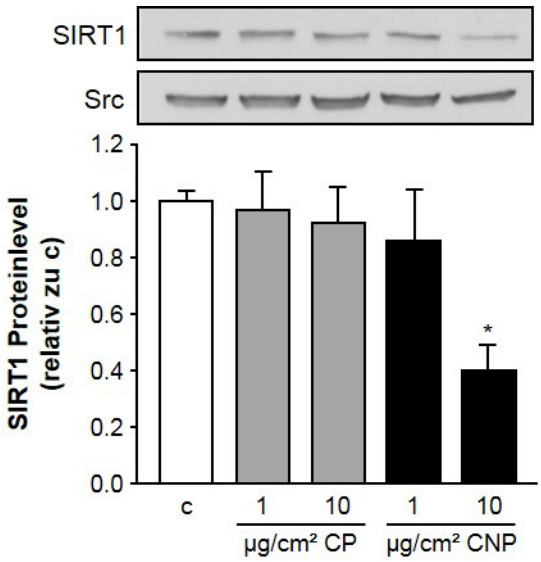

Abbildung 10: Langzeitbelastung mit Kohlenstoffnanopartikeln verursacht eine Reduktion von SIRT1. RLE-6TN Zellen wurden jeden zweiten Tag über eine Periode von 14 Tagen mit Kohlenstoffpartikeln (CP) oder Kohlenstoffnanopartikeln (CNP) belastet. c bezeichnet die unbehandelte Kontrolle. SIRT1 Proteinlevel wurden durch Immunoblot bestimmt, Src diente als Ladungskontrolle. Gezeigt sind repräsentative Immunoblots und eine semiquantitative Analyse von SIRT1 normiert auf Src. (Mittelwerte +/- Standardfehler n=6, *p<0.05 vs Kontrolle, zweiseitiger, ungepaarter t-test). (modifiziert nach **Spannbrucker** et al., 2018)

Der Verlust der proliferativen Kapazität, der Anstieg der Zellzyklusinhibitoren p16 und p21, sowie die Reduktion von SIRT1 zeigen in diesem Modell, dass Kohlenstoffnanopartikel nach zwei Wochen Seneszenz in den Zellen auslösen. Dies legt die Vermutung nahe, dass auch die interzelluläre Kommunikation gestört ist, da auch diese während des Alterungsprozesses dysfunktional wird. Eine besondere Rolle spielen hierbei die Gap Junctions, über die der Austausch von Ionen oder kleiner Signalmoleküle zwischen benachbarten Zellen stattfindet. Lungenepithelzellen stehen über sie in Kontakt oder interagieren mit mesenchymalem Gewebe (Badri et al., 2011). Gap Junctions bestehen aus Connexinen, dies sind Transmembranproteine, die sich als Hexamere anordnen können und sogenannte Connexone bilden (Evans et al., 2002). Gap Junc-

tion-Kanäle werden durch die Zusammenlagerung von jeweils zwei Connexonen benachbarter Zellen ausgebildet. Für das humane Genom sind 21 verschiedene Connexine beschrieben, für die Ratte mindestens 19 (Agardh et al., 2013; Hanner et al., 2010). Die Kombination der verschiedenen Connexine innerhalb der Gap Junction-Kanäle ist entscheidend für die jeweilige Zelltyp-spezifische selektive Permeabilität der Gap Junctions (Ek-Vitorin et al., 2013). In epithelialen Zellen ist Connexin 43 (Cx43) das vorherrschende Connexin, das in alveolären Epithelzellen meist in Kombination mit den Connexinen Cx40 und Cx32 vorkommt (Chanson et al., 2018). Frühere Studien konnten zeigen, dass die Reduktion der interzellulären Kommunikation über Gap Junctions eine kurzfristige Reaktion (4 Stunden) auf die Exposition von Lungenepithelzellen mit Kohlenstoffnanopartikeln darstellt (Ale-Agha et al., 2010). Mit den vorliegenden Versuchen sollte nun untersucht werden, ob die durch repetitive Exposition mit Kohlenstoffnanopartikeln ausgelöste zelluläre Seneszenz funktionale Defekte auf der Ebene der Cx43-abhängigen Zell-Zell-Kommunikation bedingt. Hierfür wurden zunächst mRNA- und Proteinmengen von Cx43 untersucht. Wie in Abbildung 11A ersichtlich ist, führte die Belastung mit der hohen Nanopartikelkonzentration zu einer signifikanten Reduktion von Cx43 auf transkriptioneller Ebene. Ein gleiches Resultat zeigte sich auf Proteinebene (Abbildung 11B). Die repetitive Exposition von Lungenepithelzellen mit Kohlenstoffnanopartikeln führt also zur verminderten Expression von Cx43.

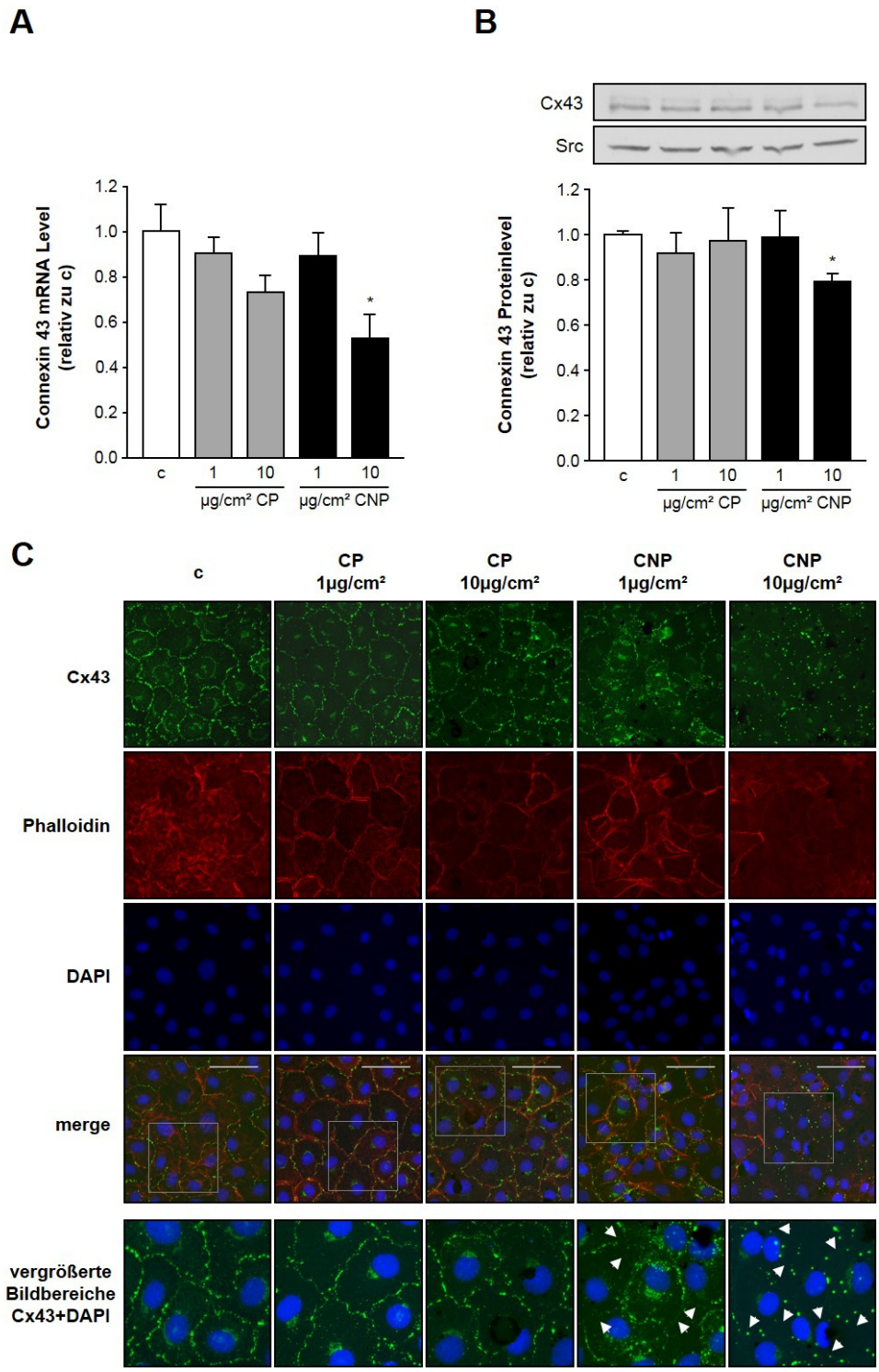

Abbildung 11: Langzeitbelastung mit Kohlenstoffnanopartikeln führt zu einer Reduktion von Connexin 43 und ändert dessen Lokalisation. RLE-6TN Zellen wurden jeden zweiten Tag über eine Periode von 14 Tagen mit Kohlenstoffpartikeln (CP) oder Kohlenstoffnanopartikeln (CNP) belastet. c bezeichnet die unbehandelte Kontrolle. (A) Connexin 43 Transkriptionslevel wurden durch semi-quantitative real-time PCR ermittelt, „60S ribosomal protein L32“ (RPL32) diente als Referenz. Gezeigt sind die Mittelwerte +/- Standardfehler (n=3, *p<0.05 vs Kontrolle, zweiseitiger, ungepaarter t-test). (B) Cx43 Proteinlevel wurde durch Immunoblot bestimmt, Src diente als Ladungskontrolle. Gezeigt sind repräsentative Immunoblots und eine semiquantitative Analyse von Cx43 normiert auf Src. Gezeigt sind die Mittelwerte +/- Standardfehler (n=6, *p<0.05 vs Kontrolle, zweiseitiger, ungepaarter t-test). (C) Immunhistochemische Analyse der Cx43 Lokalisation. c bezeichnet die unbehandelte Kontrolle. In den Zellen wurde Cx43 mit spezifischem Antikörper und Aktin mittels Phalloidin angefärbt; für die Kernfärbung wurde DAPI verwendet. Merge zeigt eine Überlagerung der Farbkanäle. Maßstab beträgt 50 µm. Die untere Zeile zeigt vergrößerte Bildbereiche. (modifiziert nach **Spannbrucker** et al., 2018)

Für eine funktionelle Zell-Zell-Kommunikation über Gap Junctions ist es erforderlich, dass Cx43 in der Zellmembran lokalisiert ist und so die Ausbildung von Connexonen ermöglicht. Da Cx43 auf Proteinebene reduziert wird, liegt die Vermutung nahe, dass sich auch Veränderungen auf der Ebene der Membranlokalisation nachweisen lassen. Mittels Immunfluoreszenzfärbung wurde daher auch die Membranständigkeit und Subzelluläre Lokalisation untersucht. In unbehandelten Zellen findet man das Protein in der Zytoplasmamembran benachbarter Zellen lokalisiert. Nach der Behandlung mit den nicht-Nanopartikeln wurde keine Veränderung der Lokalisation von Cx43 im Vergleich zur Kontrolle beobachtet. Im Gegensatz dazu führte die Behandlung mit Nanopartikeln zu einer Translokation von Cx43 aus der Zellmembran in das Zytoplasma. Dieser Effekt lässt sich bereits mit der geringen Dosierung (1 µg/cm²), bei der keine Verringerung der Proteinmenge vorliegt, beobachten (Abbildung 11C). Dies bedeutet, dass bereits geringe Konzentrationen von Kohlenstoffnanopartikeln Einfluss auf die interzelluläre Kommunikation nehmen könnten, obwohl diese Effekte auf der Ebene der Cx43 Expression noch nicht nachweisbar sind. Die Belastung mit 10 µg/cm² führt zu einer dramatischen Translokation von Cx43. Wie bereits gezeigt, geht diese Veränderung bei der hohen Belastung auch mit einer Reduktion auf Protein und mRNA Ebene einher.

Da die Translokation von Cx43 aus der Plasmamembran bereits bei der geringen Kohlenstoffnanopartikelkonzentration auftritt, jedoch nicht mit nicht-Nanopartikeln, liegt die Vermutung nahe, dass bereits geringe Dosen von Kohlenstoffnanopartikeln die interzelluläre Kommunikation stören. Daher wurde im Folgenden die interzelluläre Kommunikation untersucht. Es zeigte sich wie erwartet, dass die Gap Junction-vermittelte interzelluläre Kommunikation bei beiden Nanopartikelkonzentrationen reduziert war, während die nicht-Nanopartikel keinen Einfluss hatten. Somit konnte belegt werden, dass es auf funktionaler Ebene zu einem Kommunikationsverlust durch Nanopartikel in Lungenepithelzellen kommt (Abbildung 12).

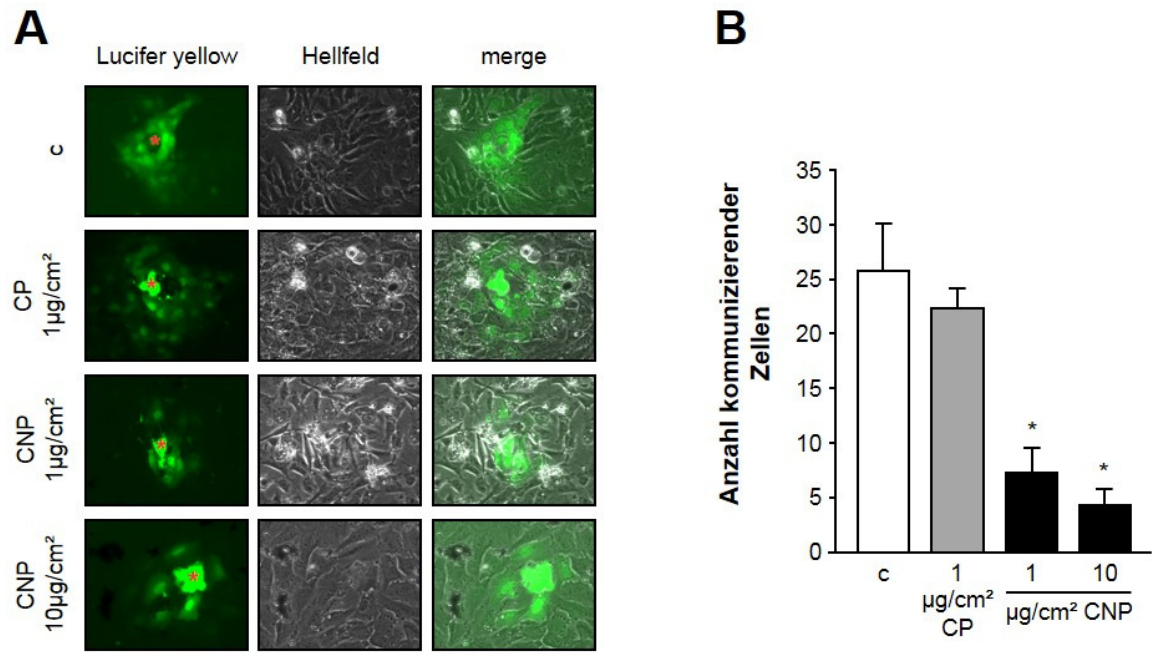

Abbildung 12: Langzeitbelastung mit Kohlenstoffnanopartikeln verringert die interzelluläre Kommunikation. RLE-6TN Zellen wurden jeden zweiten Tag über eine Dauer von 14 Tagen mit Kohlenstoffpartikeln (CP) oder Kohlenstoffnanopartikeln (CNP) belastet. c bezeichnet die unbehandelte Kontrolle. An Tag 14 wurde die interzelluläre Gap Junction Kommunikation durch Mikroinjektion von Lucifer Yellow (Dye Transfer Assay) ermittelt. (A) Repräsentative Bilder; Merge zeigt eine Überlagerung des Fluoreszenzkanals und der Hellfeldabbildung. Die Zelle, in die der Farbstoff injiziert wurde, ist mit einem Stern markiert. (B) Quantitative Analyse der interzellulären Kommunikation. Gezeigt ist die Anzahl kommunizierender Zellen. (Mittelwerte +/- Standardfehler n=4, *p<0.05 vs Kontrolle, zweiseitiger, ungepaarter t-test). (modifiziert nach **Spannbrucker** et al., 2018)

Zusammenfassend zeigen diese Arbeiten erstmalig, dass die langfristige Exposition von Lungenepithelzellen mit Kohlenstoffnanopartikeln zu einem Zellzyklusarrest, der Akkumulation der Zellzyklus-Inhibitoren p16 und p21, einer Reduktion von SIRT1 sowie einer verringerten Expression einer veränderten subzellulären Lokalisation von Cx43 führt. Die induzierte zelluläre Seneszenz geht einher mit einem Funktionsverlust der Epithelzellen auf der Ebene der Gap Junction-vermittelten interzellulären Kommunikation. Dies lässt vermuten, dass die chronische Exposition mit Kohlenstoffnanopartikeln die Organfunktion der Lunge nachhaltig beeinträchtigt und so zur Entstehung von Seneszenz-assoziierten Lungenerkrankungen beiträgt. Dies unterstreicht die Notwendigkeit, die zellulären Mechanismen, die durch Nanopartikel ausgelöst werden, noch besser zu verstehen, denn dies würde Möglichkeiten für therapeutische Ansätze eröffnen. Die Aufrechterhaltung der Cx43-abhängigen Zell-Zell-Kommunikation durch pharmakologische Ansätze, wie dem anti-arrhythmisch wirksamen Peptid AAP10, das für die Therapie kardiovaskulärer Erkrankungen vorgeschlagen wird (De Vuyst et al.,

2011; Schulz et al., 2015), könnte auch eine Interventionsstrategie gegen Lungenerkrankungen wie zum Beispiel COPD darstellen.

Koffein als mögliche Interventionsstrategie für alternsbedingte Dysfunktionalität der Mitochondrien

Neben einer reduzierten replikativen Kapazität und einer Störung der interzellulären Kommunikation kommt es während des Alterungsprozesses auch zu einer Dysfunktionalität von Mitochondrien (Lopez-Otin et al., 2013), die als mögliche Ursache für die Entstehung von idiopathischer pulmonaler Fibrose betrachtet wird (Bueno et al., 2015; Pardo et al., 2016). Interessanterweise führt die Exposition von Lungenepithelzellen mit partikulären Schadstoffen zu einem reduzierten Sauerstoffverbrauch und einem Anstieg der reaktiven Sauerstoffspezies in den Mitochondrien (Malinska et al., 2018). Frühere Studien der Arbeitsgruppen Haendeler und Unfried hatten gezeigt, dass Kohlenstoffnanopartikel zu einer Verringerung der Aktivität der Telomerase-Reverse-Transkriptase (TERT) in den Mitochondrien von Endothelzellen und Lungenepithelzellen führen (Buchner et al., 2013). Da TERT notwendig für die Aufrechterhaltung der Mitochondrienfunktion zu sein scheint, könnte die Belastung mit Kohlenstoffnanopartikeln somit zur mitochondrialen Dysfunktionalität beitragen. Faktoren, die die Mitochondrienfunktion positiv beeinflussen, könnten die Entwicklung präventiver Interventionsstrategien gegen umweltinduzierte Alterungsprozesse darstellen. Untersuchungen des als Zellzyklus-Inhibitor bekannten Proteins CDKN1B (p27) zeigten, dass dieses Protein im Herzkreislaufsystem Funktionen übernimmt, die nicht im Zusammenhang mit seiner Rolle in der Zellzyklusregulation stehen (Konecny et al., 2012). Weiterhin hat sich gezeigt, dass die Aufnahme von Koffein präventiv gegen Herzkreislauferkrankungen wirkt (Greenberg et al., 2008). Die aktuellen Untersuchungen zeigen, dass p27 auch in Mitochondrien lokalisiert ist und die mitochondriale Funktion verbessert (Ale-Agha,…, **Spannbrucker** et al., 2018). *In vivo* Untersuchungen mit p27-defizienten Mäusen zeigten eine verminderte Atmungskettenaktivität in Mitochondrien aus dem Herzen. Ein Verlust von p27 im Mitochondrium trägt daher zu Dysfunktionalität und verminderter zellmigratorischer Kapazität bei. Eine Möglichkeit, um diesen Effekten entgegenzuwirken, könnte die Aufnahme von Koffein sein. Es zeigte sich, dass es nach der Behandlung mit Koffein zu einem Anstieg von p27 in den Mitochondrien kommt. Ebenso konnte *in vivo* eine Verbesserung der Atmungsaktivität in den Herzen

von Mäusen nachgewiesen werden, die zuvor Koffein über das Trinkwasser aufgenommen hatten. Somit konnte Koffein als weiterer Faktor identifiziert werden, der die Funktionalität der Mitochondrien positiv beeinflussen kann.

Ausblick

Ziel dieser Arbeit war es, die Folgen chronischer und akuter Exposition von Lungenepithelzellen mit Kohlenstoffnanopartikeln aufzuklären. Es konnte gezeigt werden, dass es nach Exposition zu einer Liganden-unabhängigen, nicht kanonischen Aktivierung des EGF-Rezeptors kommt, die sich *ex vivo* und *in vivo* beobachten lässt. Dieser Prozess wird spezifisch von Caveolin-1 vermittelt und lässt sich so von endogenen Signalereignissen unterscheiden. Des Weiteren konnte *ex vivo* demonstriert werden, dass eine chronische Belastung mit geringen Mengen von Kohlenstoffnanopartikeln zu Seneszenz-assoziierten Endpunkten wie dem Verlust der Replikationsfähigkeit führt und die interzelluläre Kommunikation reduziert wird. Auf Grundlage dieser Erkenntnisse stellt sich die weiterführende Frage, ob ein Zusammenhang zwischen diesen Kurzzeit- und Langzeiteffekten besteht. Möglicherweise steht die akute EGFR-Aktivierung beim chronischen Verlauf im Zusammenhang mit der Seneszenz. In der Literatur findet man Hinweise, dass auch die Belastung von Lungenepithel mit Dieselrußpartikeln zu einer Aktivierung des EGFR führen kann. Im weiteren Verlauf einer Signalkaskade kann es über „Signal transducer and activator of transcription 3“ (Stat3) zu einem Anstieg von p21 und somit zu einer Inhibition der Zellproliferation kommen (Cao et al., 2010). In diesem Zusammenhang ist von Interesse, ob auch eine Langzeitexposition mit geringen Dosen von Kohlenstoffnanopartikeln zu einer Aktivierung des EGFR führt und ob diese Ereignisse an der Entstehung zellulärer Seneszenz beteiligt sind. Hier wird die Untersuchung der EGFR-abhängigen Signalkaskaden im Hinblick auf zelluläre Seneszenz *ex vivo* und *in vivo* neue Erkenntnisse bringen. Ist die EGFR-Aktivierung bei einer chronischen Belastung für diese Prozesse relevant, müssten die in dieser Arbeit vorgestellten Anzeichen zellulärer Seneszenz in Caveolin-1 defizienten Zellen bzw. Tieren gegenüber wildtypischen Tieren reduziert sein. Dies würde einen kausalen Zusammenhang zwischen der in dieser Arbeit gezeigten Aktivierung des EGFR und der reduzierten proliferativen Kapazität nach chronischer Belastung zeigen.

Die in früheren Studien beobachtete Entstehung von intrazellulären reaktive Sauerstoffspezies (Buchner et al., 2013) könnte die initiale Ursache für die hier beschriebene zelluläre Seneszenz und Dysfunktionalität von Epithelzellen aufgrund der Exposition

mit Kohlenstoffnanopartikeln darstellen. Weiterführende Studien sollten diesen Kausalzusammenhang im Hinblick auf antioxidative Strategien untersuchen. Hierfür könnten dann intrazelluläre oxidative und antioxidative Systeme untersucht werden. Interessant in diesem Zusammenhang wäre es, die Expression und Aktivität von NADPH-Oxidasen, Superoxiddismutasen, Katalasen, Glutathion und Thioredoxin-1 durch den Einsatz von verschiedenen Interventionsstrategien zu untersuchen. Speziell der kausale Zusammenhang zwischen dem Anstieg von ROS, der Induktion von Seneszenz wäre an diesem Punkt zu analysieren. Hier bieten sich Interventionsstrategien durch Vorbehandlung mit Antioxidantien wie N-Acetylcystein oder Tempol an. Es konnte bereits in Endothelzellen nachgewiesen werden, dass eine durch H_2O_2 induzierte zelluläre Seneszenz zu einem Anstieg der NADPH Oxidase 4 und einer Abnahme von Thioredoxin-1 führt (Goy et al., 2014). Daher wäre auch eine Reexpression von Thioredoxin-1 denkbar, die dann in einem chronischen Belastungsszenario eine höhere Spezifität gegenüber der Gabe von Antioxidantien hätte.

Um die *ex vivo* erhobenen Ergebnisse zu verifizieren und eine physiologische Relevanz darzulegen, könnten in *in vivo* Ansätzen adulte C57Bl/6 Mäuse repetitiv mit Partikelsuspensionen durch pharyngeale Aspiration exponiert werden. Dieses System eignet sich für mechanistische Untersuchungen, da es eine präzise Dosierung der Partikel in der Lunge ermöglicht. Die Experimente sollen dann unter Bedingungen durchgeführt, bei denen es nicht zu einer pulmonalen Inflammation kommt, das heißt, dass Partikeldosierungen verwendet werden, die keine Einwanderung von Entzündungszellen in die Lunge auslösen. Anschließend sollen die Seneszenz-assoziierten Endpunkte wie der Anstieg von p16 und p21, der Verlust von SIRT1 und eine Veränderung der zellulären Kommunikation im Lungenepithel sowie im Endothel der Aorten untersucht werden. Zusätzlich könnte auch hier eine Veränderung der Aktivität und der Translokation des EGFR nachgeprüft werden. Die Applikation von Koffein stellt eine potentielle Präventivstrategie gegen eine Partikel-induzierte mitochondriale Dysfunktion dar. Hier wäre es von Interesse, den möglichen protektiven Effekt von Koffein auf das Lungenepithel und das Endothel *ex vivo* und *in vivo* zu untersuchen. Es sollte überprüft werden, ob hierdurch die Funktionalität der Mitochondrien verbessert werden kann und sich eine Präventivstrategie gegen partikelinduzierte Alterung und Erkrankung entwickelt lässt.

Zusammenfassung

Die Exposition des Menschen mit Umweltnanopartikeln korreliert mit Alters-assoziierten degenerativen Erkrankungen der Atemwege und des Herz-Kreislaufsystems. Erste Untersuchungen der Interaktion von Kohlenstoffnanopartikeln mit Lungenepithelzellen sowie Endothelzellen zeigten Hinweise auf die Induktion von zellulärer Seneszenz. Ziel dieser Arbeit war es, die durch verbrennungsgenerierte Nanopartikel-induzierten Mechanismen zu untersuchen, die zur Entstehung krankhafter Veränderungen beitragen. Dabei wurden einerseits die molekularen Effekte einer einmaligen Exposition als auch die der repetitiven Behandlung untersucht. Dabei wurden Kohlenstoffnanopartikel als Modell für Umweltpartikel verwendet. Eine einmalige Exposition von Epithelzellen führt zu einer Liganden-unabhängigen Aktivierung des epidermalen Wachstumsfaktorrezeptors (EGFR)-Signalweges. Charakteristisch für diesen Partikel-spezifischen Mechanismus ist die Internalisierung des Rezeptors in Abhängigkeit von Caveolin-1. Die Induktion zellulärer Seneszenz durch direkte Wirkung von Kohlenstoffnanopartikeln wurde durch repetitive Exposition von Lungenepithelzellen untersucht. Dies löste einen irreversiblen Verlust der Replikationsfähigkeit, die Akkumulation der Zellzyklusinhibitoren p16 und p21 sowie den Verlust der Redox-sensitiven Histon-Deacetylase Sirtuin-1 aus. Zudem wurde ein dramatischer Verlust der Gap Junction-abhängigen interzellulären Kommunikation in diesen Zellen nachgewiesen. Dieser Funktionsverlust wird durch verringerte Expression und veränderte subzelluläre Lokalisation von Connexin 43, einem der wichtigsten Gap Junction formenden Proteine, ausgelöst. Zudem führt Exposition von Lungenepithelzellen und auch Endothelzellen mit Partikeln zu einer reduzierten Mitochondrienfunktion. Interessanterweise, zeigten Untersuchungen auf Endothelzellen, dass sich durch Koffeingabe die mitochondriale Funktionalität verbessert. Dadurch ergibt sich eine mögliche Strategie zur Prävention der durch Kohlenstoffnanopartikel ausgelösten Dysfunktionalität sowohl auf zellulärer als auch auf Organebene.

Zusammengefasst zeigen die Ergebnisse dieser Arbeit, dass durch Kohlenstoffnanopartikel intrazelluläre Prozesse ausgelöst werden, die die Funktionalität der Zellen stark einschränken und zur Seneszenz führen.

Summary

Human exposure to environmental nanoparticles correlates with age-associated degenerative diseases of the respiratory and cardiovascular systems. Initial studies of the interaction of carbon nanoparticles with lung epithelial and endothelial cells revealed evidence for the induction of cellular senescence.

The aim of this work was to investigate mechanisms induced by combustion-derived nanoparticles that contribute to the development of pathological changes. The molecular effects of a single exposure as well as the repetitive treatment were investigated. In addition, the induction of cellular senescence after repetitive treatment was studied with respect to epithelial dysfunction. Therefore, carbon nanoparticles were used as model particles. A single exposure of epithelial cells to carbon nanoparticles led to ligand-independent activation of the epidermal growth factor receptor (EGFR)-signalling pathway. Characteristic for this particle-specific mechanism was the internalization of the receptor as a function of caveolin-1. The induction of cellular senescence by direct impact of carbon nanoparticles was investigated by using repetitive exposition of lung epithelial cells. This exposure caused irreversible loss of the replicative capacity, accumulation of cell cycle inhibitors p16 and p21, and loss of redox-sensitive histone deacetylase Sirtuin-1. In addition, a dramatic loss of Gap junction-dependent cell-cell communication was demonstrated in these cells. This loss of function is triggered by decreased expression and altered subcellular localization of Connexin 43, a major Gap junction forming protein. Furthermore, the exposure of lung epithelial as well as endothelial cells with particles results in a reduction of mitochondrial function. Interestingly, further investigations showed an improved mitochondrial function after caffeine treatment in endothelial cells. This could be a possible strategy for the prevention of dysfunctionality by inhaled combustion-derived nanoparticles on cellular but also organ level.

In summary, the results of this work show that carbon nanoparticles trigger intracellular processes that severely restrict cell functionality and lead to senescence.

Literaturverzeichnis

7708, D. I. DIN ISO 7708:1996-01, Luftbeschaffenheit - Festlegung von Partikelgrößenverteilungen für die gesundheitsbezogene Schwebstaubprobenahme (ISO 7708:1995)

Aasen, T., Johnstone, S., Vidal-Brime, L., Lynn, K. S., & Koval, M. (2018). Connexins: Synthesis, Post-Translational Modifications, and Trafficking in Health and Disease. *Int J Mol Sci, 19*(5). doi:10.3390/ijms19051296

Adrain, C., & Freeman, M. (2014). Regulation of receptor tyrosine kinase ligand processing. *Cold Spring Harb Perspect Biol, 6*(1). doi:10.1101/cshperspect.a008995

Agardh, H. E., Gertow, K., Salvado, D. M., Hermansson, A., van Puijvelde, G. H., Hansson, G. K., n-Berne, G. P., & Gabrielsen, A. (2013). Fatty acid binding protein 4 in circulating leucocytes reflects atherosclerotic lesion progression in Apoe(-/-) mice. *J Cell Mol Med, 17*(2), 303-310. doi:10.1111/jcmm.12011

Ale-Agha, N., Albrecht, C., & Klotz, L. O. (2010). Loss of gap junctional intercellular communication in rat lung epithelial cells exposed to carbon or silica-based nanoparticles. *Biol Chem, 391*(11), 1333-1339. doi:10.1515/BC.2010.133

Ale-Agha, N., Goy, C., Jakobs, P., Spyridopoulos, I., Gonnissen, S., Dyballa-Rukes, N., Aufenvenne, K., von Ameln, F., Zurek, M., Spannbrucker, T., Eckermann, O., Jakob, S., Gorressen, S., Abrams, M., Grandoch, M., Fischer, J. W., Kohrer, K., Deenen, R., Unfried, K., Altschmied, J., & Haendeler, J. (2018). CDKN1B/p27 is localized in mitochondria and improves respiration-dependent processes in the cardiovascular system-New mode of action for caffeine. *PLoS Biol, 16*(6), e2004408. doi:10.1371/journal.pbio.2004408

Badri, L., Walker, N. M., Ohtsuka, T., Wang, Z., Delmar, M., Flint, A., Peters-Golden, M., Toews, G. B., Pinsky, D. J., Krebsbach, P. H., & Lama, V. N. (2011). Epithelial interactions and local engraftment of lung-resident mesenchymal stem cells. *Am J Respir Cell Mol Biol, 45*(4), 809-816. doi:10.1165/rcmb.2010-0446OC

BeruBe, K., Balharry, D., Sexton, K., Koshy, L., & Jones, T. (2007). Combustion-derived nanoparticles: mechanisms of pulmonary toxicity. *Clin Exp Pharmacol Physiol, 34*(10), 1044-1050. doi:10.1111/j.1440-1681.2007.04733.x

Borm, P. J., Cakmak, G., Jermann, E., Weishaupt, C., Kempers, P., van Schooten, F. J., Oberdorster, G., & Schins, R. P. (2005). Formation of PAH-DNA adducts after in vivo and vitro exposure of rats and lung cells to different commercial carbon blacks. *Toxicol Appl Pharmacol, 205*(2), 157-167. doi:10.1016/j.taap.2004.10.020

Borm, P. J., & Kreyling, W. (2004). Toxicological hazards of inhaled nanoparticles--potential implications for drug delivery. *J Nanosci Nanotechnol, 4*(5), 521-531.

Buchner, N., Ale-Agha, N., Jakob, S., Sydlik, U., Kunze, K., Unfried, K., Altschmied, J., & Haendeler, J. (2013). Unhealthy diet and ultrafine carbon black particles induce senescence and disease associated phenotypic changes. *Exp Gerontol, 48*(1), 8-16. doi:10.1016/j.exger.2012.03.017

Bueno, M., Lai, Y. C., Romero, Y., Brands, J., St Croix, C. M., Kamga, C., Corey, C., Herazo-Maya, J. D., Sembrat, J., Lee, J. S., Duncan, S. R., Rojas, M., Shiva, S., Chu, C. T., & Mora, A. L. (2015). PINK1 deficiency impairs mitochondrial homeostasis and promotes lung fibrosis. *J Clin Invest, 125*(2), 521-538. doi:10.1172/jci74942

Caito, S., Rajendrasozhan, S., Cook, S., Chung, S., Yao, H., Friedman, A. E., Brookes, P. S., & Rahman, I. (2010). SIRT1 is a redox-sensitive deacetylase that is post-translationally modified by oxidants and carbonyl stress. *FASEB J, 24*(9), 3145-3159. doi:10.1096/fj.09-151308

Campisi, J. (2013). Aging, cellular senescence, and cancer. *Annu Rev Physiol, 75*, 685-705. doi:10.1146/annurev-physiol-030212-183653

Cao, D., Bromberg, P. A., & Samet, J. M. (2010). Diesel particle-induced transcriptional expression of p21 involves activation of EGFR, Src, and Stat3. *Am J Respir Cell Mol Biol, 42*(1), 88-95. doi:10.1165/rcmb.2008-0455OC

Chanson, M., Watanabe, M., O'Shaughnessy, E. M., Zoso, A., & Martin, P. E. (2018). Connexin Communication Compartments and Wound Repair in Epithelial Tissue. *Int J Mol Sci, 19*(5). doi:10.3390/ijms19051354

Chilosi, M., Carloni, A., Rossi, A., & Poletti, V. (2013). Premature lung aging and cellular senescence in the pathogenesis of idiopathic pulmonary fibrosis and COPD/emphysema. *Transl Res, 162*(3), 156-173. doi:10.1016/j.trsl.2013.06.004

Chung, S., Vu, S., Filosto, S., & Goldkorn, T. (2015). Src regulates cigarette smoke-induced ceramide generation via neutral sphingomyelinase 2 in the airway epithelium. *Am J Respir Cell Mol Biol, 52*(6), 738-748. doi:10.1165/rcmb.2014-0122OC

Conti, S., Harari, S., Caminati, A., Zanobetti, A., Schwartz, J. D., Bertazzi, P. A., Cesana, G., & Madotto, F. (2018). The association between air pollution and the incidence of idiopathic pulmonary fibrosis in Northern Italy. *Eur Respir J, 51*(1). doi:10.1183/13993003.00397-2017

De Vuyst, E., Boengler, K., Antoons, G., Sipido, K. R., Schulz, R., & Leybaert, L. (2011). Pharmacological modulation of connexin-formed channels in cardiac pathophysiology. *Br J Pharmacol, 163*(3), 469-483. doi:10.1111/j.1476-5381.2011.01244.x

Disayabutr, S., Kim, E. K., Cha, S. I., Green, G., Naikawadi, R. P., Jones, K. D., Golden, J. A., Schroeder, A., Matthay, M. A., Kukreja, J., Erle, D. J., Collard, H. R., & Wolters, P. J. (2016). miR-34 miRNAs Regulate Cellular Senescence in Type II Alveolar Epithelial Cells of Patients with Idiopathic Pulmonary Fibrosis. *PLoS One, 11*(6), e0158367. doi:10.1371/journal.pone.0158367

Dockery, D. W., Pope, C. A., 3rd, Xu, X., Spengler, J. D., Ware, J. H., Fay, M. E., Ferris, B. G., Jr., & Speizer, F. E. (1993). An association between air pollution and mortality in six U.S. cities. *N Engl J Med, 329*(24), 1753-1759. doi:10.1056/nejm199312093292401

Donaldson, K., & MacNee, W. (2001). Potential mechanisms of adverse pulmonary and cardiovascular effects of particulate air pollution (PM10). *Int J Hyg Environ Health, 203*(5-6), 411-415. doi:10.1078/1438-4639-00059

Donaldson, K., Tran, L., Jimenez, L. A., Duffin, R., Newby, D. E., Mills, N., MacNee, W., & Stone, V. (2005). Combustion-derived nanoparticles: a review of their toxicology following inhalation exposure. *Part Fibre Toxicol, 2*, 10. doi:10.1186/1743-8977-2-10

Drab, M., Verkade, P., Elger, M., Kasper, M., Lohn, M., Lauterbach, B., Menne, J., Lindschau, C., Mende, F., Luft, F. C., Schedl, A., Haller, H., & Kurzchalia, T. V. (2001). Loss of caveolae, vascular dysfunction, and pulmonary defects in caveolin-1 gene-disrupted mice. *Science, 293*(5539), 2449-2452. doi:10.1126/science.1062688

Driscoll, K. E. (1996). Effects of fibres on cell proliferation, cell activation and gene expression. *IARC Sci Publ*(140), 73-96.

Ek-Vitorin, J. F., & Burt, J. M. (2013). Structural basis for the selective permeability of channels made of communicating junction proteins. *Biochim Biophys Acta, 1828*(1), 51-68. doi:10.1016/j.bbamem.2012.02.003

Evans, W. H., & Martin, P. E. (2002). Gap junctions: structure and function (Review). *Mol Membr Biol, 19*(2), 121-136. doi:10.1080/09687680210139839

Faner, R., Rojas, M., Macnee, W., & Agusti, A. (2012). Abnormal lung aging in chronic obstructive pulmonary disease and idiopathic pulmonary fibrosis. *Am J Respir Crit Care Med, 186*(4), 306-313. doi:10.1164/rccm.201202-0282PP

Geiser, M., & Kreyling, W. G. (2010). Deposition and biokinetics of inhaled nanoparticles. *Part Fibre Toxicol, 7*, 2. doi:10.1186/1743-8977-7-2

Geiser, M., Rothen-Rutishauser, B., Kapp, N., Schurch, S., Kreyling, W., Schulz, H., Semmler, M., Im Hof, V., Heyder, J., & Gehr, P. (2005). Ultrafine particles cross cellular membranes by nonphagocytic mechanisms in lungs and in cultured cells. *Environ Health Perspect, 113*(11), 1555-1560. doi:10.1289/ehp.8006

Goy, C., Czypiorski, P., Altschmied, J., Jakob, S., Rabanter, L. L., Brewer, A. C., Ale-Agha, N., Dyballa-Rukes, N., Shah, A. M., & Haendeler, J. (2014). The imbalanced redox status in senescent endothelial cells is due to dysregulated Thioredoxin-1 and NADPH oxidase 4. *Exp Gerontol, 56*, 45-52. doi:10.1016/j.exger.2014.03.005

Greenberg, J. A., Chow, G., & Ziegelstein, R. C. (2008). Caffeinated coffee consumption, cardiovascular disease, and heart valve disease in the elderly (from the Framingham Study). *Am J Cardiol, 102*(11), 1502-1508. doi:10.1016/j.amjcard.2008.07.046

Greim, H., Borm, P., Schins, R., Donaldson, K., Driscoll, K., Hartwig, A., Kuempel, E., Oberdorster, G., & Speit, G. (2001). Toxicity of fibers and particles. Report of the workshop held in Munich, Germany, 26-27 October 2000. *Inhal Toxicol, 13*(9), 737-754. doi:10.1080/08958370118273

Hanner, F., Sorensen, C. M., Holstein-Rathlou, N. H., & Peti-Peterdi, J. (2010). Connexins and the kidney. *Am J Physiol Regul Integr Comp Physiol, 298*(5), R1143-1155. doi:10.1152/ajpregu.00808.2009

Hansen, C. G., & Nichols, B. J. (2010). Exploring the caves: cavins, caveolins and caveolae. *Trends Cell Biol, 20*(4), 177-186. doi:10.1016/j.tcb.2010.01.005

Hoet, P. H., Bruske-Hohlfeld, I., & Salata, O. V. (2004). Nanoparticles - known and unknown health risks. *J Nanobiotechnology, 2*(1), 12. doi:10.1186/1477-3155-2-12

Houssaini, A., Breau, M., Kebe, K., Abid, S., Marcos, E., Lipskaia, L., Rideau, D., Parpaleix, A., Huang, J., Amsellem, V., Vienney, N., Validire, P., Maitre, B., Attwe, A., Lukas, C., Vindrieux, D., Boczkowski, J., Derumeaux, G., Pende, M., Bernard, D., Meiners, S., & Adnot, S. (2018). mTOR pathway activation drives lung cell senescence and emphysema. *JCI Insight, 3*(3). doi:10.1172/jci.insight.93203

Ibald-Mulli, A., Wichmann, H. E., Kreyling, W., & Peters, A. (2002). Epidemiological evidence on health effects of ultrafine particles. *J Aerosol Med, 15*(2), 189-201. doi:10.1089/089426802320282310

Khan, E. M., Heidinger, J. M., Levy, M., Lisanti, M. P., Ravid, T., & Goldkorn, T. (2006). Epidermal growth factor receptor exposed to oxidative stress undergoes Src- and caveolin-1-dependent perinuclear trafficking. *J Biol Chem, 281*(20), 14486-14493. doi:10.1074/jbc.M509332200

Kim, Y. M., Reed, W., Lenz, A. G., Jaspers, I., Silbajoris, R., Nick, H. S., & Samet, J. M. (2005). Ultrafine carbon particles induce interleukin-8 gene transcription and p38 MAPK activation in normal human bronchial epithelial cells. *Am J Physiol Lung Cell Mol Physiol, 288*(3), L432-441. doi:10.1152/ajplung.00285.2004

Konecny, F., Zou, J., Husain, M., & von Harsdorf, R. (2012). Post-myocardial infarct p27 fusion protein intravenous delivery averts adverse remodelling and improves heart function and survival in rodents. *Cardiovasc Res, 94*(3), 492-500. doi:10.1093/cvr/cvs138

Kroker, M., Sydlik, U., Autengruber, A., Cavelius, C., Weighardt, H., Kraegeloh, A., & Unfried, K. (2015). Preventing carbon nanoparticle-induced lung inflammation reduces antigen-specific sensitization and subsequent allergic reactions in a mouse model. *Part Fibre Toxicol, 12*, 20. doi:10.1186/s12989-015-0093-5

Lemmon, M. A., Bu, Z., Ladbury, J. E., Zhou, M., Pinchasi, D., Lax, I., Engelman, D. M., & Schlessinger, J. (1997). Two EGF molecules contribute additively to stabilization of the EGFR dimer. *Embo j, 16*(2), 281-294. doi:10.1093/emboj/16.2.281

Lemmon, M. A., Schlessinger, J., & Ferguson, K. M. (2014). The EGFR family: not so prototypical receptor tyrosine kinases. *Cold Spring Harb Perspect Biol, 6*(4), a020768. doi:10.1101/cshperspect.a020768

Lopez-Otin, C., Blasco, M. A., Partridge, L., Serrano, M., & Kroemer, G. (2013). The hallmarks of aging. *Cell, 153*(6), 1194-1217. doi:10.1016/j.cell.2013.05.039

MacNee, W., & Donaldson, K. (2003). Mechanism of lung injury caused by PM10 and ultrafine particles with special reference to COPD. *Eur Respir J Suppl, 40*, 47s-51s.

Malinska, D., Szymanski, J., Patalas-Krawczyk, P., Michalska, B., Wojtala, A., Prill, M., Partyka, M., Drabik, K., Walczak, J., Sewer, A., Johne, S., Luettich, K., Peitsch, M. C., Hoeng, J., Duszynski, J., Szczepanowska, J., van der Toorn, M., & Wieckowski, M. R. (2018). Assessment of mitochondrial function following short- and long-term exposure of human bronchial epithelial cells to total particulate matter from a candidate modified-risk tobacco product and reference cigarettes. *Food Chem Toxicol, 115*, 1-12. doi:10.1016/j.fct.2018.02.013

Mercado, N., Ito, K., & Barnes, P. J. (2015). Accelerated ageing of the lung in COPD: new concepts. *Thorax, 70*(5), 482-489. doi:10.1136/thoraxjnl-2014-206084

Nagibin, V., Egan Benova, T., Viczenczova, C., Szeiffova Bacova, B., Dovinova, I., Barancik, M., & Tribulova, N. (2016). Ageing related down-regulation of myocardial connexin-43 and up-regulation of MMP-2 may predict propensity to atrial fibrillation in experimental animals. *Physiol Res, 65 Suppl 1*, S91-S100.

Nemmar, A., Hoylaerts, M. F., Hoet, P. H., & Nemery, B. (2004). Possible mechanisms of the cardiovascular effects of inhaled particles: systemic translocation and prothrombotic effects. *Toxicol Lett, 149*(1-3), 243-253. doi:10.1016/j.toxlet.2003.12.061

Nikula, K. J., Snipes, M. B., Barr, E. B., Griffith, W. C., Henderson, R. F., & Mauderly, J. L. (1995). Comparative pulmonary toxicities and carcinogenicities of chronically inhaled diesel exhaust and carbon black in F344 rats. *Fundam Appl Toxicol, 25*(1), 80-94.

Oberdorster, G. (2001). Pulmonary effects of inhaled ultrafine particles. *Int Arch Occup Environ Health, 74*(1), 1-8.

Oberdorster, G., Oberdorster, E., & Oberdorster, J. (2005). Nanotoxicology: an emerging discipline evolving from studies of ultrafine particles. *Environ Health Perspect, 113*(7), 823-839. doi:10.1289/ehp.7339

Oberdorster, G., Oberdorster, E., & Oberdorster, J. (2007). Concepts of nanoparticle dose metric and response metric. *Environ Health Perspect, 115*(6), A290. doi:10.1289/ehp.115-1892118

Okamoto, T., & Suzuki, K. (2017). The Role of Gap Junction-Mediated Endothelial Cell-Cell Interaction in the Crosstalk between Inflammation and Blood Coagulation. *Int J Mol Sci, 18*(11). doi:10.3390/ijms18112254

Ovrevik, J., Refsnes, M., Totlandsdal, A. I., Holme, J. A., Schwarze, P. E., & Lag, M. (2011). TACE/TGF-alpha/EGFR regulates CXCL8 in bronchial epithelial cells exposed to particulate matter components. *Eur Respir J, 38*(5), 1189-1199. doi:10.1183/09031936.00171110

Pardo, A., & Selman, M. (2016). Lung Fibroblasts, Aging, and Idiopathic Pulmonary Fibrosis. *Ann Am Thorac Soc, 13 Suppl 5*, S417-s421. doi:10.1513/AnnalsATS.201605-341AW

Peuschel, H., Sydlik, U., Grether-Beck, S., Felsner, I., Stockmann, D., Jakob, S., Kroker, M., Haendeler, J., Gotic, M., Bieschke, C., Krutmann, J., & Unfried, K. (2012). Carbon nanoparticles induce ceramide- and lipid raft-dependent signalling in lung epithelial cells: a target for a preventive strategy against environmentally-induced lung inflammation. *Part Fibre Toxicol, 9*, 48. doi:10.1186/1743-8977-9-48

Pirela, S. V., Sotiriou, G. A., Bello, D., Shafer, M., Bunker, K. L., Castranova, V., Thomas, T., & Demokritou, P. (2015). Consumer exposures to laser printer-emitted engineered nanoparticles: A case study of life-cycle implications from nano-enabled products. *Nanotoxicology, 9*(6), 760-768. doi:10.3109/17435390.2014.976602

Poulose, N., & Raju, R. (2015). Sirtuin regulation in aging and injury. *Biochim Biophys Acta, 1852*(11), 2442-2455. doi:10.1016/j.bbadis.2015.08.017

Rajendrasozhan, S., Yang, S. R., Kinnula, V. L., & Rahman, I. (2008). SIRT1, an antiinflammatory and antiaging protein, is decreased in lungs of patients with chronic obstructive pulmonary disease. *Am J Respir Crit Care Med, 177*(8), 861-870. doi:10.1164/rccm.200708-1269OC

Roychoudhury, A., Haussinger, D., & Oesterhelt, F. (2012). Effect of the compatible solute ectoine on the stability of the membrane proteins. *Protein Pept Lett, 19*(8), 791-794.

Ruckerl, R., Ibald-Mulli, A., Koenig, W., Schneider, A., Woelke, G., Cyrys, J., Heinrich, J., Marder, V., Frampton, M., Wichmann, H. E., & Peters, A. (2006). Air pollution and markers of inflammation and coagulation in patients with coronary heart disease. *Am J Respir Crit Care Med, 173*(4), 432-441. doi:10.1164/rccm.200507-1123OC

Schikowski, T., Sugiri, D., Ranft, U., Gehring, U., Heinrich, J., Wichmann, H. E., & Kramer, U. (2005). Long-term air pollution exposure and living close to busy roads are associated with COPD in women. *Respir Res, 6*, 152. doi:10.1186/1465-9921-6-152

Schnitzer, J. E., Oh, P., Pinney, E., & Allard, J. (1994). Filipin-sensitive caveolae-mediated transport in endothelium: reduced transcytosis, scavenger endocytosis, and capillary permeability of select macromolecules. *J Cell Biol, 127*(5), 1217-1232.

Schulz, R., Gorge, P. M., Gorbe, A., Ferdinandy, P., Lampe, P. D., & Leybaert, L. (2015). Connexin 43 is an emerging therapeutic target in ischemia/reperfusion

injury, cardioprotection and neuroprotection. *Pharmacol Ther, 153*, 90-106. doi:10.1016/j.pharmthera.2015.06.005

Skuland, T., Ovrevik, J., Lag, M., Schwarze, P., & Refsnes, M. (2014). Silica nanoparticles induce cytokine responses in lung epithelial cells through activation of a p38/TACE/TGF-alpha/EGFR-pathway and NF-kappaBeta signalling. *Toxicol Appl Pharmacol, 279*(1), 76-86. doi:10.1016/j.taap.2014.05.006

Spannbrucker, T., Ale-Agha, N., Goy, C., Dyballa-Rukes, N., Jakobs, P., Jander, K., Altschmied, J., Unfried, K., & Haendeler, J. (2018). Induction of a senescent like phenotype and loss of gap junctional intercellular communication by carbon nanoparticle exposure of lung epithelial cells. *Exp Gerontol*. doi:10.1016/j.exger.2018.11.017

Stockmann, D., Spannbrucker, T., Ale-Agha, N., Jakobs, P., Goy, C., Dyballa-Rukes, N., Hornstein, T., Kumper, A., Kraegeloh, A., Haendeler, J., & Unfried, K. (2018). Non-Canonical Activation of the Epidermal Growth Factor Receptor by Carbon Nanoparticles. *Nanomaterials (Basel), 8*(4). doi:10.3390/nano8040267

Stöckmann, D., Spannbrucker, T., Ale-Agha, N., Jakobs, P., Goy, C., Dyballa-Rukes, N., Hornstein, T., Kümper, A., Kraegeloh, A., Haendeler, J., & Unfried, K. (2018). Non-Canonical Activation of the Epidermal Growth Factor Receptor by Carbon Nanoparticles. *Nanomaterials, 8*(4), 267.

Sydlik, U., Bierhals, K., Soufi, M., Abel, J., Schins, R. P., & Unfried, K. (2006). Ultrafine carbon particles induce apoptosis and proliferation in rat lung epithelial cells via specific signaling pathways both using EGF-R. *Am J Physiol Lung Cell Mol Physiol, 291*(4), L725-733. doi:10.1152/ajplung.00131.2006

Sydlik, U., Gallitz, I., Albrecht, C., Abel, J., Krutmann, J., & Unfried, K. (2009). The compatible solute ectoine protects against nanoparticle-induced neutrophilic lung inflammation. *Am J Respir Crit Care Med, 180*(1), 29-35. doi:10.1164/rccm.200812-1911OC

Unfried, K., Albrecht, C., Klotz, L.-O., Von Mikecz, A., Grether-Beck, S., & Schins, R. P. F. (2007). Cellular responses to nanoparticles: Target structures and mechanisms. *Nanotoxicology, 1*(1), 52-71. doi:doi:10.1080/00222930701314932

Unfried, K., Kramer, U., Sydlik, U., Autengruber, A., Bilstein, A., Stolz, S., Marini, A., Schikowski, T., Keymel, S., & Krutmann, J. (2016). Reduction of neutrophilic lung inflammation by inhalation of the compatible solute ectoine: a randomized trial with elderly individuals. *Int J Chron Obstruct Pulmon Dis, 11*, 2573-2583. doi:10.2147/COPD.S115061

Unfried, K., Sydlik, U., Bierhals, K., Weissenberg, A., & Abel, J. (2008). Carbon nanoparticle-induced lung epithelial cell proliferation is mediated by receptor-dependent Akt activation. *Am J Physiol Lung Cell Mol Physiol, 294*(2), L358-367. doi:10.1152/ajplung.00323.2007

Weissenberg, A., Sydlik, U., Peuschel, H., Schroeder, P., Schneider, M., Schins, R. P., Abel, J., & Unfried, K. (2010). Reactive oxygen species as mediators of

membrane-dependent signaling induced by ultrafine particles. *Free Radic Biol Med, 49*(4), 597-605. doi:10.1016/j.freeradbiomed.2010.05.011

WHO. (2016). *Ambient air pollution: A global assessment of exposure and burden of disease* (W. H. Organization Ed.): World Health Organisation.

Wilson, M. R., Lightbody, J. H., Donaldson, K., Sales, J., & Stone, V. (2002). Interactions between ultrafine particles and transition metals in vivo and in vitro. *Toxicol Appl Pharmacol, 184*(3), 172-179.

Yao, H., Chung, S., Hwang, J. W., Rajendrasozhan, S., Sundar, I. K., Dean, D. A., McBurney, M. W., Guarente, L., Gu, W., Ronty, M., Kinnula, V. L., & Rahman, I. (2012). SIRT1 protects against emphysema via FOXO3-mediated reduction of premature senescence in mice. *J Clin Invest, 122*(6), 2032-2045. doi:10.1172/JCI60132

Eigene Veröffentlichungen

1. **Non-canonical activation of the epidermal growth factor receptor by carbon nanoparticles**
   Stöckmann D*, **Spannbrucker T***, Ale-Agha N, Jakobs P, Goy C, Dyballa-Rukes N, Hornstein T, Kümper A, Kraegeloh A, Haendeler J, Unfried K
   Nanomaterials. 2018; 8 *Gleichberechtigte Erstautoren

2. **Induction of cellular senescence and loss of gap junctional intercellular communication by carbon nanoparticle exposure of lung epithelial cells**
   Spannbrucker T*, Ale-Agha N*, Goy C, Dyballa-Rukes N, Jakobs P, Altschmied J, Unfried K, Haendeler J
   Exp Gerontol. 2018; *Gleichberechtigte Erstautoren

3. **CDKN1B/p27 is localized in mitochondria and improves respiration-dependent processes in the cardiovascular system – new mode of action for caffeine**
   Ale-Agha N*, Goy C*, Jakobs P*, Spyridopoulos I, Gonnissen S, Dyballa-Rukes N, Aufen- venne K, Von Ameln F, Zurek M, **Spannbrucker T**, Eckermann O, Jakob S, Gorressen S, Abrams M, Grandoch M, Fischer JW, Köhrer K, Deenen R, Unfried K, Altschmied J#, Haendeler J#
   Plos Biology. 2018; *Gleichberechtigte Erstautoren; #Gleichberechtigte Letztautoren

Non-canonical activation of the epidermal growth factor receptor by carbon nanoparticles

Stöckmann D*, **Spannbrucker T***, Ale-Agha N, Jakobs P, Goy C, Dyballa-Rukes N, Hornstein T, Kümper A, Kraegeloh A, Haendeler J, Unfried K

Nanomaterials. 2018; 8, 267 *Gleichberechtigte Erstautoren

Autoren:
Stöckmann D: Erstautor, war an der Planung beteiligt, führte alle Zellexperimente und Datenanalyse durch. Zudem führte er mit Herrn Unfried und Herrn Spannbrucker die Tierexperimente durch.
Spannbrucker T: Erstautor, war an der Planung beteiligt, führte alle Zellexperimente durch. Zudem führte er mit Herrn Unfried und Herrn Stöckmann die Tierexperimente durch.

Ale-Agha N: Führte zusammen mit Herrn Stöckmann Immunfluoreszenzfärbungen durch.

Jakobs P: Führte Immunoblots und deren Datenanalyse durch

Goy C: Führte Immunoblots und deren Datenanalyse durch.

Dyballa-Rukes N: Führte zusammen mit Herrn Spannbrucker und Herrn Stöckmann Immunoblots durch.

Hornstein T: Führte alle FACS Messungen und deren Analysen durch.
Kümper A: Führte Analysen der Partikelsuspensionen zusammen mit Frau Kraegeloh durch.
Kraegeloh A: Führte Analysen der Partikelsuspensionen zusammen mit Herrn Kümper durch.
Haendeler J: War an der Versuchsplanung beteiligt, plante alle Revisionsversuche, schrieb und bearbeitete das Manuskript.
Unfried K: Senior Autor, hatte die Idee zur Studie, war an der Versuchsplanung beteiligt, schrieb und bearbeitete das Manuskript.

nanomaterials

MDPI

Article

Non-Canonical Activation of the Epidermal Growth Factor Receptor by Carbon Nanoparticles

Daniel Stöckmann [1,†], Tim Spannbrucker [1,†], Niloofar Ale-Agha [1], Philipp Jakobs [1], Christine Goy [1], Nadine Dyballa-Rukes [1], Tamara Hornstein [1], Alexander Kümper [2], Annette Kraegeloh [2], Judith Haendeler [1,3] and Klaus Unfried [1,*]

1 IUF—Leibniz-Institut für Umweltmedizinische Forschung, Auf'm Hennekamp 50, 40225 Düsseldorf, Germany; daniel_stoeckmann@email.de (D.S.); Tim.Spannbrucker@IUF-duesseldorf.de (T.S.); Niloofar.ALE-AGHA@uni-duesseldorf.de (N.A.-A.); Philipp.Jakobs@IUF-duesseldorf.de (P.J.); Christine.Goy@IUF-Duesseldorf.de (C.G.); Nadine.Dyballa@uni-duesseldorf.de (N.D.-R.); Tamara.Hornstein@IUF-duesseldorf.de (T.H.); juhae001@uni-duesseldorf.de (J.H.)

2 INM—Leibniz-Institut für Neue Materialien, Campus D2 2, 66123 Saarbrücken, Germany; akuempi@web.de (A.Kü.); Annette.Kraegeloh@leibniz-inm.de (A.Kr.)

3 Medizinische Fakultät, Heinrich-Heine-Universität Düsseldorf, 40225 Düsseldorf, Germany

* Correspondence: klaus.unfried@uni-duesseldorf.de; Tel.: +49-211-3389-362

† Those authors contributed equally to this work.

Received: 25 February 2018; Accepted: 16 April 2018; Published: 23 April 2018

Abstract: The epidermal growth factor receptor (EGFR) is an abundant membrane protein, which is essential for regulating many cellular processes including cell proliferation. In our earlier studies, we observed an activation of the EGFR and subsequent signaling events after the exposure of epithelial cells to carbon nanoparticles. In the current study, we describe molecular mechanisms that allow for discriminating carbon nanoparticle-specific from ligand-dependent receptor activation. Caveolin-1 is a key player that co-localizes with the EGFR upon receptor activation by carbon nanoparticles. This specific process mediated by nanoparticle-induced reactive oxygen species and the accumulation of ceramides in the plasma membrane is not triggered when cells are exposed to non-nano carbon particles or the physiological ligand EGF. The role of caveolae formation was demonstrated by the induction of higher order structures of caveolin-1 and by the inhibition of caveolae formation. Using an in vivo model with genetically modified mice lacking caveolin-1, it was possible to demonstrate that carbon nanoparticles in vivo trigger EGFR downstream signaling cascades via caveolin-1. The identified molecular mechanisms are, therefore, of toxicological relevance for inhaled nanoparticles. However, nanoparticles that are intentionally applied to humans might cause side effects depending on this phenomenon.

Keywords: tyrosine kinase receptor; caveolin-1; airway epithelium; lung inflammation; protein kinase B

1. Introduction

The epidermal growth factor receptor (EGFR) is an omnipresent receptor tyrosine kinase, which can be activated by the binding of specific ligands. It triggers intracellular signaling pathways involved in a plethora of cellular responses to external stimuli including proliferation, apoptosis, and pro-inflammatory reactions. As a functional protein located in the plasma membrane, the EGFR might be affected when cells are intentionally or unintentionally exposed to nanoparticles. Important evidence for an interference of nanoparticles with EGFR signaling comes from toxicological approaches using different kinds of nanoparticles in various experimental systems. Colloidal nanoparticles consisting of gold, silver, or iron oxide were demonstrated to induce changes in EGFR-dependent signaling

and the expression of gene products regulated by this signaling network in a human epithelial cell line [1]. Earlier investigations of lung epithelial cells exposed to pure hydrophobic carbon nanoparticles demonstrated that a proliferative response on this kind of exposure is mediated by the activation of the EGFR [2,3]. These reactions proved to be specific for nanoparticles since non-nano carbon particles failed to induce these reactions.

The molecular mechanism by which nanoparticles interfere with EGFR-signaling are of particular importance for identifying hazards of nanoparticles and for developing safe nanomaterials [4]. EGFR might be activated by natural ligands released by nanoparticle-triggered cell reactions. Evidence for this kind of mechanism comes from studies with an epithelial cell line exposed to different kinds of environmentally relevant particles and amorphous silica nanoparticles [5,6]. The exposure to these xenobiotics appears to activate TACE (tumour necrosis factor-α-converting enzyme), which is able to shed the ectodomain of TGF-α known as a ligand of EGFR. Signaling events, which are crucial for the pro-inflammatory response in these cells, appears to be activated by this pathway of specific ligand binding. However, the receptor might also be activated by rather unspecific cellular stressors, which are described for oxygen radicals [7]. In our earlier studies, we demonstrated that carbon nanoparticles are able to induce oxidative stress in different kinds of cells [8,9]. The intrinsic oxidative capacity of carbon nanoparticles leads to a rapid generation of reactive oxygen species [10]. In this context, we showed that intracellular reactive oxygen species are crucial for activating proliferative EGFR signaling in lung epithelial cells exposed to carbon nanoparticles [9,10]. Involving membrane-linked src-family kinases (SFK) downstream of EGFR, the activation of protein kinase B (Akt) and proliferative and pro-inflammatory mitogen-activated protein kinase (MAPK) signaling pathways were specifically triggered [11,12]. Molecular analyses of the lipid composition of exposed cells demonstrated that exposure to carbon nanoparticles led to an increase of ceramides in lipid raft membrane fractions, which caused the internalization and activation of the EGFR [9]. Interestingly, ceramide-induced receptor activation could be prevented by stabilizing the EGFR in lipid raft fractions of exposed cells. This effect was achieved by adding ectoine, which is an extremolyte known to stabilize the interaction of membrane proteins with the lipid bilayer [13]. Using this intervention strategy, we were able to demonstrate that the pro-inflammatory effects of nanoparticle-induced EGFR signaling are relevant to in vivo experiments in rats and mice [14].

Based on these previous findings, we now ask whether EGFR activation triggered by carbon nanoparticles involves specific non-canonical mechanisms, which can be distinguished from ligand-dependent activation. As Filosto et al. [15] have shown, non-canonical activation of the EGFR by reactive oxygen species is characterized by src family kinase- (SFK-) dependent processes including the generation of ceramides. After canonical ligand binding, no EGFR homodimers are formed. Moreover, activated monomers are internalized by the formation of caveolae and transported to the perinuclear region where they remain relatively stable compared to ligand-activated homodimers which are, after clathrin-dependent internalization, rapidly subjected to lysosomal degradation [16,17]. In this context caveolin-1, a protein involved in many regulatory processes is of particular importance. The oligomerization of caveolin-1 is the main structural event for the formation of caveolae, which is a specific form of endocytotic membrane invaginations. The lipid composition of the plasma membrane appears to have an impact on EGFR activation mediated by caveolin-1. Ganglioside GM3 has been identified as a negative regulator of EGFR by modulating caveolin-1 levels in raft and non-raft regions of the plasma membrane [18]. In our own studies, we observed a rapid dramatic loss of GM3 accompanied by an accumulation of ceramides after exposure of lung epithelial cells to carbon nanoparticles [9].

The current study aimed to identify signaling events triggered by carbon nanoparticles interacting with epithelial cells. Nanoparticle-specific activation of EGFR was investigated in the model system of the lung epithelium. Using an alveolar type II-derived epithelial cell line (RLE-6TN), we aimed to discriminate non-canonical events from ligand-dependent receptor activation. As a possible mediator of non-canonical EGFR activation, the role of caveolin-1 in lung epithelial cells in vitro

and in vivo was investigated. By comparing molecular events triggered by carbon nanoparticles and the natural ligand of EGFR, the epidermal growth factor (EGF), which is the importance of non-canonical EGFR activation, was elucidated. Employing different kinds of intervention strategies including pharmacological inhibitors also knock out animals for caveolin-1. The relevance of these molecular events was documented.

2. Results

2.1. Particle Characterization

Particles used in this study consist of aciniform, which is an elemental carbon. Carbon nanoparticles (CNP) as well as (non-nano) carbon particles (CP) were characterized for physical properties by using transmission electron microscopy and dynamic light scattering, which was described in the material and methods section and in an earlier publication [19]. Results are shown in Figure S1 and Table S1 in Supplementary Materials.

2.2. Caveolin-1 Is Involved in EGFR Activation after Carbon Nanoparticle Exposure

In the first set of experiments, we aimed to identify signaling events, which allow us to discriminate non-canonical EGFR activation by carbon nanoparticles from ligand-dependent activation. Therefore, the role of caveolin-1 as a potential mediator of these events was investigated in a well characterized rat lung epithelial cell line [20]. Analyses of subcellular localization of EGFR and caveolin-1 were performed by fluorescence microscopy with specific antibodies. Cells either exposed to suspensions of carbon nanoparticles (10 $\mu g/cm^2$) or to EGF as the natural ligand were compared. Earlier, we demonstrated that ceramides are accumulated in the cell membrane after exposure to carbon nanoparticles. Therefore, ceramide (C6) was applied in order to evaluate the role of this nanoparticle-specific event for non-canonical EGFR activation [9]. After five minutes of exposure, all three stimuli led to a translocation of the EGFR from the plasma membrane into the cytoplasm, which is considered a feature of receptor activation (see Figure 1A). Simultaneously, intracellular caveolin-1 accumulation occurred after exposure to carbon nanoparticles and ceramide but not after EGF application. The co-localization of EGFR and caveolin-1 in the cytoplasm of the cells is visualized by the yellow signals in the merge of the images. The co-localization of EGFR and caveolin-1 was only observed after particle and ceramide exposure but not in the presence of the natural ligand EGF. Therefore, the intracellular accumulation of caveolin-1 and its co-translocation with the EGFR can be considered a specific feature that allows to discriminate ligand-dependent from non-canonical receptor activation.

In order to verify the specificity of the observed reactions, a number of molecular events identified earlier to be involved in nanoparticle-specific activation of signaling pathways were investigated by using intervention approaches. Src family kinases (SFK) were inhibited by the pharmacological inhibitor PP2, which specifically and dose dependently diminish downstream signaling [12]. The preventive application of 1 mM ectoine is considered to stabilize EGFR membrane interaction and inhibit the activation and internalization of the receptor. The influence of reactive oxygen species was counteracted by pre-treating the cells with α-tocopherol. Filipin III was used a cholesterol-depleting substance, which is known to prevent the formation of caveolae. All these intervention approaches reduced the internalization and co-localization of EGFR and caveolin-1 after carbon nanoparticle exposure (see Figure 1B). EGF-dependent receptor activation was not influenced by these interventions. From these data points, we can conclude that formation of reactive oxygen species, activation of SFK and structural changes of the membrane including the formation of caveolae are essential components of non-canonical EGFR activation by carbon nanoparticles.

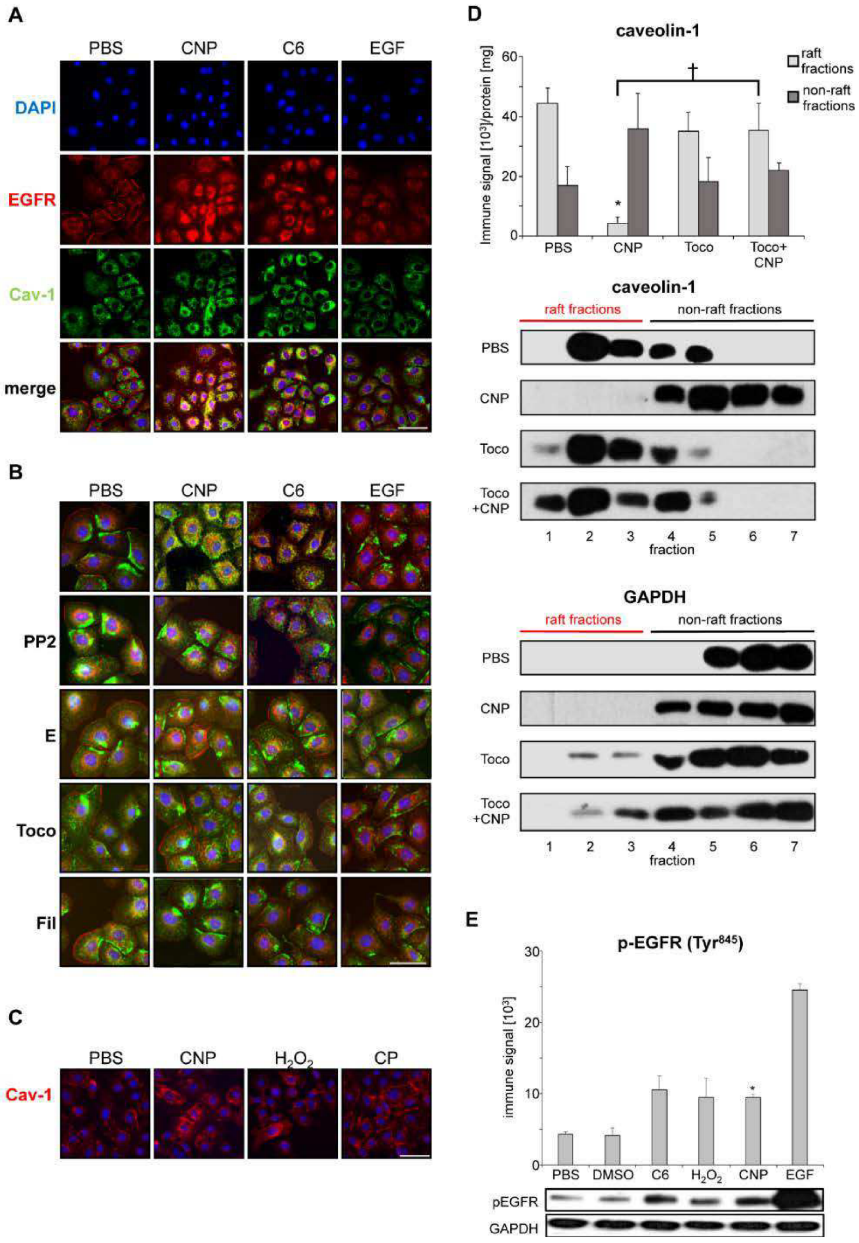

Figure 1. Caveolin-1 and EGFR co-localization as a feature of non-canonical EGFR activation. Epithelial cells (RLE-6TN) were exposed (5 min) to carbon nanoparticles (CNP), non-nano carbon particles (CP), each 10 μg/cm^2, (50 μM) H_2O_2, (5 μM) C6 ceramide, or EGF (100 ng/mL), respectively. (**A**) Subcellular localization of EGFR (red Alexa flour 594) and caveolin-1 (green Alexa flour 488). Co-localization is visualized by the yellow color in merged images; (**B**) Subcellular localization of EGFR and caveolin-1 in cells pre-treated with inhibitors of carbon nanoparticle-specific signaling prior to particle or EGF exposure: SFK inhibitor PP2 (10 μM), 1 mM ectoine (**E**), 75 μM α-tocopherol (Toco), and 1 μg/mL filipin III (Fil). Co-localization is visualized by the yellow color in merged images; (**C**) Subcellular localization of caveolin-1 (red Alexa fluor 594) after exposure to carbon nanoparticles (CNP), carbon particles (CP), or hydrogen peroxide (H_2O_2); (**D**) Quantification and representative Western blots of caveolin-1 in lipid raft fraction of RLE-6TN cells exposed to CNP (10 μg/cm^2). Raft and non-raft fraction were isolated from density gradients after ultracentrifugation. Pre-treatment of cells with α-tocopherol (Toco) was applied as an antioxidant strategy. GAPDH was used as a control protein not associated with lipid rafts. The bars in the graph represent the additive immune signals of raft and non-raft fractions, which was indicated in the representative original Western blots; (**E**) Quantification and representative Western-blot of EGFR phosphorylation at Tyr^{845}. Nuclei were stained with DAPI (blue). Scale bars represent 20 μm; *, which was significantly different to PBS control ($p < 0.05$); †, significantly different from CNP alone ($p < 0.05$).

The specificity of the translocation of caveolin-1 from the plasma membrane to the cytoplasm induced by carbon nanoparticles was tested by applying particulate and non-particulate control substances (see Figure 1C). The relevance of reactive oxygen species for signal induction was demonstrated by the translocation of caveolin-1 in cells exposed to hydrogen peroxide (50 µM). Non-nano carbon particles (CP) with a primary size of >200 nm (see supplementary files for particle characterization) were not able to trigger the specific signaling events. In our earlier studies, we were able to show that these particles at equal mass doses are not able to trigger EGFR translocation and activation as well as subsequent signaling steps and endpoints [3,9,12]. Dose response experiments suggest that this effect is linked to the considerably reduced surface area of the bigger particles compared to the nanoparticles of equal mass.

The activation of the EGFR by carbon nanoparticles is associated with the shift of the receptor molecule from detergent-resistant lipid rafts to non-raft membrane compartments that can be separated by density centrifugation [21]. We investigated whether caveolin-1 behaves similarly to EGFR in these kind of analyses. Western-blot analyses of density gradient fractions reveal that, after exposure to carbon nanoparticles caveolin-1, EGFR is shifted from the raft to the non-raft fractions (see Figure 1D). This effect could be prevented by the pre-treatment of the cells with the antioxidant α-tocopherol.

As proof of principle that co-localization and translocation of both proteins reflect receptor activation, the activating phosphorylation of the EGFR under the chosen experimental conditions has to be demonstrated. In earlier studies, we demonstrated that Tyr^{1173} phosphorylation as a marker of EGFR autophosphorylation is triggered by carbon nanoparticles through reactive oxygen species and ceramide accumulation [9]. We now tested the phosphorylation status of the receptor at Tyr^{845}. This SFK-dependent phosphorylation has been described to be crucial for kinase activity of the EGFR [22–24]. Figure 1E demonstrates that conditions under which intracellular co-localization of caveolin-1 and EGFR occurs, the amount of EGFR that is phosphorylated at Tyr^{845} is significantly increased. A similar reaction was observed when EGF was applied as a positive control.

2.3. Carbon Nanoparticles Induce Higher Order Structures of Caveolin-1

The formation of caveolae is accomplished by structural organization of caveolin molecules [25]. Oligomerization of caveolin-1 as well as its interaction with other structural proteins like cavins is an essential pre-requisite of caveolar invaginations [26]. As the application of filipin III inhibited EGFR translocation after carbon nanoparticle exposure (see Figure 1B), the formation of caveolae might be a critical step in non-canonical EGFR activation. Protein interactions can be observed by crosslinking proteins in intact cells, by applying the membrane permeable substance DSP (dithiobis-succimidylpropionate), and through subsequent protein analysis [27]. In order to test whether caveolae formation is involved in carbon nanoparticle-induced signaling processes, we quantified the formation of high molecular weight protein structures (>350 kDa) containing caveolin-1 under different exposure conditions (see Figure 2). In semi-quantitative Western-Blot analyses, we were able to demonstrate that treatment of the cells with carbon nanoparticles as well as with C6 ceramide led to an increase in high molecular weight caveolin-1 protein complexes while the treatment with EGF failed to induce this reaction (see Figure 2A). Increasing the antioxidant capacity of the cells by applying *N*-acetylcysteine as well as by adding the membrane-coupled antioxidant α-tocopherol, both reduced the amount of caveolin-1 protein complexes significantly (see Figure 2B,C). As expected, filipin III as an inhibitor of caveolae formation prevented the carbon nanoparticle-induced caveolin-1 protein complexes (see Figure 2D). These data strongly suggest that internalization of EGFR after carbon nanoparticle exposure of lung epithelial cells depends on the formation of caveolae.

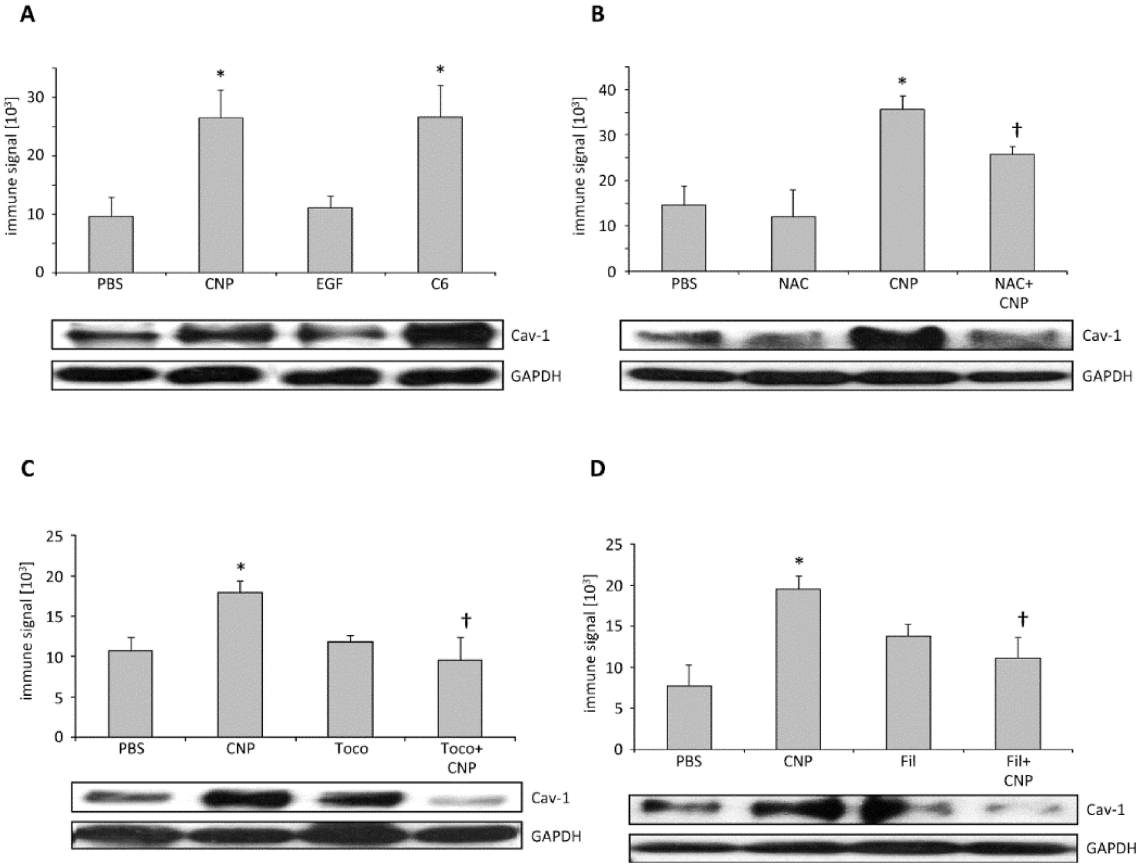

Figure 2. Caveolin-1 protein complexes in dithiobis-succimidylpropionate (DSP)-cross-linked protein extracts. After exposure RLE-6TN cells were treated with DSP (1 mM, 1 h at 4 °C) to stabilize higher order caveolin-1 structures to be detectable by Western blotting. Means and standard errors as well as representative Western-blots are depicted. (**A**) Cells were exposed (5 min) to CNP (10 μg/cm^2), EGF (100 ng/mL), or C6 ceramide (5 μM). Cell were pre-treated with (18 h) *N*-acetylcysteine (NAC, 1 mM); (**B**), or 1 h with α-tocopherol (Toco, 75 μM) (**C**), or filipin III (Fil, 1 μg/mL) (**D**). *, significantly different to PBS control ($p < 0.05$). †, significantly different from CNP alone ($p < 0.05$).

2.4. Non-Canonical EGFR Activation In Vivo

The activation of MAPK signaling pathways via EGFR was identified as a specific mechanism by which carbon nanoparticles induce endpoints like proliferation, apoptosis, and pro-inflammatory responses in lung epithelial cells [3,28]. The in vivo relevance of this cellular reaction was earlier demonstrated in the lungs of animals exposed to carbon nanoparticles [29]. Investigations of signaling events after particle exposure demonstrated that the activation of the MAPK Erk1/2 and protein kinase B (Akt) are mediated by EGFR activation [11]. These EGFR-specific signaling pathways allowed us to test the relevance of caveolin-1-dependent EGFR activation in vivo. The specific appearance of phosphorylated forms of Erk1/2 and Akt was used as an indicator of non-canonical EGFR activation in vivo. The application of carbon nanoparticles in the lungs of animals is a well-established experimental system in which the specific interaction of nanoparticles with the airway epithelium can be investigated. Signaling events triggered by the particles as well as physiological reactions can be studied in tissue samples. The use of animals that lack the caveolin-1 gene due to genetic modification tested the relevance of non-canonical EGFR activation via caveolin-1 in vivo [30]. We, therefore, employed the system of pharyngeal aspiration of carbon nanoparticles (2.5 mg/kg) in the lungs of caveolin-1 knock out mice and their wild type littermates. The induction of signaling events was investigated 6 h after exposure (see Figure 3). At this time point after exposure, signaling events in

lung epithelial cells are activated while inflammatory responses are still not at the peak. As described earlier, lungs of caveolin-1 deficient animals show morphological changes [30]. In hematoxilin eosin (HE) stained lung sections of these animals, we observed a mild phenotype of slightly thickened septa (see Figure 3A). Lung sections immuno-stained for caveolin-1 clearly show that this protein is present in wild type littermates. EGFR as well as the phosphorylated forms of Akt an Erk1/2 were detectable in lung epithelial cells. Exposure of WT-animals appeared to increase the activating phosphorylation of Akt and Erk1/2 while this reaction was not observed in exposed knock out animals. In order to verify this finding, the amount of phosphorylated signaling proteins was determined in protein preparations from lung homogenates. In these semi-quantitative analyses, the levels of phosphorylated Akt (see Figure 3B) and phosphorylated Erk1/2 (see Figure 3C) in relation to the respective amounts of total protein was elevated only in exposed WT animals. In animals lacking caveolin-1, both proteins were not activated after exposure to carbon nanoparticles.

The lack of caveolin-dependent activation of the Akt Erk1/2 signaling cascade is also obvious at the level of the inflammatory response in the lungs triggered by the nanoparticles. Neutrophilic granulocytes and macrophages as the major inflammatory cells were determined in lung lavages of exposed mice (see Figure 3D). In earlier studies, we were able to demonstrate that membrane-dependent signaling in lung epithelial cells is a major driver of neutrophil recruitment in the lung after particle exposure [14]. Accordingly, we now observed that the impairment of non-canonical EGFR activation in caveolin-1 deficient mice led to a marked reduction of this pro-inflammatory response. At the level of macrophages, such effects are not observed at this early time point after exposure. Caveolin-1 knock-out mice appear to have elevated macrophage numbers. This phenomenon appears not to influence the inflammatory response on nanoparticles. The results of the animal experiments demonstrate that carbon nanoparticles are able to address non-canonical EGFR activation via caveolin-1 in epithelial cells in vivo. However, the relevance of these signaling events in lung epithelial cells for nanoparticle-induced lung inflammation as a possible health effect of inhaled nanoparticles in humans is documented.

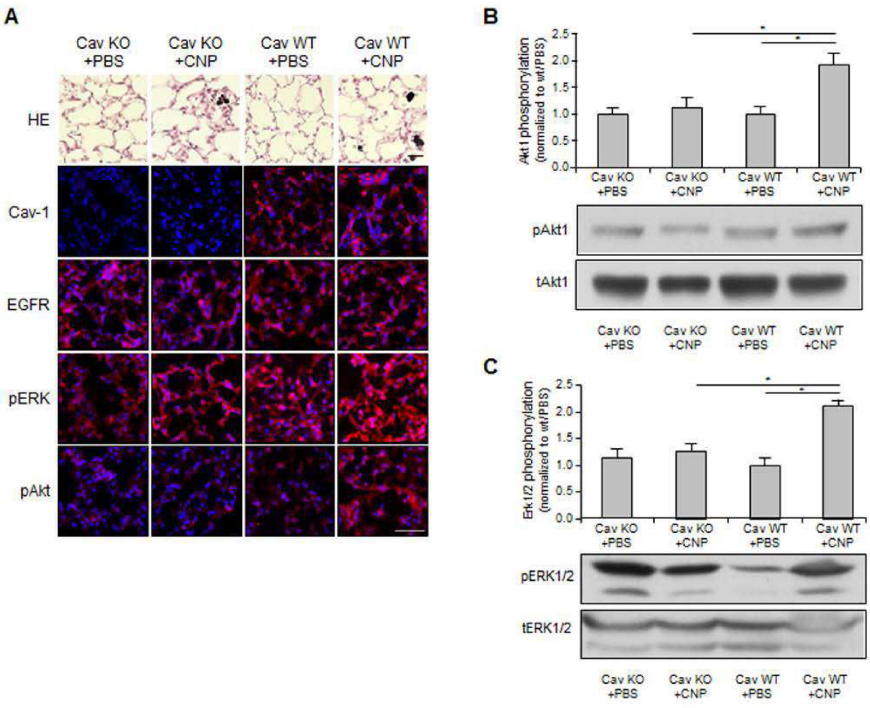

Figure 3. *Cont.*

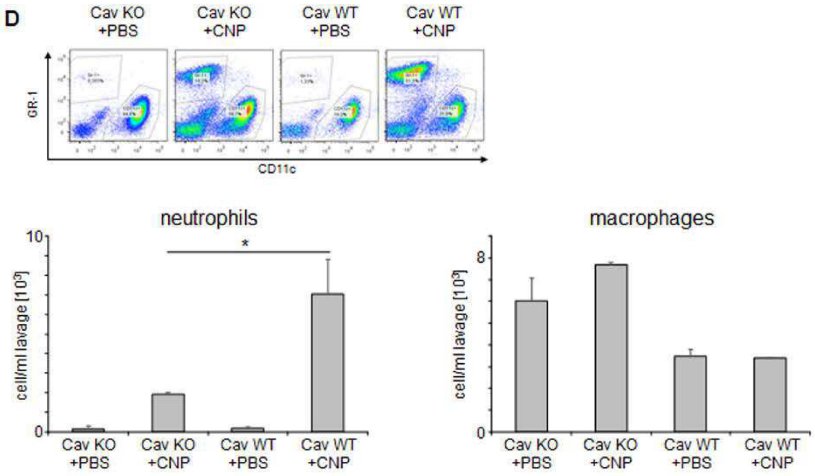

Figure 3. Non-canonical EGFR signaling in vivo. Caveolin-1 knock-out mice and their wild type littermates were exposed to carbon nanoparticles (CNP, 2.5 mg/kg) (or saline as control) by pharyngeal aspiration. Six hours after this single exposure, animals were sacrificed and subjected to bronchoalveolar lavage (BAL) followed by lung tissue preparation. (**A**) Immunohistochemistry from frozen sections of lung tissue. Lungs were either stained with Hematoxilin/Eosin (HE) or immunostained (red) for caveolin-1 (Cav-1), EGFR, phosphorylated Erk1/2 (pERK), or phosphorylated Akt (pAkt) and counterstained with DAPI (blue); (**B**) Relative phosphorylation of Akt in lung homogenates of animals were exposed as indicated. Means and standard errors of immune signals of phosphorylated Akt relative to total Akt and representative Western-blots; (**C**) Relative phosphorylation of Erk1/2 in lung homogenates of animals was exposed as indicated. Means and standard errors of immune signals of phosphorylated Erk1/2 relative to total Erk1/2 and representative Western-blots; (**D**) Flow cytometric analyses of lung lavages with respect to inflammatory cells. GR-1 positive cells (neutrophils) and CD11c positive cells (macrophages) were quantified per mL lung lavage. Scale bars represent 50 µm. *, significantly different from untreated control ($p < 0.05$).

3. Discussion

The presented data demonstrate that EGFR is an important regulator of cellular functions and tissue homeostasis, which can be activated by carbon nanoparticles in epithelial cells via a non-canonical mechanism. This depends on caveolin-1. The induction of higher order structures built by caveolin-1 after carbon nanoparticle exposure and the suppressive effect of the inhibitor filipin III indicate that the formation of caveolae is a critical step involved in these cellular reactions. Our earlier studies identified Akt as a key signaling enzyme downstream of EGFR, which is also responsible for activating MAP-kinases Erk1/2 after nanoparticle exposure [11]. The in vivo experiments demonstrate that this specific signaling cascade, which is responsible for regulating epithelial tissue homeostasis and pro-inflammatory reactions in lungs exposed to nanoparticles depends on the structural protein caveolin-1. Furthermore, the inhibitor experiments demonstrate that signaling events upstream of EGFR activation include the generation of reactive oxygen species and the accumulation of ceramides in lipid raft membrane fractions, which we earlier identified as specific for the interaction of carbon nanoparticles with lung epithelial cells, are causative for the non-canonical activation of the EGFR.

Carbon nanoparticles can be considered model particles for combustion-derived environmental nanoparticles [31]. The inhalation of these particles has been linked to many pathological endpoints including neutrophilic lung inflammation and chronic obstructive pulmonary disease (COPD). Recent investigations have shown that lung epithelial cells are the most relevant cell type for the induction of neutrophilic lung inflammation triggered by carbon nanoparticles [32]. As the current data clearly demonstrate the link between non-canonical EGFR activation in this cell type and neutrophilic lung

inflammation, the induction of this pathway may be considered as a measure for the toxicity of inhaled particles.

Besides toxicologically relevant incidents, carbon nanoparticles as well as other poorly soluble particles might be intentionally applied to the human body. There are a number of strategies that aim to employ carbon-based nanomaterials for diagnostic and therapeutic approaches in humans [33–35]. To our knowledge, a possible interference of these strategies with EGFR signaling is usually not tested. However, nanoparticle-based approaches that aim to suppress EGFR activity, like in tumor therapy, might have the side effect of an activation of this receptor pathway. Our in vivo findings indicate that these nanoparticle-specific effects can occur in vivo and can lead to physiological responses. Yet, there are applications in which the activation of membrane receptor kinases is wanted such as in regenerative therapy [36]. Recent developments of drug delivery systems aim to use nanoparticles for the application of growth factors among therapeutic targets [37]. By choosing appropriate carrier nanoparticles, non-canonical activation of EGFR and possibly other membrane receptor kinases could increase the effectivity of such therapeutic approaches.

4. Materials and Methods

4.1. Reagents

Carbon nanoparticles (CNP Printex 90, Degussa, Essen, Germany) and carbon particles (H. Haeffner, Chepstow, UK) were used for exposure experiments suspended in phosphate buffered saline (PBS). Particle characteristics as well as characteristics of the suspensions were determined as described earlier [19]. Physicochemical characteristics as well as methods of characterization are provided in the supplementary file.

4.2. Cell Culture and Exposure

RLE-6TN cells (ATCC, Manassas, VA, USA) were cultured as described earlier [3]. Cells grown to a confluence of 70–80% were used for exposure experiments. In order to discriminate exposure effects from serum-induced reactions, cells were kept at low serum conditions (0.5% fetal calf serum) for 20 h. Immediate early reactions of particle cell interaction were monitored five minutes after exposure to particle concentrations of 10 $\mu g/cm^2$, which proved to be a relevant exposure dose that does not induce cytotoxicity, according to our earlier studies [3].

Inhibitors were added to the cells at 18 h (NAC (1 mM)), 4 h (ectoine (1 mM)), or 60 min with alpha-tocopherol (75 Mm), PP2 (10 μM), and filipin III (1 μg/mL) [38] prior to treatment with CNP (10 $\mu g/cm^2$), CP (10 $\mu g/cm^2$), C6-ceramide (5 μM), H_2O_2 (50 μM), or EGF (100 ng/mL). EGF (R&D Systems, Abingdon, UK) and ectoine ((*S*)-2-methyl-1,4,5,6-tetrahydropyrimidine-4-carboxylic acid, LPS-free, ultrapure 99%, bitop AG, Witten, Germany) were solubilized in sterile PBS. Filipin III (from *Streptomyces filipinensis*, Sigma-Aldrich Chemie, Schnelldorf, Germany), PP2 (Calbiochem, Schwalbach, Germany), and DSP (dithiobis-succimidylpropionate, Thermo Scientific, Waltham, MA, USA) were solubilized in DMSO (dimethyl sulfoxide) and diluted in PBS to the indicated concentrations. α-tocopherol (D-alpha-tocopherol succinate, semi-synthetic, Sigma-Aldrich Chemie, Schnelldorf, Germany) was solubilized in ethanol and further diluted in PBS before use. In experiments using these compounds, respective vehicle controls were performed. The effect of DMSO on lipid raft composition was investigated as described before [9]. DMSO treated samples showed no difference to PBS treated samples.

4.3. Protein Isolation

The cells were lysed on ice in modified radio immunoprecipitation assay buffer (25 mM Tris-Cl pH 7.4, 150 mM NaCl, 0.1 mM EDTA, 1% Nonidet P-40, 0.1% SDS, 1% deoxycholate, 0.025% NaN_3, 1% protease inhibitor cocktail, 1% phosphatase inhibitor cocktail (both inhibitor cocktails from Sigma)), which was described in Reference [39]. Protein crosslinking by dithiobis-succimidylpropionate (DSP)

was performed as described [27]. Cells were rapidly cooled to 4 °C prior to 1 h incubation with DSP (1 mM) at 4 °C. Crosslinking was stopped by adding 1 M Tris/HCl pH 7.4 (15 mM) prior to protein preparation. Afterwards, proteins were isolated as described above. Detergent resistant membrane raft fractions were isolated and detected as described earlier in Reference [9]. Cells were mechanically disrupted and treated with Triton X-100 (4-(1,1,3,3-tetramethylbutyl)phenyl-polyethylene glycol, 1%). Raft and non-raft fractions were collected from density gradients after ultracentrifugation. Raft fractions were identified by the presence of the raft marker ganglioside GM1 in dot blot assays, as described [9].

4.4. Protein Analyses

Western blotting was performed as described earlier [9]. Equal amounts of total cell protein (5–40 µg) were separated by using SDS-PAGE (7.5% or 10%) and transferred onto PVDF membranes (Hybond-P, Amersham Biosciences, Little Chalfont, UK). DSP-cross-linked caveolin-1 protein complexes were separated on 5% PAGE gels [26]. Unless otherwise stated, all antibodies were from Cell Signaling Technology (Danvers, MA, USA). The antibodies used include caveolin-1 (Upstate Biotechnology, Lake Placid, NY, USA), phospho-EGFR (Tyr^{845}), Akt, phospho-Akt (Ser^{473}), p44/42 MAPK, phospho-p44/42 MAPK (Thr^{202}/Tyr^{204}), and GAPDH (Imgenex Corp., San Diego, CA, USA). Signal strength was detected using the ECL Plus Western Blotting Detection System (Bio-Rad, Hercules, CA, USA). Band intensities from X-ray films (immune signal) were used for statistical calculations. The depicted graphs show either absolute immune signals (high molecular caveolin-1 complexes, EGFR $pTyr^{845}$) or signals relative to the respective total proteins (Erk1/2, Akt).

4.5. Immunostaining

Cells were treated with 4% paraformaldehyde (20 minutes, room temperature). Permeabilisation and blocking was achieved by incubation with 3% bovine serum albumin and 0.3% Triton X-100 in PBS. Slides were incubated with primary antibodies (1:50) overnight at 4 °C, Akt, phospho-Akt (Ser^{473}), Erk1/2, phospho-p44/42 MAPK (Thr^{202}/Tyr^{204}) (Imgenex Corp., San Diego, CA, USA). After 1 h of incubation with secondary antibodies (Alexa Fluor 594 or Alexa Fluor 488, 1:800 or 1:500; Invitrogen, Darmstadt, Germany), nuclei were counterstained by mounting with prolonged gold anti-fade mounting medium with DAPI (1:2000, Invitrogen). Cells were visualized using an Axiovert 200M microscope using (Zeiss, Jena, Germany, 400-fold enlargement, under oil). As control for the specificity of the reactions, mock immunostainings without primary antibodies were performed.

4.6. Animal Experiments

All animal experiments were approved by the local authorities in accordance with the German animal welfare legislation. Caveolin-1 knock-out mice [30] were generated by the group of T. Kurzchalia (Dresden, Germany). Knock-out and wild type mice were obtained by mating of heterozygous animals. Littermates either homozygous knock-out or wild type were used. Adult animals of both sexes were exposed as described earlier [19] by single pharyngeal aspiration of particle solutions (n = 4) or PBS (n = 3). Animals were sacrificed six hours after exposure. Broncho alveolar lavage was prepared from each lung. Lung tissue was sampled for histopathology. Lung sections (4–6 µm) were made from cryo-preserved lung tissue. Immunostainings were performed with the respective antibodies and fluorescent secondary antibodies, which were followed by embedding the sections in mounting medium that contains DAPI. Parallel sections were stained with hematoxylin/eosin. Immunostainings were analyzed microscopically. As a control for the specificity of the reactions, mock immunostainings without primary antibodies were performed. For semi-quantitative analyses of signaling proteins, tissue samples from two independent animal experiments were used (PBS n = 4–5, CNP n = 7–8).

Broncho alveolar lavages were subjected to differential cell counting. Inflammatory cells were discriminated by flow cytometry by employing a FACScanto II Flow Cytometer (BD Bioscience, BD

Bioscience, Franklyn Lake, NJ, USA). Data were analyzed using FlowJo 7.6.5 software. Fluorescently labelled CD11c (N418) and GR-1 (RB6-8C5) (both BioLegend San Diego, CA, USA) were used to monitor changes in the inflammatory status of the lungs, which are reflected by shifts in the percentages of macrophages and neutrophils.

4.7. Statistical Analyses

For statistical analyses, one-way ANOVA followed by Bonferroni post hoc testing was performed using IBM SPSS statistics 22 (IBM Corp., Armonk, NY, USA). Results from Western-blot analyses of phosphorylated proteins were tested for statistical significance with Mann-Whitney U test. The sample size of the animal experiment was determined by power calculation using G*Power 3.1.9.2. Unless not otherwise stated, all experiments were performed as three independent replicates. Differences were considered as significant when $p < 0.05$. Bar graphs show means ± SEM.

Supplementary Materials: The following are available online at http://www.mdpi.com/2079-4991/8/4/267/s1, Figure S1: Transmission elecron micrograph of CP after drying a particle suspension (H_2O) on a holey carbon film, Table S1: Physical characteristics of CNP suspension in PBS.

Acknowledgments: The research was funded by Deutsche Forschungsgemeinschaft: individual grants UN110/4-1 and HA 2868/11-1 as well as from Research Training Group 1427). P.J. is fellowship holder in the International Research Training Group 1902. The authors acknowledge support of their work at INM and IUF in the frame of the Leibniz Research Alliance Nanosafety. The excellent technical assistance of Petra Groß, Tracy Klitz, and Winfried Brock is gratefully acknowledged.

Author Contributions: D.S. and T.S. conducted all cell experiments and analyses. Both contributed to the design of the experiments. N.A.-A. and D.S. performed immunostainings and histology. P.J., C.G., T.S., and N.D.-R. performed Western-blots, A.Kü. and A.Kr. performed analyses of particle suspensions. K.U., D.S., T.S., and T.H. performed animal experiments and subsequent analyses. J.H. and K.U. designed experiments and wrote and edited the manuscript.

Conflicts of Interest: The authors declare no conflict of interest.

References

1. Comfort, K.K.; Maurer, E.I.; Braydich-Stolle, L.K.; Hussain, S.M. Interference of silver, gold, and iron oxide nanoparticles on epidermal growth factor signal transduction in epithelial cells. *ACS Nano* **2011**, *5*, 10000–10008. [CrossRef] [PubMed]
2. Tamaoki, J.; Isono, K.; Takeyama, K.; Tagaya, E.; Nakata, J.; Nagai, A. Ultrafine carbon black particles stimulate proliferation of human airway epithelium via egf receptor-mediated signaling pathway. *Am. J. Physiol. Lung Cell. Mol. Physiol.* **2004**, *287*, L1127–L1133. [CrossRef] [PubMed]
3. Sydlik, U.; Bierhals, K.; Soufi, M.; Abel, J.; Schins, R.P.; Unfried, K. Ultrafine carbon particles induce apoptosis and proliferation in rat lung epithelial cells via specific signaling pathways both using egf-r. *Am. J. Physiol. Lung Cell. Mol. Physiol.* **2006**, *291*, L725–L733. [CrossRef] [PubMed]
4. Unfried, K.; Albrecht, C.; Klotz, L.-O.; Von Mikecz, A.; Grether-Beck, S.; Schins, R.P.F. Cellular responses to nanoparticles: Target structures and mechanisms. *Nanotoxicology* **2007**, *1*, 52–71. [CrossRef]
5. Ovrevik, J.; Refsnes, M.; Totlandsdal, A.I.; Holme, J.A.; Schwarze, P.E.; Lag, M. TACE/TGF-alpha/EGFR regulates CXCL8 in bronchial epithelial cells exposed to particulate matter components. *Eur. Respir. J.* **2011**, *38*, 1189–1199. [CrossRef] [PubMed]
6. Skuland, T.; Ovrevik, J.; Lag, M.; Schwarze, P.; Refsnes, M. Silica nanoparticles induce cytokine responses in lung epithelial cells through activation of a p38/TACE/TGF-alpha/EGFR-pathway and NF-kappabeta signalling. *Toxicol. Appl. Pharmacol.* **2014**, *279*, 76–86. [CrossRef] [PubMed]
7. Goldkorn, T.; Balaban, N.; Matsukuma, K.; Chea, V.; Gould, R.; Last, J.; Chan, C.; Chavez, C. EGF-receptor phosphorylation and signaling are targeted by H_2O_2 redox stress. *Am. J. Respir. Cell Mol. Biol.* **1998**, *19*, 786–798. [CrossRef] [PubMed]
8. Buchner, N.; Ale-Agha, N.; Jakob, S.; Sydlik, U.; Kunze, K.; Unfried, K.; Altschmied, J.; Haendeler, J. Unhealthy diet and ultrafine carbon black particles induce senescence and disease associated phenotypic changes. *Exp. Gerontol.* **2013**, *48*, 8–16. [CrossRef] [PubMed]

9. Peuschel, H.; Sydlik, U.; Grether-Beck, S.; Felsner, I.; Stockmann, D.; Jakob, S.; Kroker, M.; Haendeler, J.; Gotic, M.; Bieschke, C.; et al. Carbon nanoparticles induce ceramide- and lipid raft-dependent signalling in lung epithelial cells: A target for a preventive strategy against environmentally-induced lung inflammation. *Part. Fibre Toxicol.* **2012**, *9*, 48. [CrossRef] [PubMed]
10. Weissenberg, A.; Sydlik, U.; Peuschel, H.; Schroeder, P.; Schneider, M.; Schins, R.P.; Abel, J.; Unfried, K. Reactive oxygen species as mediators of membrane-dependent signaling induced by ultrafine particles. *Free Radic. Biol. Med.* **2010**, *49*, 597–605. [CrossRef] [PubMed]
11. Unfried, K.; Sydlik, U.; Bierhals, K.; Weissenberg, A.; Abel, J. Carbon nanoparticle-induced lung epithelial cell proliferation is mediated by receptor-dependent akt activation. *Am. J. Physiol. Lung Cell. Mol. Physiol.* **2008**, *294*, L358–L367. [CrossRef] [PubMed]
12. Peuschel, H.; Sydlik, U.; Haendeler, J.; Buchner, N.; Stockmann, D.; Kroker, M.; Wirth, R.; Brock, W.; Unfried, K. C-SRC-mediated activation of ERK1/2 is a reaction of epithelial cells to carbon nanoparticle treatment and may be a target for a molecular preventive strategy. *Biol. Chem.* **2010**, *391*, 1327–1332. [CrossRef] [PubMed]
13. Roychoudhury, A.; Haussinger, D.; Oesterhelt, F. Effect of the compatible solute ectoine on the stability of the membrane proteins. *Protein Pept. Lett.* **2012**, *19*, 791–794. [CrossRef] [PubMed]
14. Sydlik, U.; Gallitz, I.; Albrecht, C.; Abel, J.; Krutmann, J.; Unfried, K. The compatible solute ectoine protects against nanoparticle-induced neutrophilic lung inflammation. *Am. J. Respir. Crit. Care Med.* **2009**, *180*, 29–35. [CrossRef] [PubMed]
15. Filosto, S.; Khan, E.M.; Tognon, E.; Becker, C.; Ashfaq, M.; Ravid, T.; Goldkorn, T. Egf receptor exposed to oxidative stress acquires abnormal phosphorylation and aberrant activated conformation that impairs canonical dimerization. *PLoS ONE* **2011**, *6*, e23240. [CrossRef] [PubMed]
16. Goldkorn, T.; Filosto, S.; Chung, S. Lung injury and lung cancer caused by cigarette smoke-induced oxidative stress: Molecular mechanisms and therapeutic opportunities involving the ceramide-generating machinery and epidermal growth factor receptor. *Antioxid. Redox Signal.* **2014**, *21*, 2149–2174. [CrossRef] [PubMed]
17. Balbis, A.; Parmar, A.; Wang, Y.; Baquiran, G.; Posner, B.I. Compartmentalization of signaling-competent epidermal growth factor receptors in endosomes. *Endocrinology* **2007**, *148*, 2944–2954. [CrossRef] [PubMed]
18. Wang, X.Q.; Sun, P.; Paller, A.S. Ganglioside induces caveolin-1 redistribution and interaction with the epidermal growth factor receptor. *J. Biol. Chem.* **2002**, *277*, 47028–47034. [CrossRef] [PubMed]
19. Kroker, M.; Sydlik, U.; Autengruber, A.; Cavelius, C.; Weighardt, H.; Kraegeloh, A.; Unfried, K. Preventing carbon nanoparticle-induced lung inflammation reduces antigen-specific sensitization and subsequent allergic reactions in a mouse model. *Part. Fibre Toxicol.* **2015**, *12*, 20. [CrossRef] [PubMed]
20. Driscoll, K.E.; Carter, J.M.; Iype, P.T.; Kumari, H.L.; Crosby, L.L.; Aardema, M.J.; Isfort, R.J.; Cody, D.; Chestnut, M.H.; Burns, J.L.; et al. Establishment of immortalized alveolar type II epithelial cell lines from adult rats. *Cell. Dev. Biol. Anim.* **1995**, *31*, 516–527. [CrossRef]
21. Mineo, C.; Gill, G.N.; Anderson, R.G. Regulated migration of epidermal growth factor receptor from caveolae. *J. Biol. Chem.* **1999**, *274*, 30636–30643. [CrossRef] [PubMed]
22. Wu, W.; Graves, L.M.; Gill, G.N.; Parsons, S.J.; Samet, J.M. Src-dependent phosphorylation of the epidermal growth factor receptor on tyrosine 845 is required for zinc-induced ras activation. *J. Biol. Chem.* **2002**, *277*, 24252–24257. [CrossRef] [PubMed]
23. Wu, W.; Wages, P.A.; Devlin, R.B.; Diaz-Sanchez, D.; Peden, D.B.; Samet, J.M. SRC-mediated EGF receptor activation regulates ozone-induced interleukin 8 expression in human bronchial epithelial cells. *Environ. Health Perspect.* **2015**, *123*, 231–236. [CrossRef] [PubMed]
24. Mueller, K.L.; Powell, K.; Madden, J.M.; Eblen, S.T.; Boerner, J.L. EGFR tyrosine 845 phosphorylation-dependent proliferation and transformation of breast cancer cells require activation of p38 mapk. *Transl. Oncol.* **2012**, *5*, 327–334. [CrossRef] [PubMed]
25. Sargiacomo, M.; Scherer, P.E.; Tang, Z.; Kubler, E.; Song, K.S.; Sanders, M.C.; Lisanti, M.P. Oligomeric structure of caveolin: Implications for caveolae membrane organization. *Proc. Natl. Acad. Sci. USA* **1995**, *92*, 9407–9411. [CrossRef] [PubMed]
26. Hansen, C.G.; Nichols, B.J. Exploring the caves: Cavins, caveolins and caveolae. *Trends Cell Biol.* **2010**, *20*, 177–186. [CrossRef] [PubMed]

27. Ludwig, A.; Howard, G.; Mendoza-Topaz, C.; Deerinck, T.; Mackey, M.; Sandin, S.; Ellisman, M.H.; Nichols, B.J. Molecular composition and ultrastructure of the caveolar coat complex. *PLoS Biol.* **2013**, *11*, e1001640. [CrossRef] [PubMed]
28. Kim, Y.M.; Reed, W.; Lenz, A.G.; Jaspers, I.; Silbajoris, R.; Nick, H.S.; Samet, J.M. Ultrafine carbon particles induce interleukin-8 gene transcription and p38 mapk activation in normal human bronchial epithelial cells. *Am. J. Physiol. Lung Cell. Mol. Physiol.* **2005**, *288*, L432–L441. [CrossRef] [PubMed]
29. Autengruber, A.; Sydlik, U.; Kroker, M.; Hornstein, T.; Ale-Agha, N.; Stockmann, D.; Bilstein, A.; Albrecht, C.; Paunel-Gorgulu, A.; Suschek, C.V.; et al. Signalling-dependent adverse health effects of carbon nanoparticles are prevented by the compatible solute mannosylglycerate (firoin) in vitro and in vivo. *PLoS ONE* **2014**, *9*, e111485. [CrossRef] [PubMed]
30. Drab, M.; Verkade, P.; Elger, M.; Kasper, M.; Lohn, M.; Lauterbach, B.; Menne, J.; Lindschau, C.; Mende, F.; Luft, F.C.; et al. Loss of caveolae, vascular dysfunction, and pulmonary defects in caveolin-1 gene-disrupted mice. *Science* **2001**, *293*, 2449–2452. [CrossRef] [PubMed]
31. Donaldson, K.; Tran, L.; Jimenez, L.A.; Duffin, R.; Newby, D.E.; Mills, N.; MacNee, W.; Stone, V. Combustion-derived nanoparticles: A review of their toxicology following inhalation exposure. *Part. Fibre Toxicol.* **2005**, *2*, 10. [CrossRef] [PubMed]
32. Chen, S.; Yin, R.; Mutze, K.; Yu, Y.; Takenaka, S.; Konigshoff, M.; Stoeger, T. No involvement of alveolar macrophages in the initiation of carbon nanoparticle induced acute lung inflammation in mice. *Part. Fibre Toxicol.* **2016**, *13*, 33. [CrossRef] [PubMed]
33. Misra, S.K.; Ohoka, A.; Kolmodin, N.J.; Pan, D. Next generation carbon nanoparticles for efficient gene therapy. *Mol. Pharm.* **2015**, *12*, 375–385. [CrossRef] [PubMed]
34. Modugno, G.; Menard-Moyon, C.; Prato, M.; Bianco, A. Carbon nanomaterials combined with metal nanoparticles for theranostic applications. *Br. J. Pharmacol.* **2015**, *172*, 975–991. [CrossRef] [PubMed]
35. Zhang, C.; Lei, S.; Zhang, Z.; He, J.; Xiao, S.; Fan, P.; Xie, J.; Gu, X.; Li, Y.; Zheng, W. Evaluation of the clinical value of carbon nanoparticles as lymph node tracer in differentiated thyroid carcinoma requiring reoperation. *Int. J. Clin. Oncol.* **2016**, *21*, 68–74.
36. Huynh, E.; Li, J. EGF and EGFR: Promising targets for modulating inflammation and mucosal healing therapy in IBD. *Inflamm. Cell Signal.* **2015**, *2*. [CrossRef]
37. Gainza, G.; Villullas, S.; Pedraz, J.L.; Hernandez, R.M.; Igartua, M. Advances in drug delivery systems (DDSS) to release growth factors for wound healing and skin regeneration. *Nanomedicine* **2015**, *11*, 1551–1573. [CrossRef] [PubMed]
38. Henriksen, L.; Grandal, M.V.; Knudsen, S.L.; van Deurs, B.; Grovdal, L.M. Internalization mechanisms of the epidermal growth factor receptor after activation with different ligands. *PLoS ONE* **2013**, *8*, e58148. [CrossRef] [PubMed]
39. Berken, A.; Abel, J.; Unfried, K. Beta1-integrin mediates asbestos-induced phosphorylation of AKT and ERK1/2 in a rat pleural mesothelial cell line. *Oncogene* **2003**, *22*, 8524–8528. [CrossRef] [PubMed]

Induction of cellular senescence and loss of gap junctional intercellular communication by carbon nanoparticle exposure of lung epithelial cells

Spannbrucker T*, Ale-Agha N*, Goy C, Dyballa-Rukes N, Jakobs P, Altschmied J, Unfried K, Haendeler J

Exp Gerontol. 2018; *Gleichberechtigte Erstautoren

Autoren:

Spannbrucker T: Erstautor, war an der Planung und Durchführung der Versuche beteiligt, führte die Datenanalyse durch und war zudem am Entwurf des Manuskriptes beteiligt.

Ale-Agha N: Erstautorin, war an der Planung und Durchführung aller Versuche beteiligt, führte alle Mikroinjektionen und deren Datenanalyse durch und war zudem am Entwurf des Manuskriptes beteiligt.

Goy C: Führte zusammen mit Frau Dyballa-Rukes und Herrn Jakobs die Immunoblots und deren Datenanalyse durch. Korrigierte Teile des Manuskripts.

Dyballa-Rukes N: Führte zusammen mit Frau Goy und Herrn Jakobs die Immunoblots und deren Datenanalyse durch. Korrigierte Teile des Manuskripts.

Jakobs P: Führte zusammen mit Frau Goy und Frau Dyballa-Rukes die Immunoblots und deren Datenanalyse durch. Korrigierte Teile des Manuskripts.

Altschmied J: war an der Idee und Planung der Versuche beteiligt, gab konstruktive Kritik zum Manuskript und erstellte die finale Korrektur.

Unfried K: war an der Idee und Planung der Versuche beteiligt, gab konstruktive Kritik zum Manuskript und erstellte die finale Korrektur.

Haendeler J: Senior Autorin, hatte die Idee zur Studie, war an der Versuchsplanung beteiligt und schrieb sowie finalisierte das Manuskript.

Experimental Gerontology 117 (2019) 106–112

Contents lists available at ScienceDirect

Experimental Gerontology

journal homepage: www.elsevier.com/locate/expgero

Short report

Induction of a senescent like phenotype and loss of gap junctional intercellular communication by carbon nanoparticle exposure of lung epithelial cells

Tim Spannbrucker[a,c,1], Niloofar Ale-Agha[c,1], Christine Goy[c], Nadine Dyballa-Rukes[c], Philipp Jakobs[c], Kirsten Jander[d], Joachim Altschmied[d], Klaus Unfried[a,*], Judith Haendeler[b,c,*]

[a] Environmentally-induced Skin and Lung Aging, IUF-Leibniz Research Institute for Environmental Medicine, Heisenberg-group - Environmentally-induced Cardiovascular Degeneration, Medical Faculty, HHU Duesseldorf, Duesseldorf, Germany
[b] Institute of Clinical Chemistry, Medical Faculty, HHU Duesseldorf, Duesseldorf, Germany
[c] IUF-Leibniz Research Institute for Environmental Medicine, Duesseldorf, Germany
[d] Core Unit Biosafety Level 2 Laboratory, IUF-Leibniz Research Institute for Environmental Medicine, Duesseldorf, Germany

ARTICLE INFO

Keywords:
Senescence
Lung epithelial cell
Carbon nanoparticles
Cell communication
Connexin 43

ABSTRACT

Inhalation of combustion-derived particles is associated with the development of age-related diseases like chronic obstructive pulmonary disease and idiopathic pulmonary fibrosis. In both diseases senescence of lung epithelial cells has been observed. Employing an *in vitro* system of repetitive exposure to pure carbon nanoparticles we asked whether this kind of particles are able to induce a senescent like phenotype, which might be accompanied by a loss of functionality at the level of gap junctional intercellular communication. Non-cytotoxic doses of carbon nanoparticles but not of bigger carbon particles led to an irreversible reduction of the proliferative capacity accompanied by the accumulation of the cell cycle blocking proteins p21 and p16 as well as a loss of both redox sensitive histone deacetylase SIRT1 and connexin-43. Gap junction intercellular communication detected by microinjection of fluorescent lucifer yellow was dramatically decreased after exposure. This loss of functionality was associated with a reduction of Connexin 43 at the plasma membrane. As the experimental system was chosen to study the effects of pure carbon nanoparticles in the absence of inflammatory cells, the data indicate that cumulative long-term exposure of the lung epithelium to low doses of combustion-derived nanoparticles might contribute to epithelial senescence and age-associated diseases of the airways.

1. Introduction

Chronic exposure to particulate air pollution has been shown to contribute to the development of age-related diseases like chronic obstructive pulmonary disease (COPD) and idiopathic pulmonary fibrosis (IPF) (Faner et al., 2012). Both diseases show features of premature lung aging and cellular senescence like the accumulation of cell cycle blocking proteins p21 and p16 (Disayabutr et al., 2016; Houssaini et al., 2018) as well as the loss of the redox-sensitive histone deacetylase SIRT1 (Rajendrasozhan et al., 2008; Shetty et al., 2017). In COPD, the reduced proliferative and regenerative capacity of senescent lung cells may cause the formation of emphysema (Bartling and Hofmann, 2018; Chilosi et al., 2013). In IPF, senescence-associated changes in cellular signalling of epithelial cells appear to be involved in processes like epithelial to mesenchymal transition and tissue remodelling (Selman et al., 2016).

The inhalation of combustion-derived environmental carbon particles may contribute to the pathogenesis of the age-associated diseases by inducing cellular senescence in the lung epithelium. This effect could be triggered by the direct interaction of particles with lung epithelial cells. This mechanism appears to be particularly relevant for inhaled nanoparticles, which - because of their small size - are not specifically recognized and cleared from the lung by macrophages (Geiser et al., 2005). Our own earlier studies give indications that the exposure of the lung epithelium to pure carbon nanoparticles induces oxidative stress and cellular senescence (Buchner et al., 2013). For these studies we established a cell culture model using confluent cell layers of an alveolar lung epithelial cell, which was exposed repetitively for 14 days with particle doses not inducing cytotoxicity. In these cells we observed elevated levels of reactive oxygen species in parallel to an accumulation

* Corresponding authors.
E-mail addresses: Klaus.unfried@uni-duesseldorf.de (K. Unfried), juhae001@hhu.de (J. Haendeler).
[1] Both authors contributed equally to this work.

https://doi.org/10.1016/j.exger.2018.11.017
Received 13 March 2018; Received in revised form 7 November 2018; Accepted 22 November 2018
Available online 23 November 2018
0531-5565/

of p21 and p16 protein levels.

The molecular mechanisms by which inert poorly soluble pure carbon nanoparticles induce intracellular oxidative stress and cellular senescence are not fully understood (Unfried et al., 2007; Weissenberg et al., 2010). However, the comparison of chemically identical particle types differing in their primary particle size indicates a particular role of physical particle characteristics in this pathogenic mechanism (Peuschel et al., 2012). At constant mass doses, only carbon nanoparticles with a primary diameter of 20 nm induced intracellular oxidative stress and subsequent signalling events, while non-nano carbon particles (primary diameter 350 nm) failed to induce these reactions. Besides the primary size, the particle samples differ in their reactive surface area by a factor of 40. It is, therefore, assumed that the reactive surface area is a particle characteristic, which specifically influences nanoparticle cell interaction.

Cellular senescence is associated with the loss of cellular function. The communication of lung epithelial cells *via* gap junctions appears to be an important mechanism for the regulation of inflammatory reactions (Freund-Michel et al., 2016; Losa et al., 2011). Moreover, there are also indications that lung epithelial cells are able to communicate with mesenchymal cells *via* gap junction intercellular communication (GJIC) (Badri et al., 2011). Earlier studies using microinjection of a fluorescent dye demonstrated that GJIC in lung epithelial cells was reduced after exposure to carbon nanoparticles for a few hours (Ale-Agha et al., 2010). The loss of GJIC was accompanied by an acute translocation of connexin-43 from the plasma membrane to the cytoplasm. As connexin-43 appears to be downregulated during aging in other systems (Nagibin et al., 2016), age-associated downregulation of this key protein of GJIC might be an additional feature of nanoparticle induced epithelial senescence.

The current work aimed to investigate the direct influence of carbon particles of different sizes to induce a senescent like phenotype in lung epithelial cells. We used a well-established cell culture model to specifically investigate the induction of senescence by carbon particles without additional influences of inflammatory cells recruited to the airways. The specificity of such reactions was investigated by applying two different doses of particles, which earlier proved to be not cytotoxic (Buchner et al., 2013). The application of two chemically nearly identical particles, which differ in primary size and therefore also in their reactive surface area (see Table 1) allowed to investigate the role of physical particle characteristics for the induction of epithelial cellular senescence. Furthermore, as a parameter of epithelial function, GJIC was investigated by fluorescent dye injection and expression analyses of connexin-43 after repetitive exposure of lung epithelial cells.

2. Material and methods

2.1. Particles and particle suspensions

Carbon nanoparticles (CNP, Printex 90 were obtained from Degussa (Germany) and carbon particles were from H. Haeffner (CP, Chepstow, UK; as Huber 99). As described earlier, particles and particle suspensions were characterized for their physical characteristics (Table 1) (Kroker et al., 2015; Peuschel et al., 2012).

For each experiment, stock suspensions of particles (1 mg/ml) were freshly prepared in PBS by sonication for 15 min at 50–60 Hz, 120 W (Sydlik et al., 2006). The suspensions were applied to confluent monolayers of RLE-6TN cells to achieve the indicated doses.

2.2. Cell culture

RLE-6TN rat lung epithelial cells (Driscoll et al., 1995) derived from alveolar type II cells were purchased from ATCC and cultivated at 37 °C in a humidified atmosphere with 5% (v/v) CO_2 and held in Ham's F-12 (Sigma, Germany) supplemented with (final concentrations) 5% (v/v) fetal calf serum (FCS, Sigma), 1% (v/v) of Glutamax (Invitrogen), and penicillin/streptomycin (Sigma).

2.3. Cell exposure

Confluent monolayers of cells were exposed to particle suspensions every second day for 14 days to achieve doses of either 1 μg/cm^2 or 10 μg/cm^2 of particles, at each time. Prior to each exposure, the culture medium was changed. Two days after the last exposure, cells were harvested for analyses or used for immunostaining or analyses of gap junctional intercellular communication (GJIC).

2.4. Determination of gap junctional intercellular communication (GJIC)

GJIC was determined as described earlier (Ale-Agha et al., 2010). Cells were grown on 6 cm dishes and exposed to carbon nanoparticles or carbon particles as described above. GJIC was determined by microinjecting the fluorescent dye lucifer yellow CH (Sigma; 10% (w/v) in 0.33 M LiCl) into selected cells by means of a micromanipulator and a microinjector system (Eppendorf, Hamburg, Germany). One minute after injection, fluorescent cells surrounding the cells loaded with the dye were counted and taken as a measure of GJIC. Ten individual cells were loaded with dye per dish and means of the numbers of fluorescent neighboring cells were calculated (Ale-Agha et al., 2009).

2.5. Western blotting, immunocytochemistry

For Western blotting, cells were lysed in RIPA (50 mmol/l TRIS-HCl pH 8.0, 1% IGEPAL CA-630, 150 mmol/l NaCl, 0.1% (w/v) SDS, 0.5% (w/v) Desoxycholat) and protein concentrations determined by Bradford assay (Bio-Rad, Hercules, USA). Samples were applied to SDS–polyacrylamide gels of 10% (w/v) acrylamide, followed by electrophoresis and blotting. Immunodetections were performed using the following antibodies: rabbit polyclonal anti-Cx43 (Sigma-Aldrich, St. Louis, U.S.A.; 1:1500), anti-p21 (Abcam, Cambridge, UK; 1:500), anti-p16 (Abcam, Cambridge, UK, 1:200), anti-SIRT1 (Cell Signalling Technology, Danvers, U.S.A.; 1:500), anti-Src (Cell Signalling Technology, Danvers, U.S.A.; 1:500). As secondary antibodies, horseradish peroxidase conjugated goat anti-rabbit antibodies were used (GE Healthcare, Chicago, U.S.A.; 1:5000). All antibody incubations were in 5% (w/v) nonfat dry milk in Tris-buffered saline containing 0.1% (v/v) Tween 20 (TBST). Semi-quantitative analyses were performed on scanned immunoblots using ImageJ. For immunofluorescence, cells were grown on glass coverslips and treated with carbon nanoparticles or carbon particles as described above. Following the respective experimental treatments, cells were washed with PBS and fixed for 15 min with 4% (v/v) of formaldehyde, and washed three times with PBS. Non-

Table 1
Physical characteristics of carbon particles and particle suspensions.

Sample	Primary size [nm]	Zeta potential [mV]	Surface area [m^2/g]	Size in suspension [nm] *peak 1*	Size in suspension [nm] *peak 2*	Size in suspension [nm] *peak 3*
CNP	20	−22.4	442	887 (± 197) 88.8%	118 (± 126) 10.5%	1798 (± 3114.8) 0.7%
CP	350	−16.0	10.6	359 (± 22) 100%		

specific binding sites were blocked for 15 min at room temperature with 3% (v/v) normal goat serum (Sigma) diluted in PBS containing 0.3% (v/v) Triton X-100. For detection of Cx43, cells were incubated with polyclonal rabbit anti-connexin-43 (1:1500) diluted in PBS containing 1% (v/v) goat serum overnight at 4 °C. Antibodies were removed and cells washed three times with PBS, followed by incubation with an Alexa 488-coupled goat anti-rabbit IgG (H + L; 1:500) for 1 h at RT. For actin filaments staining RLE were stained with Alexa Fluor 568-coupled phalloidin for 30 min at RT (Invitrogen, Karlsruhe, Germany). Nuclei were stained with 4′,6-diamidino-2-phenylindole (DAPI, Invitrogen, Karlsruhe, Germany). Cells were washed and mounted with ProLong Gold antifade mounting medium (Invitrogen, Karlsruhe, Germany). Fluorescence images were taken with an AXIOVERT 200 M microscope (Zeiss, Jena, Germany, 1:40 oil).

2.6. Real-time PCR measurements of relative mRNA levels

RNA was isolated using TRIzol reagent according to the manufacturer's protocol (Invitrogen, Karlsruhe, Germany). Gene-specific mRNA levels were determined by semi-quantitative real-time PCR. Therefore, the RNA concentration was measured photometrically. Aliquots of total RNA were reverse transcribed using the Superscript™ III First-Strand synthesis system (Invitrogen, Karlsruhe, Germany). The PCR reactions were carried out using SYBR® Green PCR Master Mix (Applied Biosystems, Darmstadt, Germany). The following primer pairs were used: hmrCx43 for (5′-ACGAGGTATCAGCACTTTTCT-3′), hmrCx43 rev (5′-ACAGCCACACCTTCCCT-3′), hmRPL32 for (5′-GTGAAGCCCAAGAT CGTCAA-3′), hmRPL32 rev (5′-TTGTTGCACATCAGCAGCAC-3′).

2.7. Cell proliferation - BrdU assay

Proliferation was analyzed by the incorporation of 5-bromo-2′-deoxyuridine (BrdU) as a parameter for DNA synthesis using the BrdU Flow Kit (BD Biosciences, Heidelberg Germany). In brief, cells were treated with carbon nanoparticles and carbon particles as described, after 14 days cells were trypsinized and reseeded for 22 h. BrdU was added to the culture medium 1 h before cells were detached. Incorporated BrdU was labeled with a FITC-coupled anti-BrdU antibody. Cells were analyzed using a Calibur flow cytometer (BD Biosciences, Heidelberg, Germany).

2.8. Statistics

For statistical analyses two-sided, unpaired Student's *t*-test was used. Data are presented as means +/− SEM.

3. Results

3.1. Carbon particles increase p21 and p16 protein levels in lung epithelial cells

In our earlier studies we observed that repetitive exposure of lung epithelial cells with non-cytotoxic doses of 10 μg/m^2 of carbon nanoparticles led to an accumulation of p21 as a feature of cellular senescence (Buchner et al., 2013). In the first experiment, we now asked whether this reaction is specific for carbon nanoparticles compared to bigger non-nano carbon particles. Cells were exposed every second day with the indicated doses of particles for 14 days. Cells were harvested for the analysis of proteins 2 days after the last exposure. Western blot analyses revealed that carbon nanoparticles significantly increase p21 protein levels at any given dose (Fig. 1A). The exposure to similar doses of carbon particles induced much lower p21 levels, indicating that at the chosen mass doses carbon nanoparticles are more potent to trigger p21 protein induction and thus, probably epithelial cell senescence. The analyses of p16 as a second cell cycle blocking protein revealed significantly increased protein levels only after carbon nanoparticle exposure while higher treatment doses induced higher protein levels (Fig. 1B). To further analyse the induction of a senescent like phenotype by carbon particles, we next investigated SIRT1.

3.2. Carbon nanoparticles induce loss of SIRT1 protein levels in lung epithelial cells

SIRT1 has been described to be downregulated in different aging and senescence models. Therefore, we used the same experimental design as for p21 and p16. Compared to control treatment, no reduction of SIRT1 levels was observed with both concentrations of carbon particles (Fig. 1C). However, exposure to 10 μg/cm^2 carbon nanoparticles led to a dramatic loss of SIRT1. The slight reduction of SIRT1 levels by exposure to the lower dose of carbon nanoparticles appears to indicate a dose dependency in the reduction of SIRT1 levels. Thus, our data show that only carbon nanoparticles, but not non-nano particles reduce SIRT1 protein levels.

3.3. Carbon nanoparticles lead to dramatic reduction in proliferative capacity of lung epithelial cells

Another hallmark, which occurs in cellular senescence, is the reduced proliferative capacity of cells. Therefore, cells were treated with particles as before for 14 days (Fig. 1D). After that cells were reseeded at a confluency of approximately 30%. Then, the ability to incorporate BrdU - as a marker for proliferation - was measured. As demonstrated in Fig. 1D, carbon nanoparticle pretreated cells show a dramatic reduction in their proliferative capacity at lower and higher carbon nanoparticle doses. In contrast, carbon particles did not change proliferation. Thus, we would conclude that only carbon nanoparticles but not carbon particles induce signs of cellular senescence.

3.4. Carbon nanoparticles reduce localization of Connexin 43 at the plasma membrane

Another described sign of cellular senescence is the reduction in intra-cellular communication (Lopez-Otin et al., 2013). Intercellular communication is dependent on the localization of Connexins at the plasma membrane to form channels between cells. One of the most important Connexins in the lung is Connexin 43 (Cx43). Therefore, we investigated mRNA expression, total protein levels as well as localization at the plasma membrane of Cx43 after exposure to carbon nanoparticles and carbon particles for after 14 days as described above. As demonstrated in Fig. 2A, only higher doses of carbon nanoparticles significantly reduced Cx43 mRNA expression. Similar results were obtained at the total protein level (Fig. 2B). To further elucidate whether particles change the cellular localization of Cx43, we next performed immunostainings.

Immunofluorescence analyses of cells exposed to particles clearly demonstrated that carbon particles did not change the localization of Cx43 at the plasma membrane (Fig. 2C). In contrast, already lower doses of carbon nanoparticles lead to a disturbed pattern of Cx43 at the plasma membrane. This is even more pronounced in cells treated with the higher carbon nanoparticle doses (Fig. 2C). Thus, these data would suggest that long-term treatment with non-cytotoxic doses of carbon nanoparticles, but not with carbon particles indeed leads to induction of a senescent like phenotype. Since reduction of Cx43 at the plasma membrane points towards a loss in gap junction intercellular communication (GJIC), we next investigated GJIC.

3.5. Loss of GJIC in cells exposed to carbon nanoparticles

Therefore, we next measured GJIC by injecting the fluorescent dye lucifer yellow into single cells and counted the number of adjacent stained cells (Fig. 3). The repetitive treatment with both doses of carbon nanoparticles led to a dramatic loss of GJIC compared to control cells as

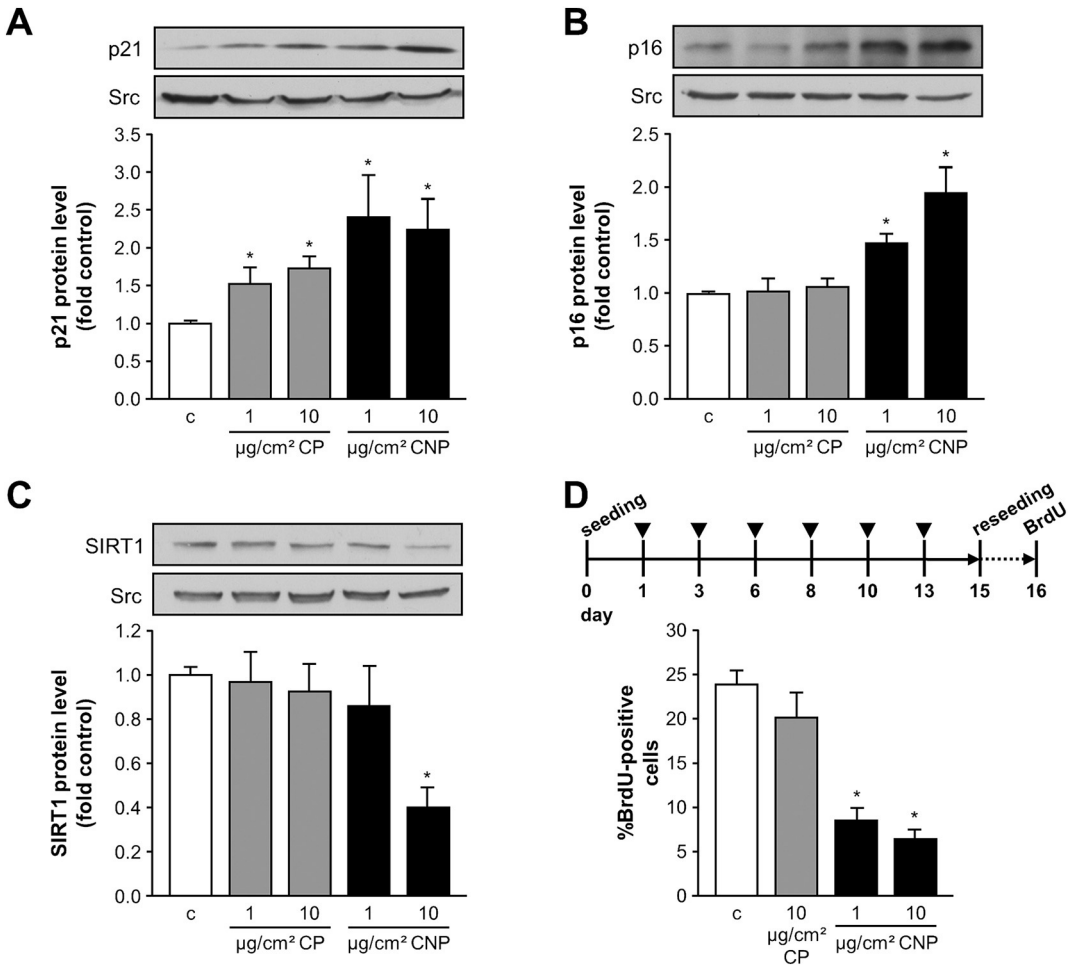

Fig. 1. Exposure to carbon nanoparticles increases senescence-associated endpoints in lung epithelial cells. RLE-6TN cells were exposed to carbon particles (CP) or carbon nanoparticles (CNP) every second day with the indicated doses for 14 days, c denotes the untreated control. (A) p21 levels were determined by immunoblot, Src served as loading control. Representative immunoblots and semiquantitative analysis of p21 normalized to Src are shown. Data are mean ± SEM, $n = 4–5$, $^*p < 0.05$ (two-sided, unpaired *t*-test). (B) p16 levels were determined by immunoblot, Src served as loading control. Representative immunoblots and semiquantitative analysis of p16 normalized to Src are shown. Data are mean ± SEM, n = 4, *p < 0.05 (two-sided, unpaired *t*-test). (C) SIRT1 levels were determined by immunoblot, Src served as loading control. Representative immunoblots and semiquantitative analysis of SIRT1 normalized to Src are shown. Data are mean ± SEM, $n = 6$, *p < 0.05 (two-sided, unpaired *t*-test). (D) Upper panel - treatment scheme of cells, the triangle indicates carbon particle (CP) and carbon nanoparticle (CNP) exposure time points. Lower bar graph - cells were exposed to carbon particles or carbon nanoparticles as indicated in the treatment scheme above. Afterwards cells were trypsinized and reseeded. BrdU was added and proliferation was measured as BrdU incorporation by flow cytometry. Data are mean ± SEM, $n = 3$, *p < 0.05 (two-sided, unpaired *t*-test).

well as to carbon particle treated cells. These data are in accordance with our findings observed in Fig. 2C that both doses of carbon nanoparticles change the subcellular localization of Connexin 43. Thus, our data indicate that only nanoparticles induce loss of cell-cell communication.

4. Discussion

Our findings demonstrate for the first time that carbon nanoparticles induce a senescent like phenotype and loss of gap junctional intercellular communication in lung epithelial cells. Due to the amount of carbon nanoparticles in ambient air pollution or at occupational settings humans can be exposed to these particulate xenobiotics for long time periods. Chronic exposure to particulate air pollution has been associated with the occurrence of biomarkers for COPD (Schikowski et al., 2014). Particularly the clear correlation of life long exposure to traffic-related air pollution and COPD in a cohort of elderly women suggests the induction of premature lung aging by this environmental stress (Schikowski et al., 2005; Unfried et al., 2016). The current work aimed to find indications that such effects can be triggered in lung epithelial cells by carbon nanoparticles as a major component of air pollution. As human real life cumulative exposure cannot be perfectly reproduced *in vitro* or in animal experiments *in vivo*, exposure models have to be applied. In order to study the induction of cellular senescence by carbon nanoparticle exposure we chose a well characterized mechanistic model, in which we applied cumulative doses of particles over a time period of 14 days. The microscopic analyses of this study again demonstrated that this treatment has no cytotoxic effect on cells, as observed earlier (Buchner et al., 2013). This model allowed investigating the effects of carbon nanoparticles on lung epithelial cells without the effects of inflammatory cells, which might contribute to oxidative stress or interfere with the senescence-associated secretome (Kumar et al., 2014; Nel et al., 2001). The relevance of data obtained with the chosen cell has earlier been demonstrated for signalling events triggered by carbon nanoparticles when these data were compared to *in vivo* data from exposed animals (Autengruber et al., 2014; Sydlik et al., 2009). The chosen particle types and doses aimed to investigate the specificity of the induction of a senescent like phenotype by carbon nanoparticles in comparison to carbon particles.

The performed studies demonstrate that repetitive treatment with

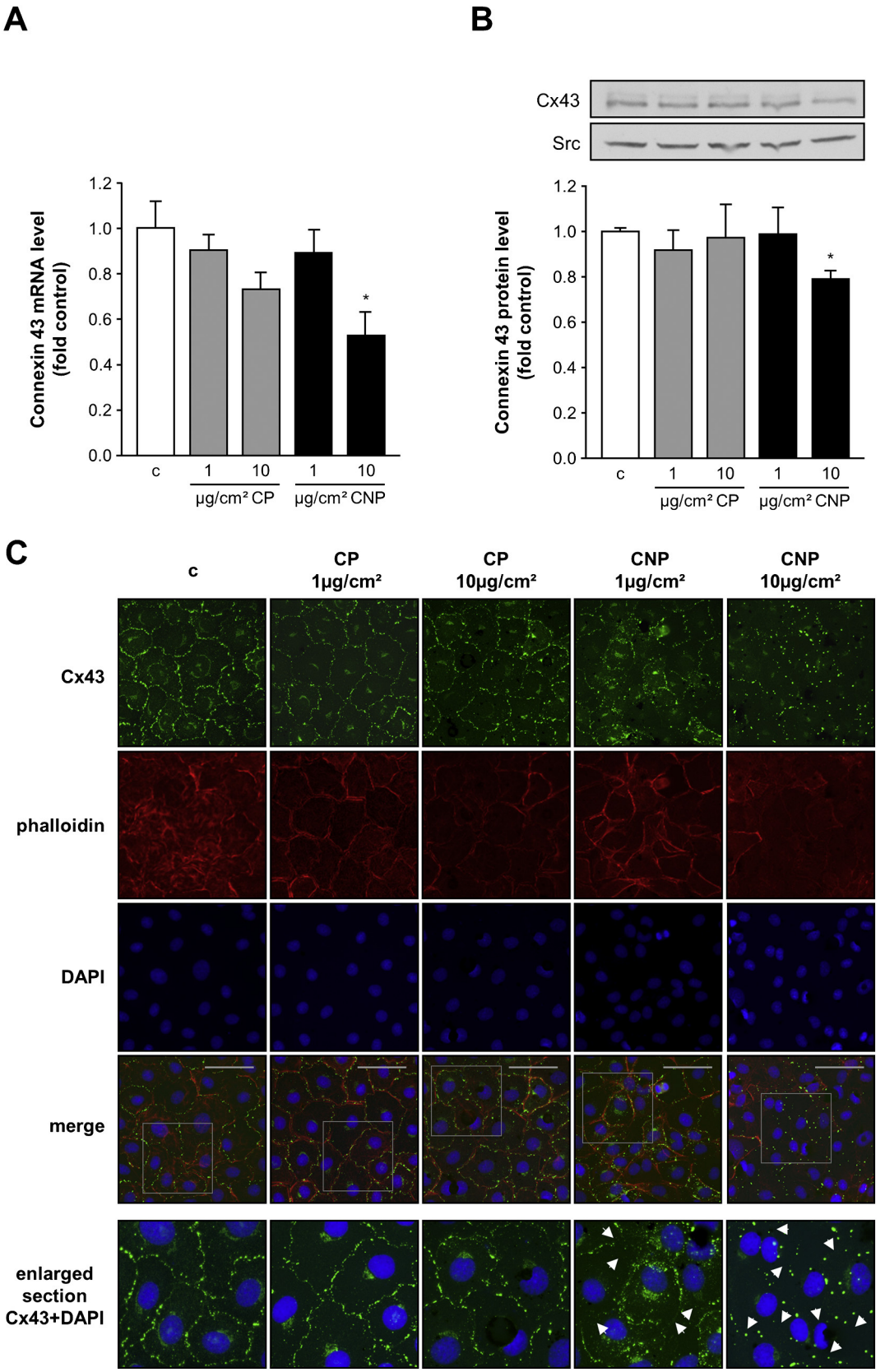

Fig. 2. Exposure to carbon nanoparticles changes Cx43 mRNA expression, total protein levels and subcellular localization in lung epithelial cells. RLE-6TN cells were exposed to carbon particles (CP) or carbon nanoparticles (CNP) every second day with the indicated doses for 14 days, c denotes the untreated control. (A) Cx43 transcript levels were determined by semiquantitative real-time PCR, RPL32 served as reference. Data are mean ± SEM, n = 3, *$p < 0.05$ (two-sided, unpaired *t*-test). (B) Cx43 levels were determined by immunoblot, Src served as loading control. Representative immunoblots, and semiquantitative analysis of Cx43 normalized to Src are shown. Data are mean ± SEM, n = 6, *p < 0.05 (two-sided, unpaired *t*-test). (C) Immunocytochemical analysis of Cx43 localization. c indicates the untreated control. The cells were stained for Cx43 and actin using phalloidin; nuclei were counterstained with DAPI, Merge shows an overlay of all fluorescence channels. The scalebar is 50 µm. Enlarged sections are displayed in the lower panels.

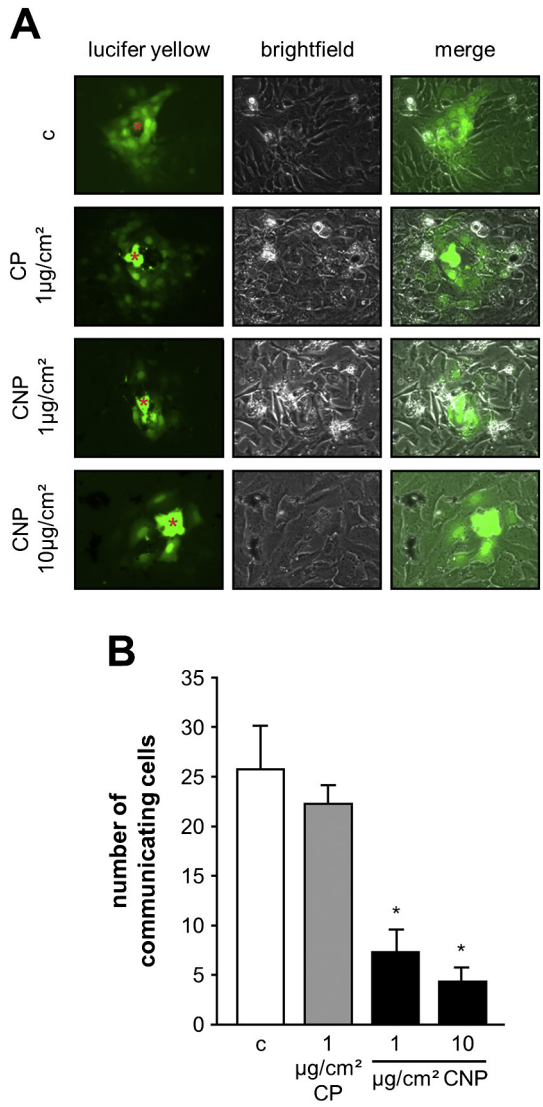

Fig. 3. Exposure to carbon nanoparticles impairs cell-cell communication. RLE-6TN cells were exposed to carbon particles (CP) or carbon nanoparticles (CNP) every second day with the indicated doses for 14 days, c denotes the untreated control. On day 14 gap junctional intercellular communication was measured by lucifer yellow dye transfer. (A) Representative microscopic pictures, merge shows an overlay of the fluorescence channel and the brightfield image. The initially injected cell is labeled with an asterisk (B) Quantitative analysis of intercellular communication. Shown are the numbers of communicating cells, data are mean ± SEM, $n = 4$, *p < 0.05 (two-sided, unpaired *t*-test).

10 µg/cm^2 carbon nanoparticles specifically triggers the accumulation of p21 and p16, the reduction of SIRT1, the loss of Connexin 43 at the plasma membrane, and the inability of those cells to proliferate. These features of cellular senescence are accompanied by a loss of epithelial cell function at the level of GJIC. The control particles, which are characterized by a bigger primary particle size appear not to induce these effects. Thus, the reduced surface area of non-nano particles compared to nanoparticles might be responsible for these differences. In earlier studies, we aimed to perform dose response experiments with respect to surface area rather than to mass (Peuschel et al., 2012). These results indicated that signalling processes indeed could be triggered by higher doses of non-nano particles. However in the current study it turned out that under repetitive conditions such high mass concentrations of carbon particles would interfere with the chosen assays.

The loss of histone deacetylase SIRT1 in the airways so far was observed in macrophages and lung epithelial cells after exposure to tobacco smoke or in chronic inflammation leading to COPD (Rajendrasozhan et al., 2008; Yao et al., 2012). Our data for the first time demonstrate that similar effects can be triggered in the absence of inflammatory cells by pure carbon nanoparticles carrying virtually no organic compounds (Borm et al., 2005). Although not yet corroborated in an *in vivo* system, these data indicate that longterm exposure to combustion-derived nanoparticles below the threshold dose for the induction of lung inflammation may contribute to the cellular senescence of epithelial cells and to the development of age-associated pulmonary diseases.

The senescent like phenotype in this study is accompanied with the dramatic loss of epithelial functionality at the level of GJIC. In earlier studies an acute redistribution of Cx43 from the plasma membrane to the cytoplasm was shown to be responsible for the loss of GJIC after exposure to combustion-derived nanoparticles. In the recent study after repetitive long term exposure, however, we can attribute the loss of GJIC to the downregulation of Cx43 at the mRNA level. Besides the reduction of Cx43, the intracellular distribution of the protein does not resemble the typical feature of redistribution due to acute stress triggered by particles (Ale-Agha et al., 2010). However, we have to acknowledge that the dramatic loss of GJIC appears not to be completely represented at the level of mRNA and protein. This effect might be due to a combination of downregulation of Cx43 and a loss of the protein at the plasma membrane. Nevertheless, the study clearly demonstrates that only carbon nanoparticles, but not carbon particles in non-cytotoxic and non-inflammatory doses induce senescence in lung epithelial cells.

5. Conclusion

In conclusion the study demonstrates that carbon nanoparticles, but not bigger carbon particles induce a senescent like phenotype, which is accompanied by a loss in GJIC in lung epithelial cells. The data indicate that long-term exposure to low doses of combustion-derived nanoparticles might lead to epithelial senescence even in the absence of inflammation and contribute to the development of age-associated lung diseases.

Acknowledgements

We thank Florian von Ameln and Olaf Eckermann for excellent technical assistance.

Funding

The research was funded by grants from the German Research Foundation (DFG) HA2868/10-1/-2, HA2868/11-1 and UN110/4-1. PJ, TS and KS are stipend holders of the IRTG1902 from the DFG.

References

Ale-Agha, N., Galban, S., Sobieroy, C., Abdelmohsen, K., Gorospe, M., Sies, H., Klotz, L.O., 2009. HuR regulates gap junctional intercellular communication by controlling beta-catenin levels and adherens junction integrity. Hepatology 50, 1567–1576.

Ale-Agha, N., Albrecht, C., Klotz, L.O., 2010. Loss of gap junctional intercellular communication in rat lung epithelial cells exposed to carbon or silica-based nanoparticles. Biol. Chem. 391, 1333–1339.

Autengruber, A., Sydlik, U., Kroker, M., Hornstein, T., Ale-Agha, N., Stockmann, D., Bilstein, A., Albrecht, C., Paunel-Gorgulu, A., Suschek, C.V., Krutmann, J., Unfried, K., 2014. Signalling-dependent adverse health effects of carbon nanoparticles are prevented by the compatible solute mannosylglycerate (firoin) in vitro and in vivo. PLoS One 9, e111485.

Badri, L., Walker, N.M., Ohtsuka, T., Wang, Z., Delmar, M., Flint, A., Peters-Golden, M., Toews, G.B., Pinsky, D.J., Krebsbach, P.H., Lama, V.N., 2011. Epithelial interactions and local engraftment of lung-resident mesenchymal stem cells. Am. J. Respir. Cell Mol. Biol. 45, 809–816.

Bartling, B., Hofmann, H.S., 2018. Reduced proliferation capacity of lung cells in chronic obstructive pulmonary disease. Z. Gerontol. Geriatr. https://doi.org/10.1007/s00391-018-1377-9.

Borm, P.J., Cakmak, G., Jermann, E., Weishaupt, C., Kempers, P., van Schooten, F.J.,

Oberdorster, G., Schins, R.P., 2005. Formation of PAH-DNA adducts after in vivo and vitro exposure of rats and lung cells to different commercial carbon blacks. Toxicol. Appl. Pharmacol. 205, 157–167.
Buchner, N., Ale-Agha, N., Jakob, S., Sydlik, U., Kunze, K., Unfried, K., Altschmied, J., Haendeler, J., 2013. Unhealthy diet and ultrafine carbon black particles induce senescence and disease associated phenotypic changes. Exp. Gerontol. 48, 8–16.
Chilosi, M., Carloni, A., Rossi, A., Poletti, V., 2013. Premature lung aging and cellular senescence in the pathogenesis of idiopathic pulmonary fibrosis and COPD/emphysema. Transl. Res. 162, 156–173.
Disayabutr, S., Kim, E.K., Cha, S.I., Green, G., Naikawadi, R.P., Jones, K.D., Golden, J.A., Schroeder, A., Matthay, M.A., Kukreja, J., Erle, D.J., Collard, H.R., Wolters, P.J., 2016. miR-34 miRNAs regulate cellular senescence in type II alveolar epithelial cells of patients with idiopathic pulmonary fibrosis. PLoS One 11, e0158367.
Driscoll, K.E., Carter, J.M., Iype, P.T., Kumari, H.L., Crosby, L.L., Aardema, M.J., Isfort, R.J., Cody, D., Chestnut, M.H., Burns, J.L., et al., 1995. Establishment of immortalized alveolar type II epithelial cell lines from adult rats. In Vitro Cell. Dev. Biol. Anim. 31, 516–527.
Faner, R., Rojas, M., Macnee, W., Agusti, A., 2012. Abnormal lung aging in chronic obstructive pulmonary disease and idiopathic pulmonary fibrosis. Am. J. Respir. Crit. Care Med. 186, 306–313.
Freund-Michel, V., Muller, B., Marthan, R., Savineau, J.P., Guibert, C., 2016. Expression and role of connexin-based gap junctions in pulmonary inflammatory diseases. Pharmacol. Ther. 164, 105–119.
Geiser, M., Rothen-Rutishauser, B., Kapp, N., Schurch, S., Kreyling, W., Schulz, H., Semmler, M., Im Hof, V., Heyder, J., Gehr, P., 2005. Ultrafine particles cross cellular membranes by nonphagocytic mechanisms in lungs and in cultured cells. Environ. Health Perspect. 113, 1555–1560.
Houssaini, A., Breau, M., Kebe, K., Abid, S., Marcos, E., Lipskaia, L., Rideau, D., Parpaleix, A., Huang, J., Amsellem, V., Vienney, N., Validire, P., Maitre, B., Attwe, A., Lukas, C., Vindrieux, D., Boczkowski, J., Derumeaux, G., Pende, M., Bernard, D., Meiners, S., Adnot, S., 2018. mTOR pathway activation drives lung cell senescence and emphysema. JCI Insight. 3. https://doi.org/10.1172/jci.insight.93203.
Kroker, M., Sydlik, U., Autengruber, A., Cavelius, C., Weighardt, H., Kraegeloh, A., Unfried, K., 2015. Preventing carbon nanoparticle-induced lung inflammation reduces antigen-specific sensitization and subsequent allergic reactions in a mouse model. Part. Fibre Toxicol. 12, 20.
Kumar, M., Seeger, W., Voswinckel, R., 2014. Senescence-associated secretory phenotype and its possible role in chronic obstructive pulmonary disease. Am. J. Respir. Cell Mol. Biol. 51, 323–333.
Lopez-Otin, C., Blasco, M.A., Partridge, L., Serrano, M., Kroemer, G., 2013. The hallmarks of aging. Cell 153, 1194–1217.
Losa, D., Chanson, M., Crespin, S., 2011. Connexins as therapeutic targets in lung disease. Expert Opin. Ther. Targets 15, 989–1002.
Nagibin, V., Egan Benova, T., Viczenczova, C., Szeiffova Bacova, B., Dovinova, I., Barancik, M., Tribulova, N., 2016. Ageing related down-regulation of myocardial connexin-43 and up-regulation of MMP-2 may predict propensity to atrial fibrillation in experimental animals. Physiol. Res. 65 (Suppl. 1), S91–s100.
Nel, A.E., Diaz-Sanchez, D., Li, N., 2001. The role of particulate pollutants in pulmonary inflammation and asthma: evidence for the involvement of organic chemicals and oxidative stress. Curr. Opin. Pulm. Med. 7, 20–26.
Peuschel, H., Sydlik, U., Grether-Beck, S., Felsner, I., Stockmann, D., Jakob, S., Kroker, M., Haendeler, J., Gotic, M., Bieschke, C., Krutmann, J., Unfried, K., 2012. Carbon nanoparticles induce ceramide- and lipid raft-dependent signalling in lung epithelial cells: a target for a preventive strategy against environmentally-induced lung inflammation. Part. Fibre Toxicol. 9, 48.
Rajendrasozhan, S., Yang, S.R., Kinnula, V.L., Rahman, I., 2008. SIRT1, an antiinflammatory and antiaging protein, is decreased in lungs of patients with chronic obstructive pulmonary disease. Am. J. Respir. Crit. Care Med. 177, 861–870.
Schikowski, T., Sugiri, D., Ranft, U., Gehring, U., Heinrich, J., Wichmann, H.E., Kramer, U., 2005. Long-term air pollution exposure and living close to busy roads are associated with COPD in women. Respir. Res. 6, 152.
Schikowski, T., Adam, M., Marcon, A., Cai, Y., Vierkotter, A., Carsin, A.E., Jacquemin, B., Al Kanani, Z., Beelen, R., Birk, M., Bridevaux, P.O., Brunekeef, B., Burney, P., Cirach, M., Cyrys, J., de Hoogh, K., de Marco, R., de Nazelle, A., Declercq, C., Forsberg, B., Hardy, R., Heinrich, J., Hoek, G., Jarvis, D., Keidel, D., Kuh, D., Kuhlbusch, T., Migliore, E., Mosler, G., Nieuwenhuijsen, M.J., Phuleria, H., Rochat, T., Schindler, C., Villani, S., Tsai, M.Y., Zemp, E., Hansell, A., Kauffmann, F., Sunyer, J., Probst-Hensch, N., Kramer, U., Kunzli, N., 2014. Association of ambient air pollution with the prevalence and incidence of COPD. Eur. Respir. J. 44, 614–626.
Selman, M., Lopez-Otin, C., Pardo, A., 2016. Age-driven developmental drift in the pathogenesis of idiopathic pulmonary fibrosis. Eur. Respir. J. 48, 538–552.
Shetty, S.K., Tiwari, N., Marudamuthu, A.S., Puthusseri, B., Bhandary, Y.P., Fu, J., Levin, J., Idell, S., Shetty, S., 2017. p53 and miR-34a feedback promotes lung epithelial injury and pulmonary fibrosis. Am. J. Pathol. 187, 1016–1034.
Sydlik, U., Bierhals, K., Soufi, M., Abel, J., Schins, R.P., Unfried, K., 2006. Ultrafine carbon particles induce apoptosis and proliferation in rat lung epithelial cells via specific signaling pathways both using EGF-R. Am. J. Phys. Lung Cell. Mol. Phys. 291, L725–L733.
Sydlik, U., Gallitz, I., Albrecht, C., Abel, J., Krutmann, J., Unfried, K., 2009. The compatible solute ectoine protects against nanoparticle-induced neutrophilic lung inflammation. Am. J. Respir. Crit. Care Med. 180, 29–35.
Unfried, K., Albrecht, C., Klotz, L.-O., Von Mikecz, A., Grether-Beck, S., Schins, R.P.F., 2007. Cellular responses to nanoparticles: target structures and mechanisms. Nanotoxicology 1, 52–71.
Unfried, K., Kramer, U., Sydlik, U., Autengruber, A., Bilstein, A., Stolz, S., Marini, A., Schikowski, T., Keymel, S., Krutmann, J., 2016. Reduction of neutrophilic lung inflammation by inhalation of the compatible solute ectoine: a randomized trial with elderly individuals. Int. J. Chron. Obstruct. Pulmon. Dis. 11, 2573–2583.
Weissenberg, A., Sydlik, U., Peuschel, H., Schroeder, P., Schneider, M., Schins, R.P., Abel, J., Unfried, K., 2010. Reactive oxygen species as mediators of membrane-dependent signaling induced by ultrafine particles. Free Radic. Biol. Med. 49, 597–605.
Yao, H., Chung, S., Hwang, J.W., Rajendrasozhan, S., Sundar, I.K., Dean, D.A., McBurney, M.W., Guarente, L., Gu, W., Ronty, M., Kinnula, V.L., Rahman, I., 2012. SIRT1 protects against emphysema via FOXO3-mediated reduction of premature senescence in mice. J. Clin. Invest. 122, 2032–2045.

CDKN1B/p27 is localized in mitochondria and improves respiration-dependent processes in the cardiovascular system – new mode of action for caffeine

Ale-Agha N*, Goy C*, Jakobs P*, Spyridopoulos I, Gonnissen S, Dyballa-Rukes N, Aufenvenne K, Von Ameln F, Zurek M, **Spannbrucker T**, Eckermann O, Jakob S, Gorressen S, Abrams M, Gran- doch M, Fischer JW, Köhrer K, Deenen R, Unfried K, Altschmied J#, Haendeler J#

Plos Biology. 2018 *Gleichberechtigte Erstautoren; #Gleichberechtigte

Letztautoren

Autoren:

Ale-Agha N: Erstautorin, war an der Planung aller Versuche beteiligt, führte alle Tierexperimente und deren Datenanalyse durch. Schrieb Teile des Manuskripts.

Goy C: Erstautorin, plante mit Frau Haendeler alle Endothelzellversuche, führte alle Zellexperimente und alle Oroborosmessungen und deren Datenanalyse durch. Schrieb Teile des Manuskripts.

Jakobs P: Erstautor, war an der Planung aller Versuche in der Revision beteiligt und führte Zellexperimente und Datenanalyse durch. Schrieb mit Frau Haendeler und Herrn Altschmied die Revision und die Antworten für die Gutachter.

Spyridopoulos I: War an der Konzeption der Studie beteiligt, half mit den statistischen Analysen und korrigierte das Manuskript.

Gonnissen S: Führte zusammen mit Frau Aufenvenne, Herrn Spannbrucker und Frau Ale-Agha Immunfluoreszenzfärbungen durch.

Dyballa-Rukes N: Führte zusammen mit Frau Goy Immunoblots und deren Auswertung durch

Aufenvenne K: Führte zusammen mit Frau Gonnissen, Herrn Spannbrucker und Frau Ale-Agha Immunfluoreszenzfärbungen durch

Von Ameln F: Führte zusammen mit Frau Goy und Herrn Jakobs Immunoblots

durch und isolierte RNA für Transkriptomanalysen. Führte zusammen mit Herrn Eckermann die Klonierungen durch. Führte die Messungen des ATP Gehaltes mit Herrn Altschmied durch.

Zurek M: Etablierte die Zellkultur der kardialen Fibroblasten zusammen mit Herrn Jakobs und führte Immunoblots durch.

Spannbrucker T: Führte zusammen mit Frau Aufenvenne, Frau Gonnissen und Frau Ale-Agha Immunfluoreszenzfärbunge durch.

Eckermann O: Führte zusammen mit Herrn von Ameln die Klonierungen durch. Generierte die Lentiviren und transduzierte kardiale Fibroblasten. Führte die Expressionsnachweise.

Jakob S: Führte alle FACS Messungen und deren Datenanalyse durch.

Gorressen S: Führte zusammen mit Frau Ale-Agha, Herrn Abrams und Frau Grandoch die Experimente an Tieren auf diabetogener Ernährung

PLOS BIOLOGY

RESEARCH ARTICLE

CDKN1B/p27 is localized in mitochondria and improves respiration-dependent processes in the cardiovascular system—New mode of action for caffeine

Niloofar Ale-Agha[1☯], Christine Goy[1☯], Philipp Jakobs[1☯], Ioakim Spyridopoulos[2], Stefanie Gonnissen[3], Nadine Dyballa-Rukes[1], Karin Aufenvenne[1], Florian von Ameln[1,3], Mark Zurek[1], Tim Spannbrucker[4], Olaf Eckermann[1], Sascha Jakob[1], Simone Gorressen[5], Marcel Abrams[5], Maria Grandoch[5], Jens W. Fischer[5], Karl Köhrer[6], René Deenen[6], Klaus Unfried[4], Joachim Altschmied[3‡*], Judith Haendeler[1‡*]

1 Heisenberg-group—Environmentally-induced Cardiovascular Degeneration, Medical Faculty, HHU Duesseldorf and IUF-Leibniz Research Institute for Environmental Medicine, Duesseldorf, Germany, **2** Institute of Genetic Medicine, Newcastle University, Newcastle upon Tyne, United Kingdom, **3** Core Unit Biosafety Level 2 Laboratory, IUF-Leibniz Research Institute for Environmental Medicine, Duesseldorf, Germany, **4** Environmentally-induced Skin and Lung Aging, IUF-Leibniz Research Institute for Environmental Medicine, Duesseldorf, Germany, **5** Institute for Pharmacology and Clinical Pharmacology, Medical Faculty, HHU Duesseldorf, Duesseldorf, Germany, **6** Biological and Medical Research Center (BMFZ), HHU, Duesseldorf, Germany

☯ These authors contributed equally to this work.
‡ JA and JH also contributed equally to this work.
* juhae001@uni-duesseldorf.de (JH); joalt001@uni-duesseldorf.de (JA)

Citation: Ale-Agha N, Goy C, Jakobs P, Spyridopoulos I, Gonnissen S, Dyballa-Rukes N, et al. (2018) CDKN1B/p27 is localized in mitochondria and improves respiration-dependent processes in the cardiovascular system—New mode of action for caffeine. PLoS Biol 16(6): e2004408. https://doi.org/10.1371/journal.pbio.2004408

Academic Editor: Cecilia Lo, University of Pittsburgh, United States of America

Received: October 3, 2017

Accepted: May 18, 2018

Published: June 21, 2018

Data Availability Statement: The authors confirm that all data underlying the findings are fully available without restriction. All relevant data except for the original microarray data used as a basis for Fig 5C are within the paper and its supporting information files. The microarray data have been deposited in the NCBI Gene Expression Omnibus (https://www.ncbi.nlm.nih.gov/geo/) under the accession number GSE100489.

Abstract

We show that the cyclin-dependent kinase inhibitor 1B (CDKN1B)/p27, previously known as a cell cycle inhibitor, is also localized within mitochondria. The migratory capacity of endothelial cells, which need intact mitochondria, is completely dependent on mitochondrial p27. Mitochondrial p27 improves mitochondrial membrane potential, increases adenosine triphosphate (ATP) content, and is required for the promigratory effect of caffeine. Domain mapping of p27 revealed that the N-terminus and C-terminus are required for those improvements. Further analysis of those regions revealed that the translocation of p27 into the mitochondria and its promigratory activity depend on serine 10 and threonine 187. In addition, mitochondrial p27 protects cardiomyocytes against apoptosis. Moreover, mitochondrial p27 is necessary and sufficient for cardiac myofibroblast differentiation. In addition, p27 deficiency and aging decrease respiration in heart mitochondria. Caffeine does not increase respiration in p27-deficient animals, whereas aged mice display improvement after 10 days of caffeine in drinking water. Moreover, caffeine induces transcriptome changes in a p27-dependent manner, affecting mostly genes relevant for mitochondrial processes. Caffeine also reduces infarct size after myocardial infarction in prediabetic mice and increases mitochondrial p27. Our data characterize mitochondrial p27 as a common denominator that improves mitochondria-dependent processes and define an increase in mitochondrial p27 as a new mode of action of caffeine.

Funding: Deutsche Forschungsgemeinschaft (DFG) www.dfg.de (grant number HA2868/10-1 and HA2868/10-2). received by JH. The funder had no role in study design, data collection and analysis, decision to publish, or preparation of the manuscript. Deutsche Forschungsgemeinschaft (DFG) www.dfg.de (grant number IRTG1902 P1 and P2). recieved by JH and JA. The funder had no role in study design, data collection and analysis, decision to publish, or preparation of the manuscript. Deutsche Forschungsgemeinschaft (DFG) www.dfg.de (grant number SFB1116 A04). received by JH and JA. The funder had no role in study design, data collection and analysis, decision to publish, or preparation of the manuscript.

Competing interests: The authors have declared that no competing interests exist.

Abbreviations: αSMA, α smooth muscle actin; aa, amino acid; ADP, adenosine diphosphate; ATP, adenosine triphosphate; CDI, cyclin-dependent kinase inhibitor; CDK4, cyclin-dependent kinase 4; CDKN1A, cyclin-dependent kinase inhibitor 1A; CDKN1B, cyclin-dependent kinase inhibitor 1B; DAPI, 4′,6-diamidino-2-phenylindole; GO, gene ontology; GRP75, 75 KDa glucose-regulated protein; HPF, high power field; HSPA9, heat shock protein 70 kDa; LAD, left anterior descending coronary artery; PDE, phosphodiesterase; PI, propidium iodide; siRNA, small interfering RNA; TGFβ1, transforming growth factor β1; TIM23, translocase of inner mitochondrial membrane 23; TOM40, translocase of outer mitochondrial membrane 40; Trx-1, thioredoxin-1.

Author summary

The protein p27 is a nuclear cell cycle inhibitor that can be shuttled to the cytoplasm to inactivate its inhibitory role, and this mechanism is thought to be used by cancer cells to unlock cell cycle arrest. Recent reports, however, have shown that p27 has other roles independent of cell cycle regulation, and it was observed that p27 mutant mice had increased mortality to myocardial infarction. Here, we have analyzed the potential role of p27 in the major cell types of the heart and shown that it is also present in mitochondria, the cellular powerhouses, where it fulfils important functions. We find that p27 is required for migration of endothelial cells by enhancing mitochondrial functions and that caffeine concentrations reached after consumption of 4 cups of coffee induce its translocation into mitochondria. Moreover, we observe that mitochondrial p27 protects heart muscle cells from cell death and is necessary for the conversion of fibroblasts into mechanically strong, contractile myofibroblasts, a process critical after myocardial infarction. Molecularly, we show that p27 is essential for caffeine-induced gene expression changes that mainly affect mitochondria and for mitochondrial respiration. We conclude that mitochondrial p27 improves mitochondria-dependent processes in heart cells and that physiological concentrations of caffeine have a protective effect.

Introduction

The cyclin-dependent kinase inhibitor 1B (CDKN1B), also known as p27, was initially discovered as a nuclear-localized cell cycle inhibitor [1]. Previous data demonstrating that p27 can be exported to the cytoplasm [2,3] were considered as a mechanism to inactivate the cell cycle inhibitory effects of p27 in the nucleus and to allow human cancer cells to escape cell cycle arrest. However, McAllister and colleagues demonstrated that nonnuclear p27 is required for migration of fibroblasts, since p27-deficient mouse embryonic fibroblasts failed to migrate, while reconstitution with p27 rescued the motility defect. Its promigratory effect was independent of its cell cycle arrest functions but rather required serine 10 phosphorylation–dependent nuclear export and a C-terminal scatter domain [4]. Moreover, it was suggested that knockout of a cell cycle inhibitor like p27 could be beneficial in the experimental setup of myocardial infarction. This was based on the reasoning that myocardial infarction leads to loss of cells in the heart and that enhanced proliferation of cells in p27-deficient mice may result in smaller infarct size and reduced mortality; however, exactly the opposite was observed [5,6]. Moreover, over the last several years, it has become evident that functional mitochondria, not only in cardiomyocytes but also in endothelial cells [7,8] and in cardiac fibroblasts [9], are required for proper functionality of those cells and are essential for protective actions in cardiovascular diseases.

Furthermore, in recent years, a number of cohort studies have convincingly demonstrated that habitual coffee consumption is associated with a lower risk of developing type 2 diabetes [10,11]. Coffee consumption was inversely correlated with total as well as cause-specific mortality, such as heart disease, respiratory disease, stroke, and diabetes, whereas no relation or a positive correlation was found with cancer-related deaths [12,13]. In addition, several studies have shown that consumption of caffeinated coffee is associated with lower risk for coronary heart disease mortality, specifically in older subjects [14,15]. Finally, the beneficial effect of caffeine appeared to be dose-dependent, as coffee consumption of 4 cups or more per day resulted in a further reduced risk for adverse events when compared to lower coffee consumption. We established previously that 4 cups of coffee lead to a serum concentration of approximately 30 μM

caffeine in humans [8]. Therefore, mechanisms explaining the protective effects of caffeine should be attributed to serum concentrations of less than 100 μM. Over decades, the effects of caffeine have been ascribed to its antagonist activity on adenosine receptors, inhibition of phosphodiesterases (PDEs), and elevated intracellular calcium levels. Since a raise of intracellular calcium in different cell types requires at least 500 μM caffeine, which in humans would result in lethal intoxication [16–18], effects on intracellular calcium can be excluded as a potential mechanism. Similarly, inhibition of PDEs by caffeine requires concentrations of 250 μM or higher, depending on the isoforms investigated [19,20]. Studies regarding the responses to activation or inhibition of adenosine receptors in the cardiovascular system are controversial. Activation of the adenosine 2A receptor has beneficial effects in the infarcted porcine myocardium [21], whereas blockade of the adenosine 2A receptor reduces cardiac reactive oxygen species production and expression of NADPH oxidase 2 in the heart [22]. Thus, it remains unclear whether unspecific inhibition of adenosine receptors or PDEs by caffeine could explain the protective effects of coffee consumption. Importantly, we demonstrated that caffeine in physiologically relevant concentrations improves the functional capacity of endothelial cells ex vivo and in vivo in a mitochondria-dependent manner [8].

Given the described protective role of caffeine and its association with mitochondria, we hypothesized that a common denominator exists in endothelial cells, cardiomyocytes, and cardiac fibroblasts that improves the mitochondria-dependent functionalities of those cells ex vivo and in vivo. Since the role of nonnuclear p27 in nontumor cells was never examined in detail, we investigated whether p27 is present in the mitochondria and is indeed required to improve mitochondria-dependent functionalities and whether the protective caffeine effects are causally related to mitochondrial p27, which would present a new mode of action for caffeine, explaining its protective function in the cardiovascular system.

Results

Mitochondrial p27 is indispensable for functional improvement of endothelial cells

Physiologically relevant concentrations of caffeine, which have beneficial cardiovascular effects, have been attributed to 4 or more cups of daily coffee consumption. Four cups of coffee lead to a serum caffeine concentration of approximately 30 μM in humans [8]. Since 4 or more cups of coffee seem to have a beneficial effect, we used 50 μM caffeine in all cellular studies presented here, as well as concentrations of caffeine in the drinking water of mice, which result in approximately 30–50 μM in the serum of the animals [8]. To assess a potential involvement of adenosine receptors in the caffeine-mediated effects, we first investigated the impact of caffeine on endothelial cell migration, as a measure for functional capacity, in the presence of adenosine receptor 2A and 2B blockers SCH442416 and GS6201, respectively. Neither inhibition of adenosine receptor 2A nor 2B changed the ability of 50 μM caffeine to induce migration in human primary endothelial cells (S1 Fig). Moreover, caffeine did not change phosphorylation of PDEs 4A and 5A, respectively (S2 Fig), which is in accordance with the literature that caffeine concentrations higher than 250 μM are needed to modulate activity of those enzymes and thus to change intracellular cyclic nucleotide levels [19,20].

McAllister and colleagues showed that p27 is necessary for migration of HepG2 cells and embryonic fibroblasts. Furthermore, its promigratory effect was independent of its cell cycle arrest functions but rather required serine 10 phosphorylation–dependent nuclear export and a C-terminal scatter domain [4]. Therefore, we down-regulated p27 with 2 different small interfering RNAs (siRNAs; Figs 1A, 1B and S3) and determined first the effect on cell viability (siRNA1: 106.9 ± 11.9%; siRNA2: 134.6 ± 21.4% of scrambled control, $n = 5$, means ± SEM,

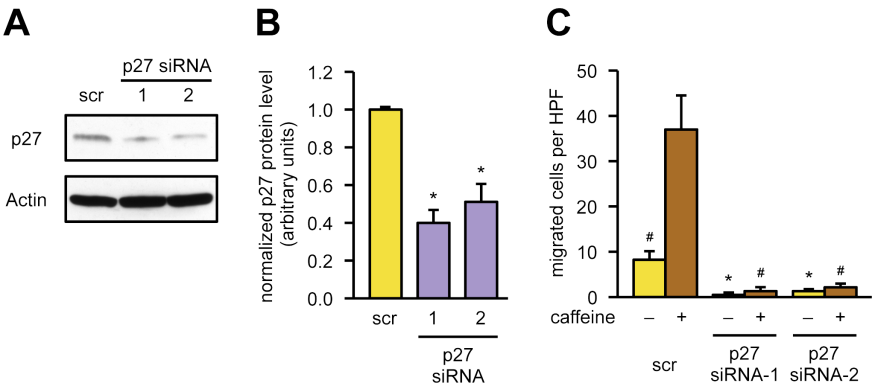

Fig 1. p27 is required for endothelial cell migration. (A, B) p27 was knocked down in endothelial cells by transfection with 2 different siRNAs targeting the p27 mRNA ("p27 siRNA-1," "p27 siRNA-2") or a scrambled siRNA ("scr") as control, and p27 levels were determined by immunoblot. **(A)** Representative immunoblots, Actin served as loading control. **(B)** Knockdown efficiency was determined by semiquantitative analysis of immunoblots. Data are mean ± SEM, $n = 5$, $^{*}p < 0.05$ versus scr (one-way ANOVA). **(C)** Endothelial cells were transfected with the same siRNAs as before, a wound was set 48 hours after transfection, and the cells were treated with 50 μM caffeine for another 18 hours or left untreated. Migratory capacity was assessed by counting cells migrated into the wound using Image J. Data are mean ± SEM, $n = 5$, $^{*}p < 0.05$ versus scr −caffeine, $^{\#}p < 0.05$ versus scr +caffeine (one-way ANOVA). Underlying data are provided in S1 Data. HPF, high power field; siRNA, small interfering RNA.

https://doi.org/10.1371/journal.pbio.2004408.g001

not significant) as well as on cellular and mitochondrial morphology (S4 Fig). Since transfection of p27-specific siRNAs affected neither cell viability nor morphology, we next investigated the effect on endothelial cell migration. Basal as well as caffeine-induced migration was completely blunted upon knockdown of p27 (Fig 1C). These data demonstrate that primary human endothelial cells require p27 for migration.

Since functional mitochondria are necessary for endothelial cell migration [8] and protein translocation to these organelles is a major determinant of their functional capacity [23], we wanted to establish a causal link between mitochondria and p27. Therefore, we investigated whether p27 is localized in mitochondria. As shown by immunoblots following biochemical separation, a fraction of p27 is localized in mitochondria. The purity of the mitochondrial preparations was confirmed by detection of the nonmitochondrial protein thioredoxin-1 (Trx-1) and the mitochondrial translocase of inner mitochondrial membrane 23 (TIM23), respectively. As an additional control, we also detected the cyclin-dependent kinase inhibitor 1A (CDKN1A), also known as p21, a member of the same protein family. As demonstrated in Fig 2A, p21 is not localized in the mitochondria, and caffeine does not affect the protein levels. Moreover, treatment with caffeine significantly increased mitochondrial p27 (Figs 2A, 2B and S5). To further verify that p27 is truly localized in the mitochondria and not simply attached to these organelles, we performed a proteinase K digest of isolated mitochondria. As demonstrated in Fig 2C, p27 is indeed localized within the mitochondria. Digestion of the outer mitochondrial membrane with proteinase K in hypotonic buffer results in mitoplasts, mitochondria stripped of their outer membrane, leaving only the inner mitochondrial membrane and the matrix. The immunoblot analysis confirmed loss of translocase of outer mitochondrial membrane 40 (TOM40) but revealed inner mitochondrial membrane proteins like TIM23 and matrix proteins like the mitochondrial heat shock protein 70, also called heat shock protein 70 kDa protein 9 (HSPA9; or 75 KDa glucose-regulated protein [GRP75]), respectively, and also p27 (Fig 2C). To causally link migration to mitochondrial p27, we cloned targeted variants of p27, which are exclusively localized in the nucleus or mitochondria, and expressed them in endothelial cells. Overexpression of nuclear- as well as mitochondrially targeted p27 revealed comparable expression levels (Fig 2D). Moreover, mitochondrially targeted

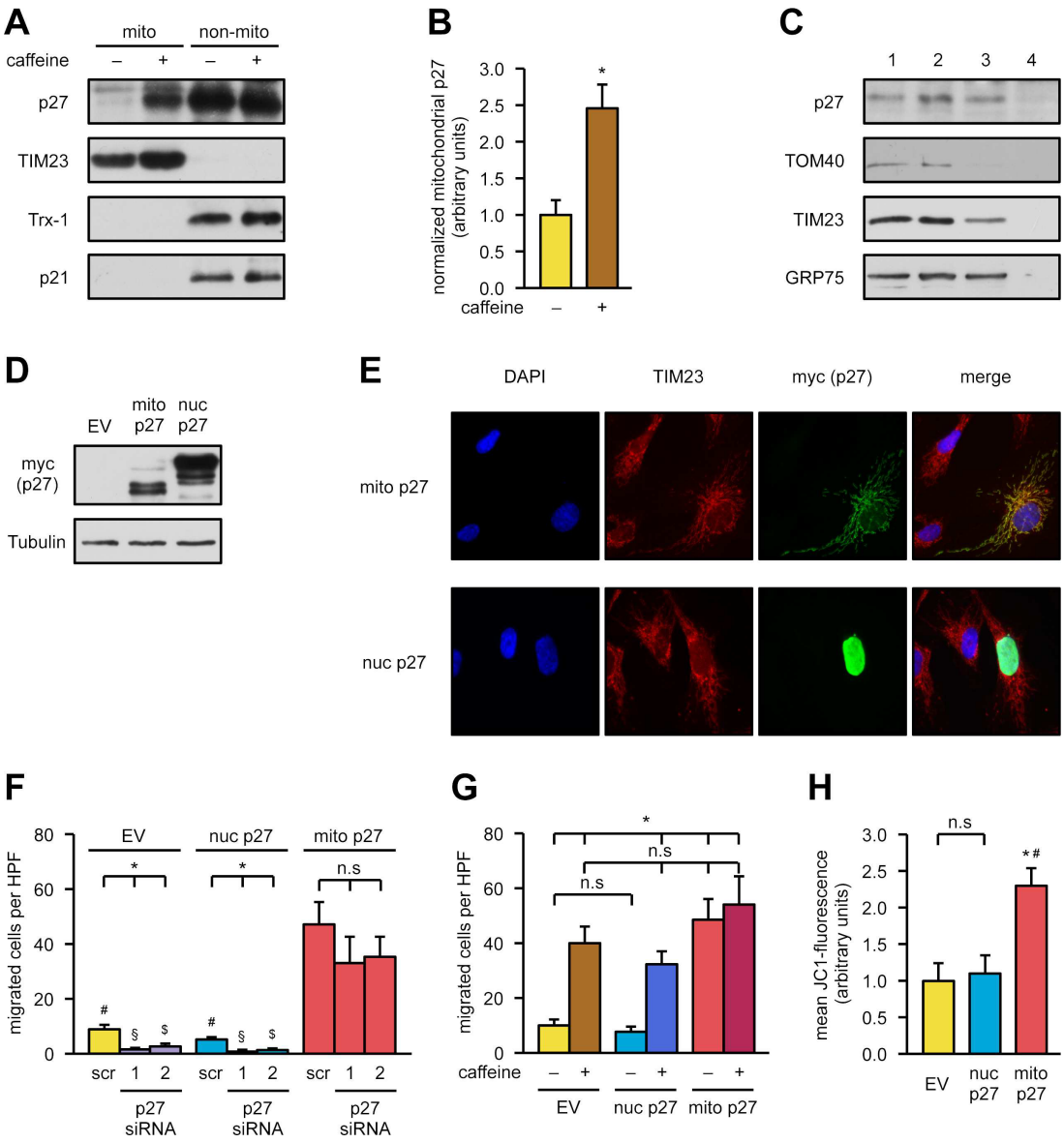

Fig 2. Mitochondrial p27 is sufficient to induce endothelial cell migration. (A, B) Endothelial cells were treated with 50 μM caffeine for 18 hours, and mitochondrial ("mito") and nonmitochondrial ("non-mito") fractions were separated. p27 and the closely related p21 protein were detected by immunoblot; TIM23 and Trx-1 served as purity controls for the fractions. **(A)** Representative immunoblots. **(B)** Semiquantitative analysis of mitochondrial p27 normalized to TIM23. Data are mean ± SEM, $n = 6$, $^{*}p < 0.05$ (two-tailed unpaired t test). **(C)** Proteinase K digestion of mitochondria. The different digestion conditions yield intact mitochondria (1), mitochondria stripped of attached proteins (2), and mitoplasts (3); 4 denotes complete digestion. p27 and marker proteins for the outer (TOM40) or inner (TIM23) mitochondrial membrane and the mitochondrial matrix (GRP75) were detected by immunoblot. **(D, E)** Endothelial cells were transfected with an empty vector ("EV") or expression vectors for nuclear ("nuc p27") or mitochondrial p27 ("mito p27"). Expression and localization of the organelle-targeted p27 proteins were analyzed by immunoblot and immunofluorescence. **(D)** Representative immunoblot, Tubulin served as loading control. Because of the presence of a trimeric nuclear localization signal at the C-terminus, the nuclear-targeted protein has a larger molecular weight. **(E)** Representative immunostainings: nuclei were visualized with DAPI (blue), mitochondria by staining for TIM23 (red), and the targeted p27 variants by staining for the myc epitope ("myc (p27)," green). Merge shows an overlay of all fluorescence channels. **(F)** Endothelial cells were transfected with the siRNAs used in Fig 1. Forty-eight hours later, cells were transfected with an empty vector ("EV") or the expression vectors for nuclear ("nuc p27") or mitochondrial p27 ("mito p27"). Three hours later, a wound was set. Migratory capacity was assessed 18 hours later by counting cells migrated into the wound using Image J. Data are mean ± SEM, $n = 5$: p27 siRNA-1/EV, p27 siRNA-2/EV, p27 siRNA-1/nuc p27, p27 siRNA-1/mito p27; $n = 6$: all others, $^{*}p < 0.05$ versus corresponding scr, $^{\#}p < 0.05$ versus scr/mito p27, $^{\S}p < 0.05$ versus p27 siRNA-1/mito p27, $^{\$}p < 0.05$ versus p27 siRNA-2/mito p27 (one-way ANOVA). **(G)** Endothelial cells were transfected with an empty vector ("EV") or expression vectors for nuclear ("nuc p27") or mitochondrial p27 ("mito p27"). Three hours later, a wound was set, and cells were treated with 50 μM

caffeine for 18 hours or left untreated. Migratory capacity was assessed by counting cells migrated into the wound using Image J. Data are mean ± SEM, $n = 5–7$, $^{*}p < 0.05$ versus EV −caffeine (Mann-Whitney pairwise comparison with Bonferroni-corrected p-values). **(H)** Endothelial cells were transfected with an empty vector ("EV") or expression vectors for nuclear ("nuc p27") or mitochondrial p27 ("mito p27"). Twenty-four hours after transfection, the mitochondrial membrane potential was measured with JC1 using flow cytometry. Data are mean ± SEM, $n = 5$, $^{*}p < 0.05$ versus EV, $^{\#}p < 0.05$ versus nuc p27 (one-way ANOVA). Underlying data are provided in S1 Data. DAPI, 4′,6-diamidino-2-phenylindole; HPF, high power field; n.s., not significant; TIM23, translocase of inner mitochondrial membrane 23; TOM40, translocase of outer mitochondrial membrane 40; Trx-1, thioredoxin-1.

https://doi.org/10.1371/journal.pbio.2004408.g002

p27 is exclusively found in the mitochondria; conversely, nuclear-targeted p27 could only be detected in the nucleus (Fig 2E). We then established a rescue experiment in which endogenous p27 was first knocked down by siRNAs, followed by overexpression of nuclear- or mitochondrially targeted p27. Only mitochondrially targeted p27 rescued the migratory defect induced by knockdown of p27, whereas nuclear-targeted p27 did not improve the migratory capacity (Fig 2F). Next, we investigated whether induction of migration by mitochondrial p27 can be further increased by caffeine. Therefore, we overexpressed mitochondrial p27 in endothelial cells, treated the cells with caffeine, and measured migratory capacity; nuclear-targeted p27 and an empty vector served as controls. Caffeine increased migratory capacity in cells transfected with the empty vector or expressing nuclear p27 (Fig 2G). Without caffeine, only mitochondrially targeted p27 induced migration of endothelial cells; however, the combination of caffeine and mitochondrial p27 did not show any additive effects. Thus, caffeine and mitochondrial p27 either share a common promigratory pathway, or each individual stimulus already induced maximal migratory capacity in these cells (Fig 2G). To evaluate whether mitochondrial p27, but not nuclear p27, improves mitochondrial parameters, we measured mitochondrial membrane potential in endothelial cells overexpressing mitochondrial p27 or nuclear p27, respectively. Only mitochondrially targeted p27 significantly enhanced mitochondrial membrane potential (Fig 2H).

The N- and C-terminus of mitochondrial p27 with serine 10 and threonine 187 are required for migratory capacity of endothelial cells

Given the novelty of our findings, we wanted to understand which domains in p27 could be responsible for its effects on cell migration and mitochondrial functions. Subcellular distribution of p27 was described to be regulated by phosphorylation of at least 4 phosphorylation sites at serine 10, threonine 157, threonine 187, and threonine 198, all of which have been suggested to be important for nonnuclear localization. The role of phosphorylation at these sites is discussed controversially, as it could differ dependent on cell and tumor type or organ system. Nevertheless, as nuclear p27 cannot compensate for the loss of migratory capacity after knockdown of the endogenous protein, it is suggestive that these sites may play a role in migration, which depends on mitochondria. Therefore, we decided to generate p27 mutants with a mitochondrial targeting sequence, in which either the N-terminus with serine 10 (ΔN, amino acids [aas] 25–198 retained), the C-terminus with the other phosphorylation sites (ΔC, aas 1–151 retained), or both (ΔN/ΔC, aas 25–151 retained) were deleted, leaving the cyclin-dependent kinase inhibitor (CDI) domain intact in every construct (Fig 3A). We first confirmed by immunoblotting that all of the mutants are expressed at comparable levels (Fig 3B). Then, we confirmed that the mutants are exclusively localized in the mitochondria (Fig 3C). Next, we examined their impact on functional capacity of human primary endothelial cells by measuring migration and adenosine triphosphate (ATP) content. Cells overexpressing the ΔN or the ΔC mutant showed only a reduced migratory capacity compared to full-length p27, whereas the ΔN/ΔC mutant completely lost the ability to induce migration (Fig 3D). Full-length p27

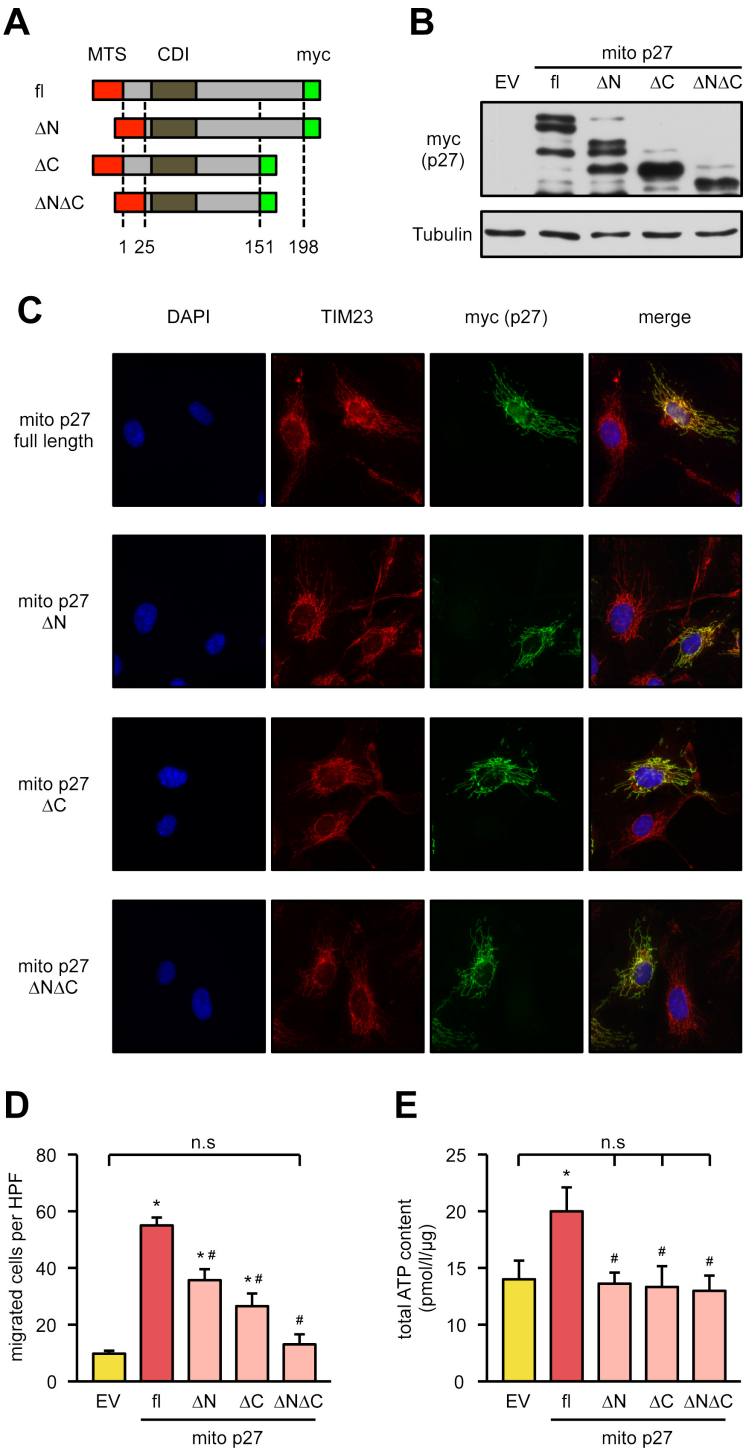

Fig 3. The N- and C-terminus of p27 are required for endothelial cell migration and ATP content. (A) Schematic representation of mitochondrially targeted p27 deletion mutants lacking the N-terminus ("ΔN"), the C-terminus ("ΔC"), or both ("ΔNΔC"). The full-length protein ("fl") and all mutants contain an N-terminal mitochondrial targeting sequence ("MTS," red) and a C-terminal myc tag (green). Numbers indicate the deletion endpoints within p27. **(B-E)** Endothelial cells were transfected with an empty vector ("EV") or expression vectors for the mitochondrially targeted p27 mutants depicted in (A). **(B, C)** Expression and localization of the mitochondrially targeted mutant p27 proteins were analyzed by immunoblot and immunofluorescence. **(B)** Representative immunoblot, tubulin served as loading control. **(C)** Representative immunostainings: nuclei were visualized with DAPI (blue), mitochondria by staining for TIM23 (red), and the targeted p27 mutants by staining for the myc epitope

("myc (p27)," green). Merge shows an overlay of all fluorescence channels. **(D)** Migratory capacity was measured in a scratch wound assay by counting cells migrated into the wound using Image J. Data are mean ± SEM, $n = 6$, $^{*}p < 0.05$ versus EV, $^{\#}p < 0.05$ versus fl mito p27 (one-way ANOVA). **(E)** ATP content was measured with a luminometric assay. Data are mean ± SEM, $n = 5$, $^{*}p < 0.05$ versus EV, $^{\#}p < 0.05$ versus fl mito p27 (one-way ANOVA). Underlying data are provided in S1 Data. ATP, adenosine triphosphate; CDI, cyclin-dependent kinase inhibitor; DAPI, 4′,6-diamidino-2-phenylindole; HPF, high power field; n.s., not significant; TIM23, translocase of inner mitochondrial membrane 23.

https://doi.org/10.1371/journal.pbio.2004408.g003

increased mitochondrial ATP content (Fig 3E). In contrast, this was not observed in cells overexpressing any of the p27 deletion mutants (Fig 3E). These data demonstrate that both the N- and C-terminus of p27 are required for the functional capacity of endothelial cells.

To further narrow down the aas relevant for mitochondrial p27, we focused on serine 10 and threonine 187 as the more likely candidates for phosphorylation because threonine 157 and 198 have been described as relevant for p27/cyclin D1/cyclin-dependent kinase 4 (CDK4) complex assembly and as such for cell cycle regulation [24]. Moreover, for the cardiovascular system, it has been shown that p27 phosphorylation at serine 10 is reduced in murine and human atherosclerotic arteries and that prevention of this phosphorylation aggravates atherosclerosis independent of cell proliferation [25]. Phosphorylation at threonine 187 has been demonstrated to result in proteasomal degradation of p27 in several cancer cells [26]; however, in the cardiovascular system, loss of this phosphorylation did not affect aortic p27 protein levels [27]. Therefore, we first examined whether caffeine induces phosphorylation of p27 at serine 10 and threonine 187. Indeed, 50 μM caffeine increased phosphorylation at both sites by approximately 2-fold (Fig 4A and 4B). Since both the N- and C-terminus are required for the functional capacity of p27 in endothelial cells (Fig 3D and 3E), we generated a mitochondrially targeted, nonphosphorylatable p27(S10A/T187A) double mutant and measured the impact on migratory capacity compared to mitochondrially targeted full-length p27. Besides comparable expression levels between p27 wild type and the mutant (Fig 4C), immunostainings confirmed the mitochondrial localization (Fig 4D). Strikingly, overexpression of this mutant did not induce migration in endothelial cells (Fig 4E). Thus, serine 10 and threonine 187, at least in the mitochondrial fraction of p27, are required for migratory capacity. To elucidate whether these two residues are also necessary for the import of p27 into the mitochondria, we generated an analogous but untargeted p27(S10A/T187A) mutant. Following expression of this variant and the corresponding wild-type protein in endothelial cells, their protein levels in mitochondrial fractions were measured. Interestingly, the ability of p27(S10A/T187A) to become imported into the mitochondria was severely restricted (Fig 4F and 4G), suggesting that the amino acids, which are critical for migratory capacity, are also involved in the translocation into the mitochondria.

Caffeine effects in the heart are linked to mitochondrial p27

It had been assumed that knockout of a cell cycle inhibitor like p27 could be beneficial in the experimental setup of myocardial infarction. This was based on the reasoning that myocardial infarction leads to loss of cells in the heart and that enhanced proliferation of cells in p27-deficient mice may result in smaller infarct size and reduced mortality. However, exactly the opposite was observed. Mice showed bigger infarct size, and the mortality was significantly increased [5,6]. Since functional mitochondria in the heart are required not only to provide energy for the pumping function but also to cope with externally or internally induced changes—e.g., during and after myocardial infarction—we hypothesized that a non-cell cycle–related function of p27, according to our data most likely in the mitochondria, could also be important for the heart. Therefore, we first analyzed the role of mitochondrial p27 in cell death induction in cardiomyocytes—a hallmark of cardiac pathologies [28]. We lentivirally expressed mitochondrially targeted

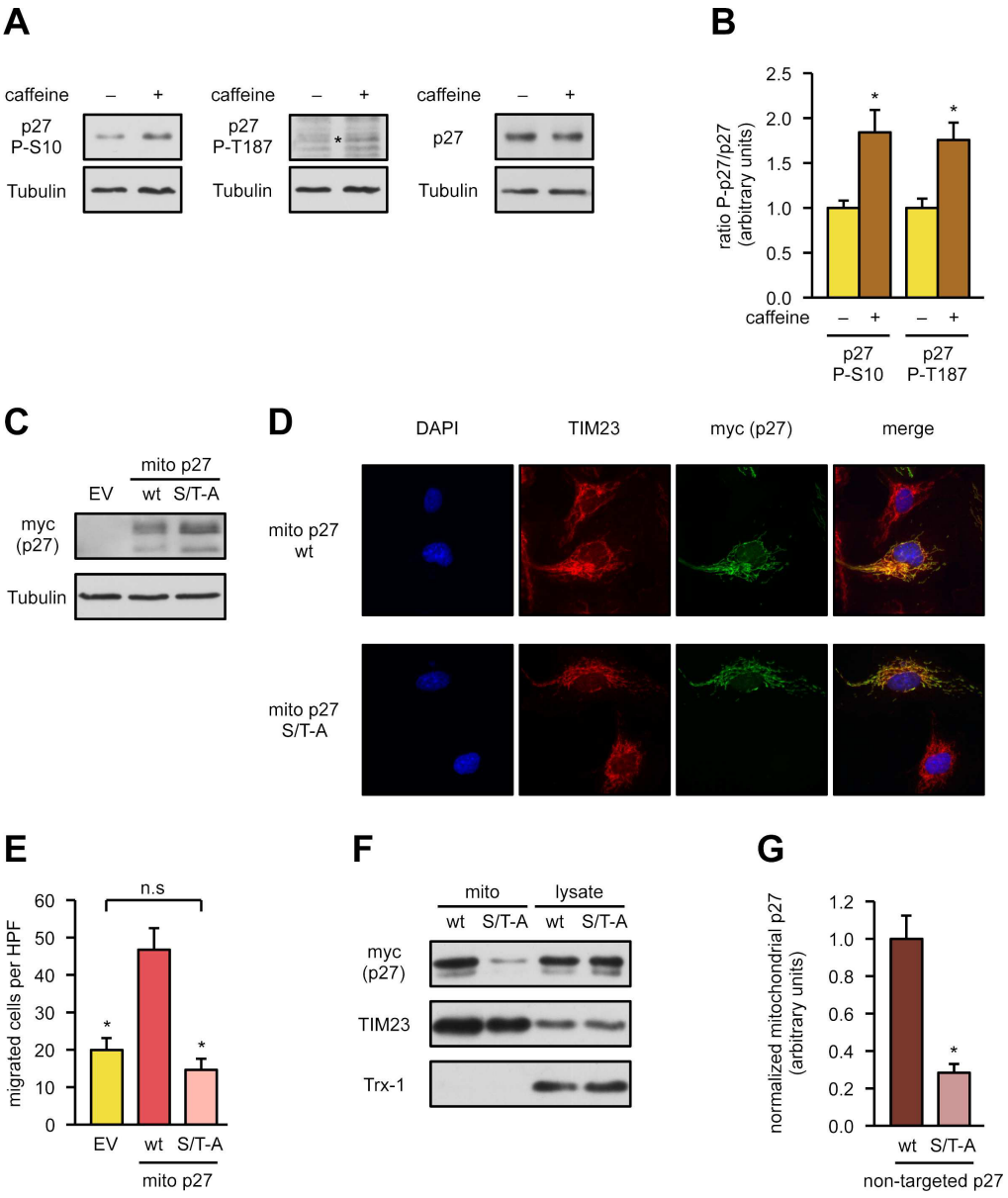

Fig 4. Serine 10 and threonine 187 of p27 are required for endothelial cell migration and mitochondrial import. **(A, B)** Endothelial cells were treated with caffeine for 18 hours or left untreated, and phosphorylation of serine 10 ("p27 P-S10") and threonine 187 ("p27 P-T187), as well as total p27 ("p27"), were detected by immunoblot. **(A)** Representative immunoblots with the corresponding loading control (Tubulin) below the respective immunoblot. The asterisk denotes p27 phosphorylated on threonine 187. **(B)** Semiquantitative analyses of the ratio of phosphorylated p27 to total p27 for both phosphorylation events. Data are mean ± SEM, $n = 7$: p27 P-S10, $n = 6$: p27 P-T187, $^{*}p < 0.05$ (two-tailed unpaired t test). **(C, D)** Endothelial cells were transfected with an empty vector ("EV") and expression vectors for mitochondrially targeted p27 ("mito p27 wt") or a mutant in which serine 10 and threonine 187 were replaced by alanine ("mito p27 S/T-A"). Expression and localization of the corresponding proteins were analyzed by immunoblot and immunofluorescence. **(C)** Representative immunoblot, tubulin served as loading control. **(D)** Representative immunostainings: nuclei were visualized with DAPI (blue), mitochondria by staining for TIM23 (red), and the targeted p27 mutants by staining for the myc epitope ("myc (p27)," green). Merge shows an overlay of all fluorescence channels. **(E)** Endothelial cells were transfected as in (C), a wound was set, and migratory capacity was assessed by counting cells migrated into the wound using Image J. Data are mean ± SEM, $n = 5$, $^{*}p < 0.05$ versus mito p27 wt (one-way ANOVA). **(F, G)** Endothelial cells were transfected with expression vectors for p27 wild type or the corresponding S/T-A mutant, both without a mitochondrial targeting sequence. Mitochondrial fractions ("mito") were prepared, and the expressed proteins were detected by immunoblot. **(F)** Representative immunoblots: the p27 proteins were detected with an anti-myc antibody ("myc (p27)"), TIM23 served as a loading control, and Trx-1 as purity control for the mitochondrial fractions. Analysis of total cell lysates ("lysate") ensures similar expression levels. **(G)**

Semiquantitative analysis of mitochondrial p27 normalized to TIM23. Data are mean ± SEM, $n = 5$, $^{*}p < 0.05$ versus p27 wt (two-tailed unpaired t test). Underlying data are provided in S1 Data. DAPI, 4′,6-diamidino-2-phenylindole; HPF, high power field; n.s., not significant; TIM23, translocase of inner mitochondrial membrane 23; Trx-1, thioredoxin-1.

https://doi.org/10.1371/journal.pbio.2004408.g004

p27 in cardiomyocytes and measured basal and oxidative stress-induced apoptosis. Mitochondrial p27 dramatically reduced basal apoptosis and completely blunted H_2O_2-induced cell death (Fig 5A). As functional mitochondria play a pivotal role in protection against heart disease and p27-deficient mice show increased mortality after myocardial infarction [6], we measured oxygen consumption in heart mitochondria isolated from adult p27-deficient mice and their wild-type littermates as a readout for mitochondrial function. Mitochondria isolated from p27-deficient mice displayed significantly reduced complex I respiration, which demonstrates that those animals have impaired mitochondrial functionality (Fig 5B). To further establish a causal link between caffeine and p27, p27-deficient animals were given 0.05% caffeine in drinking water for 10 days, a concentration for which we had previously shown to result in a serum concentration of approximately 30–50 μM and a time sufficient to completely restore the carotid endothelium after wire injury [8]. Strikingly, caffeine did not improve respiration in hearts of p27-deficient mice (Fig 5B), whereas respiration in wild-type littermates was increased by caffeine. Next, we wanted to determine whether a connection between caffeine and mitochondrial p27 also exists on the transcriptome level. Therefore, p27-deficient animals and their wild-type littermates were given 0.05% caffeine in drinking water for 10 days. After that, RNA was isolated from whole hearts, and microarray analyses were performed. As shown in the Venn diagram in Fig 5C, all but 3 of the 245 transcripts differentially expressed after caffeine administration in wild-type mice were p27-dependent, since only 3 were also regulated in p27-deficient animals. Interestingly, among the most highly enriched gene ontology (GO) categories for biological processes are GO terms describing pathways, which take place in the mitochondria (S1 Table). Strikingly, more than one-third of the transcripts in all other GO categories are translated into proteins localized in the mitochondria (S1 Table), demonstrating that the caffeine-induced, p27-dependent transcriptome changes affect to a large part the mitochondria.

Mitochondrial p27 is required for proper cardiac myofibroblast differentiation

Over the last several years, it has become evident that in several healing processes, including wound healing and the early phase after myocardial infarction, fibroblasts have to differentiate into myofibroblasts to fill the gaps caused by cell loss. Recent findings demonstrated that intact mitochondria are needed for differentiation of fibroblasts into myofibroblasts in response to factors like transforming growth factor β1 (TGFβ1) [9]. Thus, we isolated cardiac fibroblasts from p27-deficient mice and wild-type littermates and induced myofibroblast differentiation by TGFβ1 in the absence or presence of caffeine. TGFβ1 induced myofibroblast differentiation, measured by the up-regulation of α smooth muscle actin (αSMA), only in wild-type cardiac fibroblasts but not in p27-deficient cells (Fig 6). Moreover, caffeine treatment alone slightly but significantly increased αSMA levels, probably by improving mitochondrial function, again only in cells isolated from wild-type animals (Fig 6).

To investigate whether mitochondrial p27 is sufficient to rescue the p27-deficient cells from the differentiation defect, we lentivirally expressed mitochondrially targeted p27 in p27-deficient cardiac fibroblasts. As demonstrated in Fig 7, reexpression of mitochondrial p27 restored the ability of p27-deficient cardiac fibroblasts to differentiate into myofibroblasts upon TGFβ1

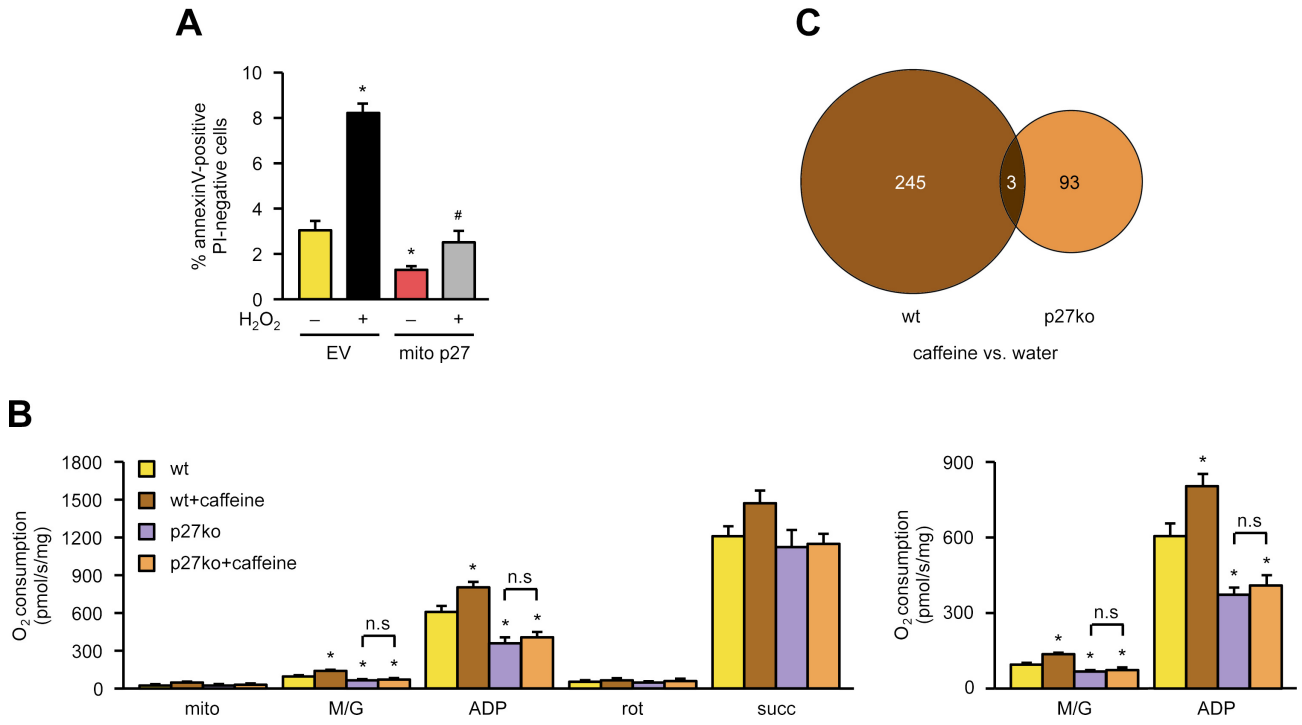

Fig 5. Caffeine effects in the heart depend on p27. (A) The mouse cardiomyocyte cell line HL-1 was lentivirally transduced with an empty vector ("EV") or an expression vector for mitochondrially targeted p27 ("mito p27") and treated with 500 μM H_2O_2 for 48 hours. Apoptosis was measured as annexin V positive/7-PI negative cells by flow cytometry. Data are mean ± SEM, $n = 5$, $^{*}p < 0.05$ versus EV $-H_2O_2$, $^{\#}p < 0.05$ versus EV $+H_2O_2$ (one-way ANOVA). **(B)** Respiration was determined in isolated heart mitochondria of adult wild-type mice ("wt") and p27-deficient littermates ("p27ko"), who had received drinking water without caffeine or water supplemented with 0.05% caffeine for 10 days. Respiration was measured as O_2 consumption without the addition of substrates ("mito") and after the successive addition of malate/glutamate ("M/G"), ADP, rotenone ("rot"), and succinate ("succ") (left panel). The right panel shows a magnification of O_2 consumption after the addition of M/G and ADP, respectively. Data are mean ± SEM, $n = 5$–8 per group, $^{*}p < 0.05$ versus wt without caffeine (one-way ANOVA). **(C)** Adult p27-deficient animals and their wild-type littermates received drinking water or water supplemented with 0.05% caffeine for 10 days. RNAs were isolated from the hearts of those mice, and microarray analyses were conducted. Data are represented as a Venn diagram. The numbers in the circles indicate the number of transcripts regulated in the two genotypes ($n = 3$ animals per genotype and treatment, $p < 0.05$). Underlying data are provided in S1 Data. ADP, adenosine diphosphate; n.s., not significant; PI, propidium iodide.

https://doi.org/10.1371/journal.pbio.2004408.g005

treatment. Thus, we also established a causal link between mitochondrial p27 and the ability of fibroblasts to differentiate into myofibroblasts.

Caffeine—in concert with mitochondrial p27—is protective in mouse models with mitochondrial dysfunction

One hallmark of the murine and human aging process is reduced mitochondrial respiratory capacity. Therefore, we wanted to determine whether a 10-day treatment with caffeine in 22-month-old mice could enhance respiration. Indeed, caffeine increased respiration (Fig 8A). Moreover, the mitochondrial ATP content was increased to roughly the same extent as the mitochondrial oxygen consumption of complex I (Fig 8B). Interestingly, mitochondrial respiration in hearts of adult p27-deficient mice was similar as in 22-month-old wild-type animals (S6 Fig), suggesting that loss of mitochondrial p27 impairs the heart as strongly as aging. This is in accordance with increased infarct size and early mortality after myocardial infarction in p27-deficient mice [6]. Furthermore, 10 days of caffeine treatment in old animals was sufficient to raise the mitochondrial respiration to the levels observed in 6-month-old mice (S6 Fig). In addition, the analysis of cardiac mitochondria from old mice showed a roughly 2-fold

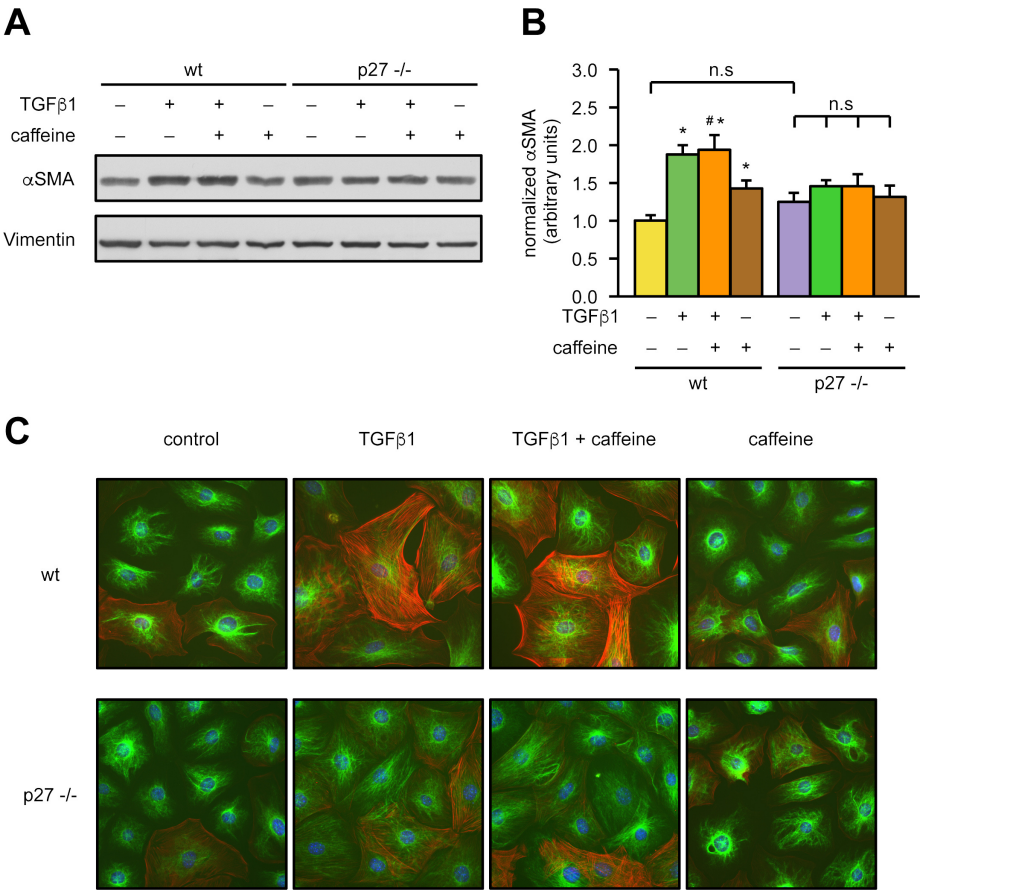

Fig 6. p27 is required for myofibroblast differentiation of cardiac fibroblasts. Cardiac fibroblasts were isolated from hearts of wild-type ("wt") mice and p27-deficient ("p27 −/−") littermates. Myofibroblast differentiation was induced by treatment with 2 ng/ml TGFβ1 for 48 hours in the presence or absence of 50 μM caffeine. Induction of αSMA was detected by immunoblot and immunostaining. **(A)** Representative immunoblots, Vimentin served as loading control. **(B)** Semiquantitative analysis of αSMA normalized to Vimentin. Data are mean ± SEM, $n = 8$: wt untreated, wt +TGFβ1, p27 −/− untreated, p27 −/− +TGFβ1; $n = 5$: all others, $^{*}p < 0.05$ versus wt untreated, $^{\#}p < 0.05$ versus wt +caffeine (one-way ANOVA). **(C)** Representative immunostainings: αSMA was stained in red and Vimentin in green, nuclei were counterstained with DAPI (blue), shown are the overlays of all fluorescence channels. Underlying data are provided in S1 Data. αSMA; α smooth muscle actin; DAPI, 4′,6-diamidino-2-phenylindole; n.s., not significant; TGFβ1, transforming growth factor β1.

https://doi.org/10.1371/journal.pbio.2004408.g006

increase in mitochondrial p27 content after 10 days of caffeine (Figs 8C and 8D and S7), demonstrating that caffeine-induced improved respiration is paralleled by an increase in mitochondrial p27. The amount of mitochondrial p27 in heart mitochondria of old mice after caffeine consumption was comparable to mitochondrial p27 in heart mitochondria of 6-month-old mice (S6 Fig). Thus, treatment of old mice with caffeine for 10 days markedly improved mitochondrial p27 and thus respiration in the heart. In addition, we also treated adult 6-month-old littermates with caffeine for 10 days and analyzed mitochondrial p27 by immunoblot. Similar to old mice, caffeine also increased mitochondrial p27 in adult 6-month-old mice when compared to their wild-type littermates (Fig 8E and 8F).

Not only aging but also obesity and type 2 diabetes have been demonstrated to be associated with mitochondrial dysfunction [29,30]. Therefore, we used a second animal model in which we fed 2-month-old mice a diabetogenic diet (S2 Table) for a total of 9.5 weeks, leading to obesity and a prediabetic state. After that, mice were separated into 2 groups, one of which

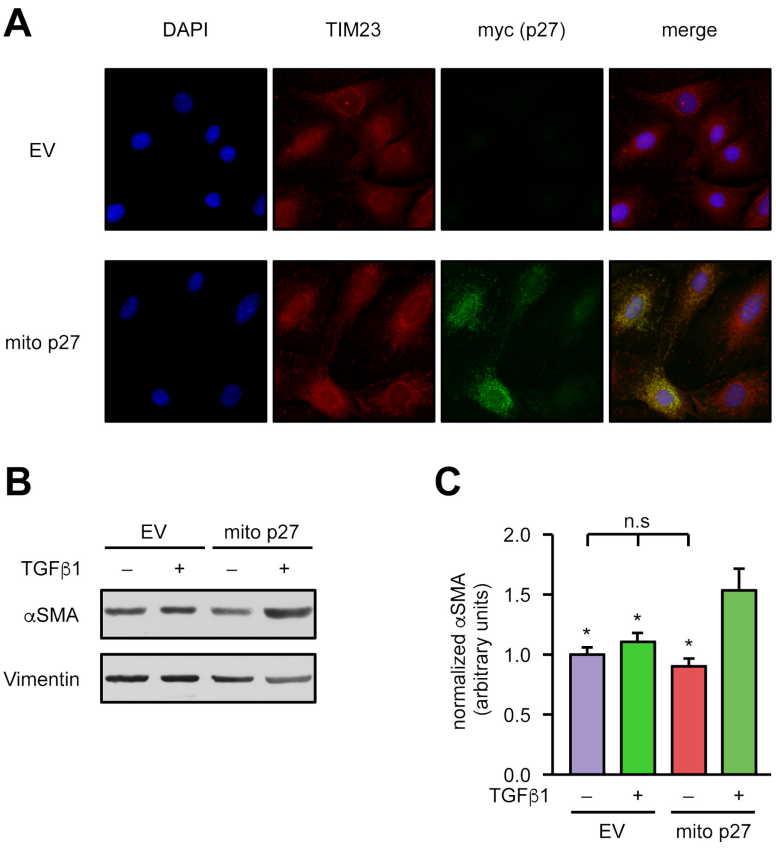

Fig 7. Mitochondrial p27 restores the impaired αSMA up-regulation in p27-deficient cardiac fibroblasts. Fibroblasts isolated from the hearts of p27-deficient mice were lentivirally transduced with an expression vector for mitochondrially targeted p27 ("mito p27") or a corresponding empty vector ("EV"). **(A)** Representative immunostainings: nuclei were visualized with DAPI (blue), mitochondria by staining for TIM23 (red), and the mitochondrially targeted p27 by staining for the myc epitope ("myc (p27)," green). Merge shows an overlay of all fluorescence channels. **(B, C)** Myofibroblast differentiation was induced by treatment with 2 ng/ml TGFβ1 for 48 hours, and αSMA was detected by immunoblot. **(B)** Representative immunoblots, Vimentin served as loading control. **(C)** Semiquantitative analysis of αSMA normalized to Vimentin. Data are mean ± SEM, $n = 5$, $^{*}p < 0.05$ versus mito p27 +TGFβ1 (one-way ANOVA). Underlying data are provided in S1 Data. αSMA; α smooth muscle actin; DAPI, 4′,6-diamidino-2-phenylindole; n.s., not significant; TGFβ1, transforming growth factor β1; TIM23, translocase of inner mitochondrial membrane 23.

https://doi.org/10.1371/journal.pbio.2004408.g007

received caffeine in the drinking water for 10 days. Then, ischemia reperfusion injury was set, and animals were analyzed 3 weeks later. We first measured the scar size of the left ventricle and the minimum left ventricular wall thickness in both groups. Ten days of caffeine treatment significantly reduced scar size and improved wall thickness (Fig 9A, 9B and 9C). Next, we investigated whether caffeine induces translocation of p27 into the mitochondria in this mouse model analogous to our observations in cells and in healthy adult as well as in old mice. Therefore, coimmunostainings of heart slices for p27 and the inner mitochondrial membrane protein TIM23 were performed in the border zone of the infarcted area. Indeed, colocalization of p27 and TIM23 was increased in the animals that had received caffeine, whereas p27 was mostly nuclear in the hearts of the mice on the diabetogenic diet without caffeine supplementation (Fig 9D). To further support the results obtained in tissue slices of the heart, we isolated mitochondria from hearts of mice fed a diabetogenic diet for 11 weeks, with the last 10 days on drinking water or water supplemented with caffeine. In accordance with our

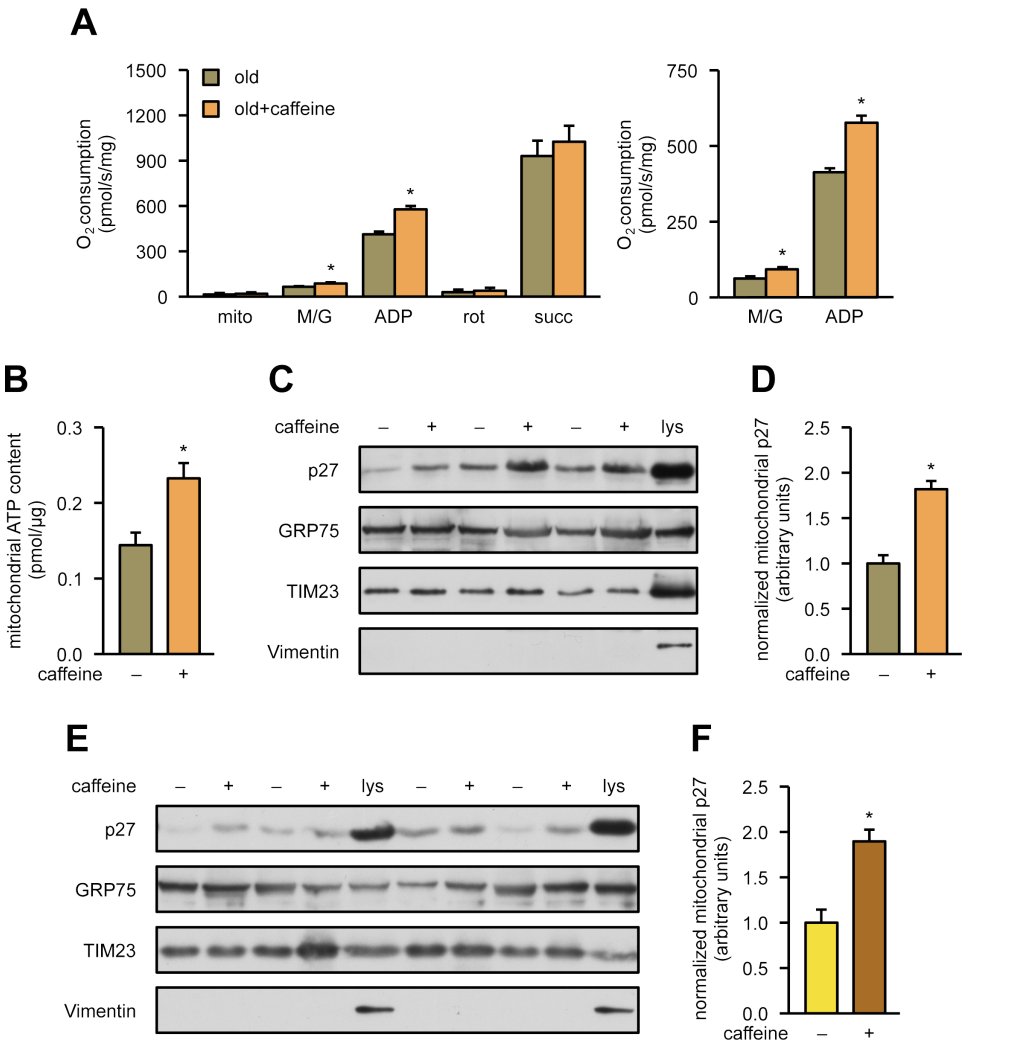

Fig 8. Caffeine enhances respiration, ATP content, and mitochondrial localization of p27 in old mouse hearts. **(A-D)** Twenty-two-month-old wild-type mice received drinking water ("old") or water supplemented with 0.05% caffeine for 10 days ("old+caffeine"). **(A)** O_2 consumption was measured in isolated heart mitochondria without the addition of substrates ("mito") and after the successive addition of malate/glutamate ("M/G"), ADP, rotenone ("rot"), and succinate ("succ") (left panel). The right panel shows a magnification of O_2 consumption after the addition of malate/glutamate and ADP, respectively. Data are mean ± SEM, $n = 6$ per group, $^*p < 0.05$ (one-way ANOVA). **(B)** Mitochondrial ATP content was measured with a luminometric assay. Data are mean, $n = 5$ per group, $^*p < 0.05$ (one-way ANOVA). **(C)** Heart mitochondria were isolated, and p27 was detected by immunoblot; GRP75 and TIM23 served as loading controls. To control for purity of the mitochondria, a total heart lysate ("lys") was used in parallel, and Vimentin was detected. Shown is a representative immunoblot. **(D)** Semiquantitative analysis of mitochondrial p27; data are mean ± SEM, $n = 7$ per group, $^*p < 0.05$ (one-way ANOVA). **(E, F)** Six-month-old wild-type mice received drinking water or water supplemented with 0.05% caffeine for 10 days. **(E)** Heart mitochondria were isolated, and p27 was detected by immunoblot; GRP75 and TIM23 served as loading controls. To control for purity of the mitochondria, a total heart lysate ("lys") was used in parallel, and Vimentin was detected. Shown is a representative immunoblot. **(F)** Semiquantitative analysis of mitochondrial p27; data are mean ± SEM, $n = 5$ per group, $^*p < 0.05$ (one-way ANOVA). Underlying data are provided in S1 Data. ADP, adenosine diphosphate; ATP, adenosine triphosphate; GRP75, 75 KDa glucose-regulated protein; TIM23, translocase of inner mitochondrial membrane 23.

https://doi.org/10.1371/journal.pbio.2004408.g008

coimmunostainings in Fig 9D, p27 was significantly increased in the mitochondria of mice that had received caffeine in their drinking water (Figs 9E, 9F and S7).

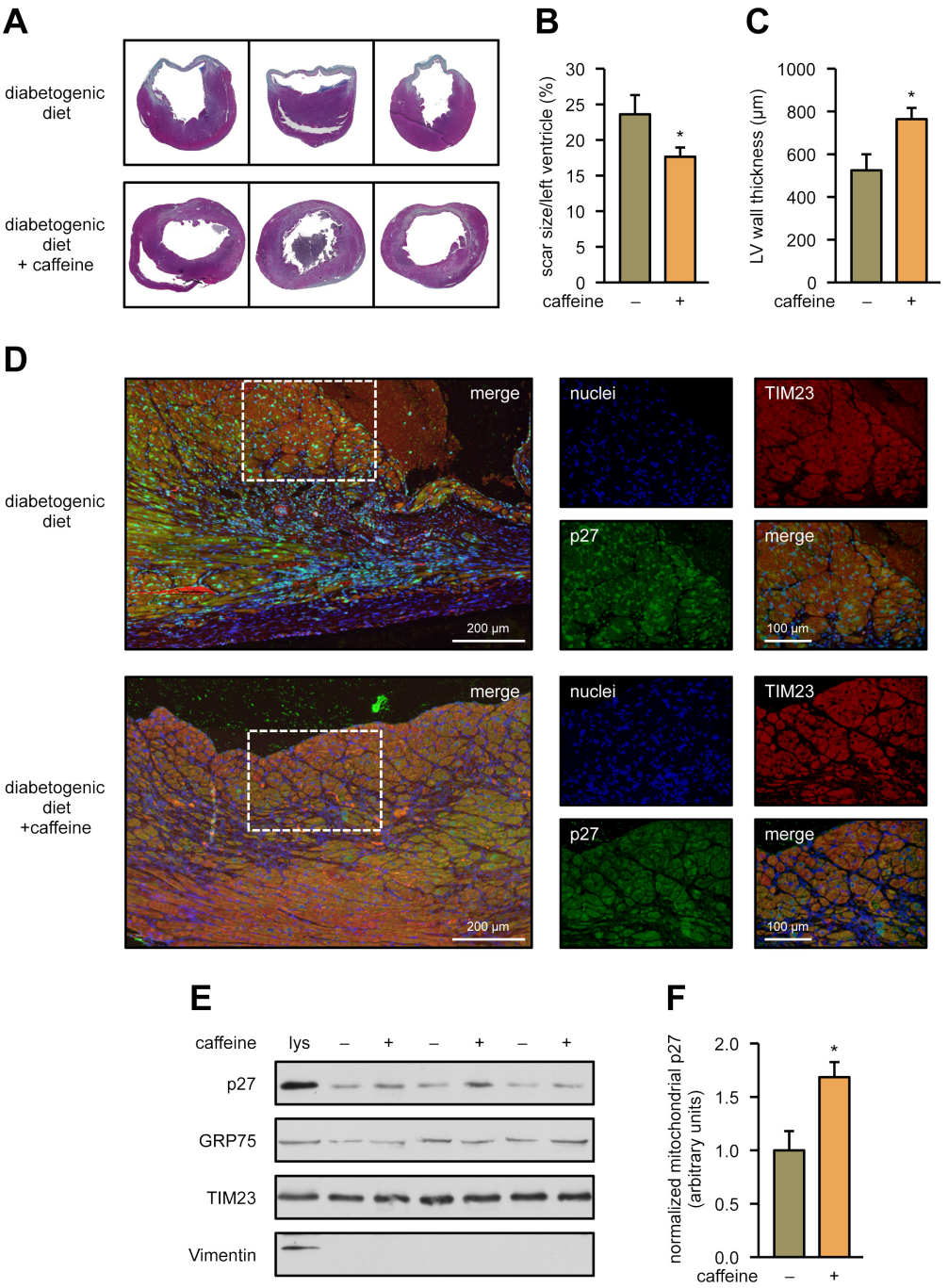

Fig 9. Caffeine improves outcomes after myocardial infarction in prediabetic mice and induces mitochondrial translocation of p27. Two-month-old wild-type mice were fed a diabetogenic diet for 11 weeks. For the last 10 days, one group of animals received drinking water supplemented with 0.05% caffeine. Afterward, myocardial infarction was induced by ligation of the left anterior descending coronary artery for 60 minutes followed by reperfusion. Twenty-one days after infarction, hearts were excised, sectioned, and the sections stained. **(A)** Representative Gomori stainings of sections of 3 different hearts for each dietary regimen. **(B)** Infarct size per left ventricle and **(C)** minimum left ventricular ("LV") wall thickness in the infarcted myocardium. Data are mean ± SEM, $n = 8$: diabetogenic diet, $n = 10$: diabetogenic diet +caffeine, $^{*}p < 0.05$ (one-way ANOVA). **(D)** Representative immunostainings of border zone sections for each dietary regimen. TIM23 is stained in red, p27 in green, nuclei were counterstained with DAPI (blue), merge shows an overlay of all fluorescence channels. The dotted rectangles indicate the sections shown in higher magnifications. **(E)** Heart mitochondria were isolated, and p27 was detected by immunoblot; GRP75 and TIM23 served as loading controls. To control for purity of the mitochondria, a total heart lysate ("lys") was used in parallel,

and Vimentin was detected. Shown is a representative immunoblot. **(F)** Semiquantitative analysis of mitochondrial p27; data are mean ± SEM, $n = 5$, $^{*}p < 0.05$ (one-way ANOVA). Underlying data are provided in S1 Data. DAPI, 4′,6-diamidino-2-phenylindole; GRP75, 75 KDa glucose-regulated protein; TIM23, translocase of inner mitochondrial membrane 23.

https://doi.org/10.1371/journal.pbio.2004408.g009

These data demonstrate that caffeine treatment in obese mice can reduce myocardial infarction injury and, in parallel, increase the levels of mitochondrial p27.

Discussion

Here, we demonstrate that p27 is localized in the mitochondria. Serine 10 and threonine 187 within p27 are required for import into the mitochondria and functional improvements induced by mitochondrial p27. Moreover, mitochondrial p27 is sufficient to improve cellular processes, which depend on functional mitochondria, in different cells of the cardiovascular system. Moreover, it is suggestive to assume that the translocation of p27 into mitochondria might be critically involved in the improved outcomes after myocardial infarction upon caffeine administration. In summary, we present an increase in mitochondrial p27 as a new mode of action for how measurable caffeine concentrations in humans improve the functionality of the cardiovascular system or can even be protective in states associated with increased risk for cardiovascular diseases.

p27 was initially discovered as a nuclear-localized cell cycle inhibitory protein [1]. Previous data demonstrating that p27 can be exported to the cytoplasm [2,3] were considered as a mechanism to inactivate the cell cycle inhibitory effects of p27 in the nucleus and to allow human cancer cells to escape cell cycle arrest. However, McAllister and colleagues demonstrated that nonnuclear p27 is required for migration of fibroblasts, since p27-deficient mouse embryonic fibroblasts failed to migrate, while reconstitution with p27 rescued the motility defect [4]. Here, we show that only mitochondrial p27—but not nuclear p27—rescues the loss of migratory capacity induced by knockdown of endogenous p27, revealing a causal, direct link between mitochondrial localization of p27 and endothelial cell migration. Moreover, serine 10 and threonine 187 are required for import into mitochondria and the promigratory action of mitochondrial p27.

Interestingly, p27 is not the only protein initially described as a cell cycle inhibitor that was subsequently shown to elicit cytoplasmic and mitochondrial functions. In fact, prohibitin and prohibitin-2 were originally characterized as tumor suppressor proteins with antiproliferative activity when present in the nucleus [31–33]. However, when localized in the mitochondria, prohibitins act as mitochondrial membrane–bound chaperones for the stabilization of mitochondrial proteins [34], and interaction of prohibitin with subunits of complex I of the respiratory chain increases mitochondrial activity [35]. Similarly, we show here that p27 is localized within the mitochondria, where it improves mitochondrial functions. Interestingly, prohibitin has also been shown to be required for cell migration [36]. Thus, it is tempting to speculate that mitochondrial p27 exerts chaperone and/or assembly functions by interacting with mitochondrial proteins such as prohibitins, in analogy to nuclear p27, which is required for cyclin D/CDK complex assembly [37]. It is important to note that mitochondrial import of the nonphosphorylatable p27 S10A/T187A mutant is markedly impaired. Thus, serine 10 and threonine 187 are required not only for p27 functions within the mitochondria but also for its import into these organelles. Similar to the p27 S10A/T187A mutant, the mutant that lacks larger regions of the N- and C-termini also showed an impaired impact on migratory capacity compared to intact p27, even when exclusively localized in the mitochondria. These results

confirm the importance of the N- and C-termini of mitochondrial p27 and therein serine 10 and threonine 187 for improving migration of endothelial cells.

Importantly, preserved endothelial cell function accounts for up to 40% of insulin-mediated glucose metabolism in humans [38]. Thus, caffeine-mediated stimulation of the functional capacity of the endothelium may indeed provide a direct mechanistic link for the inverse relationship between habitual coffee consumption and the risk for developing type 2 diabetes mellitus [11]. Moreover, our results with the diabetogenic diet in mice demonstrate that caffeine reduces infarct size in obese, prediabetic mice. Since obesity and type 2 diabetes mellitus increase the risk for myocardial infarction [39,40], coffee consumption—in addition to adequate medication, body weight lowering, and moderate exercise—could help to reduce this risk. Two large cohort studies revealed an association between coffee drinking and reduced mortality. In a prospective study of the National Institutes of Health, coffee drinking was inversely associated with subsequent mortality among 229,119 men and 173,141 women for deaths due to heart disease, respiratory disease, stroke, injuries and accidents, diabetes, and infections [12]. Similar results were obtained in a study with 521,330 participants in 10 European countries [13].

With respect to aging and thus to the elderly population, our data demonstrate that the mitochondrial capacity of the old heart is improved by caffeine to that of the adult heart. Since improving cardiovascular functionality in the elderly population is of major importance for extending health span, coffee consumption or caffeine per se could be considered as an additional protective dietary factor for the elderly population. Indeed, epidemiological analyses provided evidence that habitual intake of caffeinated beverages reduces the risk of heart disease mortality among elderly [14,15]. Moreover, since the caffeine effects are linked to increased mitochondrial p27 and thus improved mitochondrial function, enhancing mitochondrial p27 could serve as a potential therapeutic strategy not only in cardiovascular diseases but also in improving health span.

Materials and methods

Ethics statement

The study does not involve human participants and/or tissue. All experimental protocols for animal studies were approved by the Animal Ethics Committee of the LANUV, Duesseldorf (Az.: 84–02.05.50.15.023, Az.: 84–02.04.2016.A204, Az.: 84–02.04.2015.A322). The anesthetics used are detailed in the sections "Preparation of mouse heart mitochondria" and "Myocardial ischemia and reperfusion".

Experimental animals

p27-deficient mice (B6.129S4-*Cdkn1btm1Mlf*/J) [41] were originally obtained from V. Andres (Madrid, Spain) and backcrossed onto C57BL/6NTac (Taconic) for more than 10 generations. Only heterozygous p27-deficient animals were used as breeders, and the offspring was genotyped with a multiplex PCR using DNA prepared from tail clips with the DirectPCR Lysis Reagent (Mouse Tail; Viagen Biotech). The primers used were p27ko for1 (5′-AGTTGTGCC TTGTATGCTGGT-3′), p27ko rev1 (5′-ACAACAAGCTGGAACCCTGT-3′), and mPGKpA for1 (5′-ATTAAGGGCCAGCTCATTCC-3′). Amplifications were performed for 10 cycles with an annealing temperature starting at 65˚C and a decrease of 1˚C per cycle, followed by 30 cycles with a constant annealing temperature of 56˚C; the extension time in all cycles was 30 seconds. Amplification products were resolved on 1.5% agarose gels, the wild-type allele yields a product of 553 bp, the null allele a product of 325 bp. For all experiments, in which no p27-deficient littermates were required, C57BL/6 animals were purchased from Janvier.

Isolation and cultivation of cardiac fibroblasts and induction of myofibroblast differentiation

Mice were sacrificed by cervical dislocation, the hearts were excised, and all fat and large vessels were removed with a scalpel. Hearts were placed in a culture dish with room-temperature PBS (Thermo Fisher Scientific) supplemented with 1% penicillin/streptomycin (Thermo Fisher Scientific) and 2 mM $CaCl_2$ ($PBS^{(++)}$), and the blood was squeezed out with tweezers. After transfer to a new culture dish with $PBS^{(++)}$, hearts were chopped into small pieces. The pieces were distributed into two 2-ml Eppendorf tubes, each containing 1 ml of a freshly prepared, ice-cold collagenase solution (1 U/ml Collagenase NB 8 Broad Range [Serva] in $PBS^{(++)}$, filter sterilized), and incubated for 15 minutes at 37˚C with gentle mixing every 5 minutes. The cell-containing supernatants were transferred to 2-ml Eppendorf tubes containing DMEM GlutaMAX (Thermo Fisher Scientific) supplemented with 20% fetal bovine serum (Thermo Fisher Scientific) and 1% penicillin/streptomycin to stop the collagenase reaction. After centrifugation for 5 minutes at 400 xg at 4˚C, the pelleted cells were resuspended in 1 ml DMEM GlutaMAX/20% fetal bovine serum/1% penicillin/streptomycin and placed on ice. In parallel, the remainder of the heart pieces was digested again with collagenase under identical conditions. The collagenase digestions were repeated until no more pieces were visible. Finally, all cells were pooled, plated onto a 10-cm culture dish, and placed in a humidified tissue culture incubator at 37˚C in an atmosphere containing 5% CO_2. After 2 hours, all nonadherent cells were carefully aspirated off. Attached cells were washed twice with DMEM GlutaMAX/10% fetal bovine serum/1% penicillin/streptomycin and from then on grown in this medium.

Cell culture

All cells were cultivated in a humidified tissue culture incubator at 37˚C in an atmosphere containing 5% CO_2. Primary human endothelial cells were obtained from Lonza and cultured in endothelial basal medium supplemented with 1 μg/ml hydrocortisone, 12 μg/ml bovine brain extract, 50 μg/ml gentamicin, 50 ng/ml amphotericin B, 10 ng/ml epidermal growth factor (Lonza), and 10% fetal bovine serum until the third passage. After detachment with trypsin, cells were grown for at least 18 hours before transfection or treatment. All experiments were performed in the presence of complete medium including 10% fetal bovine serum.

The murine cardiac muscle cell line HL-1 [42] was a gift from W. C. Claycomb and was cultivated in Claycomb medium (Sigma Aldrich) supplemented with 1% penicillin/streptomycin, 100 μM norepinepherine (Sigma Aldrich), 2 mM L-glutamine (Sigma Aldrich), and 10% fetal bovine serum for as many passages as the cells showed contractile activity in the culture dish.

The human embryonic kidney cell line HEK293FT was obtained from Invitrogen and cultured in DMEM GlutaMAX supplemented with 10% heat-inactivated fetal bovine serum, 1% penicillin/streptomycin, 0.5 mg/ml geneticin (Thermo Fisher Scientific) as selective antibiotic, and 1% nonessential amino acids (Thermo Fisher Scientific).

Cardiac fibroblasts were cultivated in DMEM GlutaMAX supplemented with 10% fetal bovine serum and 1% penicillin/streptomycin (Thermo Fisher Scientific). For the induction of myofibroblast differentiation, the cells were grown for 24 hours in DMEM GlutaMAX/1% fetal bovine serum/1% penicillin/streptomycin before recombinant human TGFβ1 (2 ng/ml; Peprotech) was added for another 48 hours.

Cell lines and primary murine cardiac fibroblasts were routinely tested to be free of mycoplasmas using a PCR-based approach, which detects the most common species of mycoplasmas and includes appropriate internal and positive controls [43].

Transient transfections

Endothelial cells were transfected on 6-cm culture dishes with 3 μg plasmid DNA and 25 μl Superfect (Qiagen) as described previously, with a transfection efficiency of 40% [44]. Endogenous p27 was down-regulated by transfection with 2 different siRNAs (p27 siRNA-1 duplex sense strand: 5′-GCGCAAGUGGAAUUUCGAU-3′; p27 siRNA-2 duplex sense strand: 5′-GAGCCAACAGAACAGAAGA-3′) using JetSi reagent (Eurogentec) according to the manufacturer's instructions. Expression of nuclear- or mitochondrially targeted p27 after knockdown of the endogenous protein was achieved by transfection with Superfect (Qiagen) 18 hours later, using Superfect as described above.

Measurements of cell viability with 3-(4,5-dimethylthiazol-2-yl)-2,5-diphenyltetrazolium (MTT)

Cells were incubated with 0.25 mg/ml MTT in medium for 4 hours. After removing the medium, cells were washed with PBS, and formazan crystals were dissolved with dimethyl sulfoxide (DMSO). The resulting supernatant was measured in a TECAN plate reader at an absorbance of 550 nm. Absorbance of DMSO at 550 nm was subtracted as background.

Scratch wound assay of endothelial cells

For detection of cell migration, wounds were created by scraping confluent cell monolayers with a sterile disposable rubber policeman [45]. Therefore, endothelial cells were grown on 6-cm dishes, which were previously labeled with a trace line. After injury, nonattached cells were removed by gently washing with culture medium. In cases in which migration of transfected cells was analyzed, the wound was set 5 hours after transfection. For caffeine treatments, caffeine was added after the wound was set. Endothelial cell migration from the edge of the injured monolayer was quantified by staining the cells with 20 ng/ml 4′,6-diamidino-2-phenylindole (DAPI; Carl Roth) in PBS after the cells had been fixed with 4% paraformaldehyde for 15 minutes at room temperature. Microscopic pictures were taken using a Zeiss Axiovert 100, and the cells, which had invaded the wound from the trace line, were automatically counted using the particle analysis feature of ImageJ 1.42q [46] after watershed separation of overlapping nuclei.

Cloning of p27 expression vectors

The human p27 coding sequence (NM_004064) without the translation termination codon was amplified from endothelial cell cDNA with primers containing Sal I and Not I restriction sites and inserted into pCMV/myc/nuc and pCMV/myc/mito (Invitrogen) opened with these enzymes to generate expression vectors for nuclear and mitochondrially targeted p27, respectively. An analogous expression vector for nontargeted p27 was created by inserting the p27 coding sequence into pCMV/myc/cyto (Invitrogen). Deletion mutants were created by amplifying subregions of the p27 coding sequence with appropriate primers and insertion into the same vector backbones. Point mutations were introduced by site-directed mutagenesis using the QuikChange Multi Site-Directed Mutagenesis Kit (Agilent Technologies). The starting plasmids were used as empty vectors in the respective transfection experiments.

The lentiviral transfer vector for the expression vector of mitochondrially targeted p27 was created by inserting a DNA fragment containing the CMV promoter and the p27 coding sequence with the N-terminal mitochondrial targeting sequence from the expression vector for mitochondrially targeted p27 into pLKO.1-puro (Sigma Aldrich), which also served as an empty vector for the respective transductions.

The identity of all plasmids was verified by restriction digestion and DNA sequencing. Plasmid DNAs for transfections were purified with the HiSpeed Plasmid Maxi kit (Qiagen) according to the manufacturer's specifications. Concentrations were measured spectrophotometrically using a Nanodrop, and the identity and purity of each preparation was reconfirmed by restriction digestion.

Lentiviral production and transduction

VSV-G pseudotyped lentiviral transduction particles were generated as previously described [47]. Briefly, HEK293FT cells were cotransfected with a transfer vector and expression vectors for the VSV-G envelope protein and lentiviral Gag/Pol, using the Calcium Phosphate Transfection Kit (Invitrogen) according to the manufacturer's instructions. Virus-containing culture supernatants were collected over several days, filtered through a 0.45 μm PVDF membrane, and concentrated by ultrafiltration using Vivacell 100 ultrafiltration units with a PES membrane and a molecular weight cutoff of 100.000 (Sartorius). Concentrated virus particles were dispensed in aliquots and stored at −80˚C. Viral titers were determined with the QuickTiter Lentivirus Titer Kit (Lentivirus-Associated HIV p24; Cell Biolabs). HL-1 cells or murine cardiac fibroblasts were transduced with a multiplicity of infection of approximately 20. The day after transduction, the cells were washed 3 times, the medium was replaced, and the H_2O_2 treatment was started.

Total cell lysis

Cells were scraped off the plates and centrifuged for 10 minutes at 800 xg at 4˚C. After washing with PBS, cells were resuspended in RIPA-buffer (50 mM Tris/HCl pH 8, 1% IGEPAL CA-630, 150 mM NaCl, 0.1% SDS, 0.5% desoxycholate) supplemented with protease inhibitor cocktail and phosphatase inhibitor cocktail (both Bimake) and lysed for 30 minutes at 4˚C. Lysates were centrifuged at 18.000 xg, and supernatants were transferred to fresh, precooled Eppendorf tubes.

Fractionation of cells

Cells were scraped off the plates and centrifuged for 10 minutes at 800 xg at 4˚C. After washing with PBS, cells were resuspended in mitochondrial isolation buffer (20 mM HEPES, pH 7.4, 10 mM KCl, 5 mM $MgCl_2$, 1 mM EDTA, 1 mM EGTA, 250 mM sucrose), incubated for 3 minutes on ice, and then disrupted using a Dounce homogenizer. Cellular debris was removed by centrifugation for 10 minutes at 3.000 xg at 4˚C. The resulting supernatant was transferred to a new tube and centrifuged again for 15 minutes at 10.000 xg at 4˚C. The resulting pellet was washed at least 3 times with mitochondrial isolation buffer. Finally, the pellet was resuspended in mitochondrial isolation buffer and used for further analyses. The resulting supernatant was collected as a nonmitochondrial fraction.

Proteinase K digestion of mitochondria

Proteinase K digestion of mitochondria was performed essentially as previously described by us [53]. Briefly, to determine where in the mitochondria a protein is localized, 300 μg of mitochondria were distributed in 4 equal aliquots. Mitochondria were pelleted for 5 minutes at 10.000 xg at 4˚C and incubated at 4˚C on a shaker in 40 μl of 3 different buffers for 20 minutes. Buffer 1 (isotonic buffer): 250 mM sucrose, 1 mM EGTA, 10 mM HEPES, pH 7; Buffer 2 (hypotonic buffer): 1 mM EGTA, 10 mM HEPES, pH 7, 25 μg/ml proteinase K; Buffer 3 (hypotonic buffer with detergent): 1 mM EGTA, 10 mM HEPES, pH7, 1% Triton-X100, 25 μg/ml

proteinase K. After 20 minutes, digestion was stopped by adding phenylmethylsulfonyl fluoride to a final concentration of 2 mM, and incubation continued for a further 5 minutes with shaking. Aliquot 3 was boiled for 5 minutes in Laemmli-buffer. Aliquot 1 and 2 were washed once with Buffer 1 and resuspended in 40 μl RIPA-buffer (50 mM Tris/HCl pH 8, 1% IGEPAL CA-630, 150 mM NaCl, 0.1% SDS, 0.5% desoxycholate) and boiled for 5 minutes in Laemmli-buffer.

Sodium dodecyl sulfate polyacrylamide gel electrophoresis (SDS-PAGE) and immunoblotting

Electrophoretic separation of proteins with SDS-PAGE and blotting onto polyvinylidene difluoride membranes were performed according to standard methods. Detection of the different proteins was performed with antibodies directed against p27 (clone D37H1, Cell Signaling Technology, 1:300), phospho-p27 (S10; clone EP233(2)Y, Abcam, 1:300), phospho-p27 (T187; polyclonal, ab75908, Abcam, 1:300), TIM23 (clone 32, BD Biosciences, 1:2,000), TOM40 (polyclonal sc11414 and monoclonal, sc365467, Santa Cruz Biotechnology, 1:400), Trx-1 (clone 3A1, Abcam, 1:1,000), GRP75 (clone D13H4, Cell Signaling Technology, 1:500), γ-Actin (clone 2–2.1.14.17, Sigma Aldrich,1:5,000), α-Tubulin (clone DM1A, Sigma Aldrich, 1:50,000), myc-tag (rabbit clone 71D10 or mouse clone 9B11, Cell Signaling Technology, 1:500), Vimentin (clone EPR3776, Abcam, 1:12,000), αSMA (polyclonal, ab5694, Abcam, 1:6,000), PDE5A (polyclonal, #2395, Cell Signaling Technology, 1:10,00), phospho-PDE5A (S92 in mouse, S102 in human; polyclonal, GTX36930, Genetex, 1:250), PDE4A (polyclonal, ab200383, Abcam, 1:500), and phospho-PDE4A (serine 686/688; polyclonal, NB300-635, Novus Biological, 1:1,000). After protein transfer, membranes were incubated with primary antibodies overnight at 4˚C before they were washed and incubated with secondary antibodies (anti-mouse IgG, HRP-linked whole Ab from sheep, NA931V, GE Healthcare Life Sciences, anti-rabbit IgG, HRP-linked whole Ab from donkey, NA934V, GE Healthcare Life Sciences) according to standard procedures. Detection was performed by enhanced chemiluminescence using the ECL reagent (GE Healthcare) and standard X-ray films. Semiquantitative analyses were performed on scanned X-ray films using ImageJ 1.42q [46].

ATP measurements

ATP levels in total cell lysates and mitochondria preparations were determined with the luminescence-based ATP Kit SL (BioThema). ATP concentrations were calculated according to the manufacturer's recommendations.

Mitochondrial membrane potential

JC1 dye exhibits potential-dependent accumulation in mitochondria, indicative by a fluorescence emission shift from green (approximately 529 nm) to red (approximately 590 nm). Consequently, mitochondrial depolarization is indicated by a decrease in the red/green fluorescence intensity ratio. Therefore, cells were incubated with JC1 at a final concentration of 0.5 μM for 30 minutes. Cells were washed twice with PBS, and fluorescence intensities were determined using a FACSCalibur (Becton Dickinson). Mean red JC1 fluorescence was calculated.

Immunostaining of cells

For the detection of nuclear- and mitochondrially targeted p27, cells were fixed in 4% paraformaldehyde and permeabilized using 0.3% Triton-X 100/3% bovine serum albumin in PBS. For

coimmunostaining, cells were first incubated with a mouse antibody against myc-tag (clone 9E10, Santa Cruz Biotechnology, 1:50) at 4˚C overnight, and a Rhodamine Red-X-conjugated Fab fragment anti-mouse was used as secondary antibody (Jackson ImmunoResearch, 1:300, 1 hour, room temperature). Afterward, cells were incubated with a rabbit anti-TOM40 antibody (polyclonal, sc11414, Santa Cruz Biotechnology, 1:50) at room temperature overnight and an Alexa 488 anti-rabbit secondary antibody (Invitrogen, 1:200, 1 hour, room temperature). Nuclei were counterstained with DAPI.

For the localization studies of mitochondrially targeted p27 deletion mutants, endothelial cells were stained for mitochondria using Mito Tracker Red CMXRos (Thermo Fisher Scientific, 1:50,000, 30 minutes, room temperature). Subsequently, cells were washed with PBS and fixed for 15 minutes with 4% paraformaldehyde. For permeabilization, 0.3% Triton X-100 and 3% bovine serum albumin in PBS were used for 15 minutes. Afterward, cells were incubated with an FITC-coupled anti-myc-tag antibody (clone 9E10, Santa Cruz Biotechnology, 1:50) at 4˚C overnight. Nuclei were visualized with 20 ng/ml DAPI in PBS. Cells were washed with PBS and mounted with ProLong Gold antifade mounting medium (Invitrogen).

A direct immunostaining of αSMA and Vimentin was performed in mouse cardiac fibroblasts. Cells were fixed and permeabilized as described above. An Alexa-Fluor 594 conjugated antibody against αSMA (clone 1A4, Abcam, 1:100) and an Alexa-Fluor 488 conjugated anti-Vimentin antibody (clone, D21H3, Cell Signaling Technology, 1:100) were incubated at 4˚C overnight. Afterward, nuclei were stained with DAPI, and cells were mounted as above. All primary antibodies were diluted in PBS containing 1% bovine serum albumin.

Fluorescence images were taken with a Zeiss AXIOVERT 200 M or a Zeiss Axio Imager M2.

Apoptosis measurement

Detection of apoptosis was performed by flow cytometry using annexin V–APC binding and 7-amino-actinomycin (7-AAD) staining as described previously [48]. Only annexin V positive/ 7-AAD negative cells were counted truly apoptotic.

RNA isolation and microarrays

RNA was isolated from mouse hearts using Trizol according to the manufacturer's instruction (Invitrogen) and subjected to a second purification step using RNeasy columns (Qiagen). RNA integrity was checked on an Agilent 2100 Bioanalyzer, and concentrations were determined by photometric Nanodrop measurement. All samples in this study showed common high-quality RNA Integrity Numbers (RIN 9.7–10).

To study the differences in gene expression between wild-type mice and their p27-deficient littermates in response to caffeine, we used oligonucleotide-based microarrays. The *Mus musculus* AROS Oligo Set V4.0 was obtained from Operon. Oligonucleotides (70 mers) were dissolved in amino spotting buffer to a concentration of 20 μM (Genetix) and spotted onto UltraGap slides (Corning). After the printing process, the oligonucleotides were UV cross-linked (630 mJ/cm2) to the slide surface (NCBI Gene Expression Omnibus Platform GPL5403).

Labeled cRNA probes were synthesized from 500 ng of total RNA using the Quick Amp Labeling Kit (one-color; Agilent Technologies) according to the manufacturer's protocol. Prior to hybridization, the slides were incubated in a prewarmed BSA blocking solution containing 5x SSC, 0.1% SDS, and 0.1 mg/ml BSA at 42˚C for 45 to 60 minutes. Subsequently, slides were rinsed twice in 0.1x SSC for 5 minutes and for 30 seconds in double-distilled water, both at room temperature. The slides were then dried in a nitrogen flow. Cy3-labeled cRNA samples (2.5 μg) were dissolved in hybridization buffer (final concentration 50% formamide,

5x SSC, 0.1% SDS). Hybridization was carried out in a humid chamber at 42˚C for 16 hours. After the hybridization step, unbound cRNA and hybridization buffer were removed by several washing steps (2 times for 10 minutes 2x SSC, 0.1% SDS; 5 times for 1 minute 0.1x SSC; and 10 seconds 0.01x SSC).

Fluorescence signals were visualized by a GenePix 4000B laser scanner (Axon). GenePix Pro software (v. 6.0) was used to calculate fluorescence intensities. Data analyses on microarray probe signal intensities were conducted with GeneSpring GX software (v. 11.0.2; Agilent Technologies). Probe signal intensities were quantile normalized across all samples to reduce inter-array variability. Input data preprocessing was concluded by baseline transformation to the median of all samples. To further improve signal-to-noise ratio, a given probe had to be expressed above background (i.e., fluorescence signal of the probe was detected within the 20th and 100th percentiles of the raw signal distribution of a given array) in all 3 replicates in at least 1 of 2 or both conditions to be subsequently analyzed in pairwise comparisons. Differential gene expression was statistically determined by unpaired *t* tests. The significance threshold was set to $p < 0.05$.

GO analyses were performed using DAVID [49,50]. GO category enrichment was statistically evaluated by modified Fisher Exact testing in DAVID (EASE scoring). Additionally, fold enrichment was determined as the ratio of 2 proportions: (1) number of genes associated with a defined biological process in the experimental data set/total number of differentially expressed genes in the experimental data set versus (2) total number of genes associated with a defined biological process in the reference data set/total number of genes in the reference data set. Information about subcellular localization of differentially expressed transcripts was taken from the COMPARTMENTS database [51].

Preparation of mouse heart mitochondria

Animals were killed by exsanguination under deep anesthesia using Ketamine/Xylazine (12/1.6 mg/kg body weight). Hearts were prepared after perfusion with ice-cold PBS and cut into halves. The halves were snap frozen in liquid nitrogen and stored at −80˚C. After thawing, intact heart mitochondria were prepared as described earlier for mitochondria from rat organs [52]. Buffer volumes were reduced by a factor of approximately 2 to account for the lower organ size in mice. In detail, fat, clotted blood, auricles, and fasciae were removed from dry hearts. Hearts were cut into 1–2 mm pieces. Pieces were collected in 10 ml of washing buffer (0.3 M sucrose, 10 mM HEPES pH 7.2, 0.2 mM EDTA), 250 μl Trypsin (bovine pancreas type I, Sigma) of a 2.5 mg/ml stock solution was added, and minced tissue was further homogenized with an Ultra Turrax (IKA-TIO Basic; 3 × 5 seconds). After constant stirring for 15 minutes, 5 ml of mitochondria isolation buffer (20 mM HEPES, pH 7.4, 10 mM KCl, 5 mM $MgCl_2$, 1 mM EDTA, 1 mM EGTA, 250 mM sucrose) containing 3.25 mg Trypsin inhibitor (*Glycine max*, Sigma) was added. Samples were centrifuged for 10 minutes at 900 xg at 4˚C to remove debris. The resulting supernatant was transferred to a fresh Eppendorf tube and centrifuged again for 15 minutes at 10,000 xg at 4˚C. After centrifugation, the supernatant was discarded, and the pellet was rinsed twice with fresh mitochondrial isolation buffer, removing the fluffy white outer rim layer. The resulting brown pellet containing intact mitochondria was resuspended in mitochondria isolation buffer.

Mitochondrial respiration

The rate of mitochondrial respiration was monitored at 25˚C using an Oxygraph-*2k* system (Oroboros) equipped with 2 chambers and DatLab software as previously described, with slight modifications [53]. In detail, 200–300 μg of heart mitochondria were added to 2 ml of a

buffer containing 200 mM sucrose, 10 mM potassium phosphate, 0.1% bovine serum albumin, 10 mM Tris-HCl, 10 mM $MgSO_4$, and 2 mM EDTA, pH 7.0; and respiration was measured. Oxygen consumption was measured after the addition of the NADH-generating substrates malate (0.5 mM) and glutamate (0.5 mM). Then, ADP (0.15 mM) was added. To inhibit complex I activity, rotenone was added to a final concentration of 100 nM. Then, succinate (10 mM) was added, and complex II–dependent respiration was determined. Finally, KCN (2 mM) was added to inhibit complex IV activity.

Heart mitochondria from p27-deficient and wild-type littermates were always measured blinded in parallel, using the same conditions. The same setup was applied to measure respiration of heart mitochondria isolated from mice that had received caffeine with the drinking water or water. For each preparation, a second set of measurements was performed in a cross-over design.

Diabetogenic diet

Male mice at the age of 7–8 weeks were fed a diabetogenic diet (S7200-E010, EF Bio-Serv F1850mod; containing 24% sucrose, 35.85% lard, Ssniff) for 9.5 weeks, leading to a prediabetic state and increased body weight gain. After that, animals were randomized to a control group (diabetogenic diet) or a group receiving additional 0.05% caffeine in the drinking water (diabetogenic diet + caffeine) 10 days prior to ischemia induction. Caffeine treatment was continued until the end of the experiment 3 weeks post ischemia. The composition of the diabetogenic diet is detailed in S2 Table.

Myocardial ischemia and reperfusion

A closed-chest model of reperfused myocardial infarction was utilized. Mice were anesthetized by intraperitoneal injection of ketamine (100 mg/kg body weight) and xylazine (10 mg/kg body weight), intubated, and ventilated with a tidal volume of 10 μl/g body weight at a rate of 140 strokes/minute (two-thirds air, one-third oxygen and isoflurane 2.0 vol.% [Forene, Abbott GmbH]). Mice were placed in a supine position on a 38˚C warmed plate to maintain body temperature. After a left lateral thoracotomy between the third and four rib, the pericardium was dissected, and a 7–0 surgical suture was passed underneath the left anterior descending coronary artery (LAD). Both ends of the surgical suture were threaded through a 1-mm section of PE-20 tubing, forming a loose snare around the LAD, and were exteriorized to the left side of the thorax. The suture was left in the subcutaneous tissue. At 3 days postinstrumentation, the animals were reanesthetized by mask inhalation of isoflurane 2.0 vol.% and a mixture of one-third oxygen and two-thirds room air. Mice were placed in a supine position on a 38˚C warmed plate to maintain body temperature. The skin was reopened, and after dissecting the loop, both ends of the applied suture were gently pulled tight until ST-elevation appeared on the ECG. After 60 minutes of ischemia, reperfusion was accomplished by cutting the suture close to the chest wall. Reperfusion was confirmed by reduction of ST-elevation. Reperfusion was performed for 21 days. We strictly adhered to ischemia induction between 8 AM and 11 AM to ensure equal ischemia and reperfusion tolerance.

Wall thickness and scar size determination

Three weeks post ischemia and reperfusion, animals were killed by CO_2, and hearts were excised and rinsed in PBS. After dehydration, hearts preserved in Roti-Histofix 4% (Carl Roth) for 24 hours were paraffin-embedded and cut into 5-μm sections in 10 levels (approximately 100 μm) beginning from the apex up to the ligation side, discarding 250 μm between each level. To calculate scar size, fibrous area, and wall thickness, sections were stained with

Gomori's one-step trichrome staining. The heat-fixed sections were deparaffinized twice in Roti-Clear (Carl Roth) for 15 minutes and then rehydrated with a graded ethanol series to dH_2O. Sections were incubated in Bouin's solution (Sigma Aldrich) at 58˚C for 15 minutes. After 5 minutes of rinsing under running water, nuclear staining was performed with Weigert's iron hematoxylin A and B for 5 minutes (1:1, Sigma Aldrich). The sections were rinsed again for 5 minutes with running water followed by 25 minutes of incubation with Gomori's staining solution (chromotrope 2R, methylenblue, glacial acetic acid, phosphotungstic acid). Sections were briefly rinsed with water and 0.5% acetic acid 2x 2 minutes. Then sections were treated with an ascending alcohol series and Roti-Clear (2 x 5 minutes) and covered with Roti-Mount mounting medium (Carl Roth). Images were taken with a Zeiss Axio Imager M2. The circumference of the entire endocardium and epicardium and the thickness and length of the infarcted portion, fibrous area, and the left ventricle cavity area were determined using Diskus View software (Hilgers). Setting of the myocardial infarctions and scoring of scar size and left ventricular wall thickness were conducted in a blinded fashion and confirmed by an independent blinded observer.

Immunostaining of heart slices

The sections were stained with antibodies against p27 (polyclonal, PA5-27188, Thermo Fisher Scientific, 1:25) and TIM23 (clone 32, BD Biosciences, 1:100). The sections were deparaffinized with xylene and rehydrated by a descending alcohol series. For p27 and TIM23, a basic target retrieval solution boiled for 20 minutes in Tris/EDTA buffer pH 9.0 (Dako) was required. The sections were cooled down, washed with PBS, and incubated with 4% formalin for 20 minutes in a wet chamber. Then, slices were rinsed with PBS and were treated with blocking solution Tris Buffered Saline (50 mM Tris-HCl, 150 mM NaCl, 2.5 mM KCl, pH 8.0) supplemented with 10% fetal bovine serum/3% goat serum/0.1%Triton-X 100 for 1 hour in a wet chamber. The sections were incubated with the primary antibodies overnight at 4˚C in a wet chamber. Next, the slices were washed with PBS; the incubation with the respective secondary antibodies (anti-rabbit IgG (H + L) cross-absorbed antibody, Alexa Fluor 647, A21244, Thermo Fisher Scientific, 1:200; and anti-mouse IgG (H + L) cross-absorbed antibody, Alexa Fluor 568, A11004, Thermo Fisher Scientific, 1:200) was performed for 1 hour in a wet chamber. The sections were covered with ProLong Diamond antifade mounting medium with DAPI (Invitrogen). Fluorescence images were taken with a Zeiss Axio Imager M2.

Statistics

The number of experiments (*n*) given in the figure legends represents independent biological replicates. Normal distribution for all data sets was confirmed by Shapiro-Wilk test; homogeneity of variances (from means) between groups was verified by Levene's test. Pairwise comparisons were performed with two-sided, unpaired Student *t* tests on raw data. Multiple comparisons were performed using one-way ANOVA with post-hoc Tukey HSD test. Sample sizes for experiments, which were based on the respective statistical tests for data analyses, were calculated employing G*Power version 3.1.9.2 [54]. Effect strength for this power calculation was taken from our earlier studies [8,44,53]. Significance level (α-error) and sensitivity (β-error) were set to 0.05 and 0.95, respectively.

Supporting information

S1 Fig. Caffeine induces migration despite specific adenosine receptor 2A or 2B inhibition. **(A)** A wound was set in a confluent monolayer of primary human endothelial cells, and the cells were treated with or without 50 μM caffeine and/or 100 nM SCH442416, a specific

adenosine 2A receptor inhibitor, for 18 hours. Migratory capacity was assessed by counting cells migrated into the wound, using Image J. Data are mean ± SEM, $n = 5–6$, $^{*}p < 0.05$ versus untreated, $^{\#}p < 0.05$ versus SCH442416 (one-way ANOVA). **(B)** A wound was set, and cells were treated with or without 50 μM caffeine and/or 100 nM GS6201, a specific adenosine 2B receptor inhibitor, for 18 hours. Migratory capacity was assessed by counting cells migrated into the wound, using Image J. Data are mean ± SEM, $n = 6–7$, $^{*}p < 0.05$ versus untreated, $^{\#}p < 0.05$ versus GS6201 (one-way ANOVA). Underlying data are provided in S1 Data. n.s., not significant.
(TIF)

S2 Fig. Caffeine does not induce phosphorylation of PDE4A and PDE5A. Endothelial cells were treated with 50 μM caffeine for 18 hours, and PDE4A P-S686/688 and PDE5A P-S102, as well as total PDE4A and PDE5A, were detected by immunoblot. **(A)** Shown are 3 independent biological replicates for PDE4A P-S686/688 and PDE4A with the corresponding loading controls (Tubulin). **(B)** Semiquantitative analyses of the ratios of phospho PDE4A to total PDE4A. Data are mean ± SEM, $n = 5$ (two-tailed unpaired *t* test). **(C)** Shown are 3 independent biological replicates for PDE5A P-S102 and PDE5A with the corresponding loading controls (Tubulin). **(D)** Semiquantitative analyses of the ratios of phospho PDE5A to total PDE45A. Data are mean ± SEM, $n = 5$ (two-tailed unpaired t-test). Underlying data are provided in S1 Data. n.s., not significant; PDE4A, phosphodiesterase 4A; PDE4A P-S686/688, phosphorylation of serine 686 and 688 in PDE4A; PDE5A, phosphodiesterase 5A; PDE5A P-S102, phosphorylation of serine 102 in PDE5A.
(TIF)

S3 Fig. Original blots used for the quantitation of the siRNA-mediated p27 knockdown. p27 was knocked down in endothelial cells by transfection with 2 different siRNAs targeting the p27 mRNA (p27 siRNA-1, p27 siRNA-2) or a scrambled siRNA ("scr") as control, and p27 levels were determined by immunoblot. Shown are the blots for the 5 biological replicates used for the quantitation shown in Fig 1B. The levels of p27 were normalized to actin or tubulin, respectively. siRNA, small interfering RNA.
(TIF)

S4 Fig. siRNA-mediated knockdown of p27 does not affect cellular and mitochondrial morphology. p27 was knocked down in endothelial cells by transfection with 2 different siRNAs targeting the p27 mRNA (siRNA p27-1, siRNA p27-2) or a scrambled siRNA ("scr") as control. Intact cell morphology is shown in the brightfield images. To show the mitochondrial network and p27 distribution and levels, nuclei were visualized with DAPI (blue), mitochondria by staining for TIM23 (red), and p27 with a p27 antibody (green). Merge shows an overlay of all fluorescence channels. DAPI, 4′,6-diamidino-2-phenylindole; siRNA, small interfering RNA; TIM23, translocase of inner mitochondrial membrane 23.
(TIF)

S5 Fig. Original blots used for the quantitation of the caffeine-induced mitochondrial translocation of p27. Endothelial cells were treated with 50 μM caffeine for 18 hours, and mitochondrial ("mito") and nonmitochondrial ("non-mito") fractions were separated. p27 levels in the mitochondrial fractions were determined by immunoblot and normalized to TIM23. Shown are the blots for the 6 biological replicates used for the quantitation shown in Fig 2B. TIM23, translocase of inner mitochondrial membrane 23.
(TIF)

S6 Fig. Caffeine improves respiratory capacity and increases mitochondrial p27 in old mice to the level of adult mice. (A) For better comparability, the data for malate/glutamate- ("M/G") and ADP-stimulated respiration of the mitochondria from the hearts of adult wild-type ("adult wt") and p27-deficient ("adult p27ko") mice from Fig 5B were combined with the data from the mitochondria from 22-month-old wild-type mice receiving water ("old wt") or water with caffeine ("old wt+caffeine") shown in Fig 8A. **(B)** Heart mitochondria from adult wild-type mice, old mice, and old mice that had received drinking water with 0.05% caffeine for 10 days were analyzed for mitochondrial p27 by immunoblot. To control for purity of the mitochondria, a total heart lysate ("lys") was used in parallel, and Vimentin was detected. Underlying data are provided in S1 Data.
(TIF)

S7 Fig. Digestion of mouse mitochondria with proteinase K. Forty μg of mouse mitochondria from old (22 months) and adult (6 months) mice as well as mice on a diabetogenic diet—presented in Figs 8C, 8E and 9E—were digested with proteinase K to obtain mitoblasts. Forty μg of undigested mitochondria and the resulting mitoblasts were loaded. Immunoblots for p27, TOM40, and TIM23 are shown. The absence of TOM40 and the presence TIM23 verify the proteinase K digest. TIM23, translocase of inner mitochondrial membrane 23; TOM40, translocase of outer mitochondrial membrane 40.
(TIF)

S1 Table. GO terms for biological processes significantly ($p < 0.05$) enriched in hearts of wild-type mice after receiving 0.05% caffeine in the drinking water for 10 days compared to animals on drinking water alone, and subcellular localization of gene products. GO, gene ontology.
(XLSX)

S2 Table. Composition of diabetogenic diet.
(XLSX)

S1 Data. Excel spreadsheet containing, in separate sheets, the underlying numerical data for figure panels 1B, 1C, 2B, 2F, 2G, 2H, 3D, 3E, 4B, 4E, 4G, 5A, 5B, 6B, 7C, 8A, 8B, 8D, 8F, 9B, 9C, 9F, S1A, S1B, S2B, S2D, and S6A.
(XLSX)

Acknowledgments

We thank Vicente Andres for providing us with the initial p27-deficient founder mice.

Author Contributions

Conceptualization: Ioakim Spyridopoulos, Joachim Altschmied, Judith Haendeler.

Data curation: Joachim Altschmied, Judith Haendeler.

Formal analysis: Niloofar Ale-Agha, Christine Goy, Ioakim Spyridopoulos, Nadine Dyballa-Rukes, Mark Zurek, Karl Köhrer, René Deenen, Klaus Unfried, Joachim Altschmied, Judith Haendeler.

Funding acquisition: Joachim Altschmied, Judith Haendeler.

Investigation: Niloofar Ale-Agha, Christine Goy, Philipp Jakobs, Ioakim Spyridopoulos, Stefanie Gonnissen, Karin Aufenvenne, Florian von Ameln, Mark Zurek, Tim Spannbrucker,

Olaf Eckermann, Simone Gorressen, Marcel Abrams, Maria Grandoch, Jens W. Fischer, Karl Köhrer, René Deenen, Klaus Unfried.

Methodology: Niloofar Ale-Agha, Christine Goy, Philipp Jakobs, Stefanie Gonnissen, Nadine Dyballa-Rukes, Karin Aufenvenne, Florian von Ameln, Mark Zurek, Tim Spannbrucker, Olaf Eckermann, Sascha Jakob, Simone Gorressen, Marcel Abrams, Maria Grandoch, Jens W. Fischer, Karl Köhrer, René Deenen, Klaus Unfried.

Project administration: Judith Haendeler.

Resources: Joachim Altschmied, Judith Haendeler.

Software: Philipp Jakobs, René Deenen.

Supervision: Klaus Unfried, Joachim Altschmied, Judith Haendeler.

Validation: Niloofar Ale-Agha, Christine Goy, Philipp Jakobs, Nadine Dyballa-Rukes, Florian von Ameln, Sascha Jakob, Karl Köhrer, René Deenen, Joachim Altschmied.

Visualization: Niloofar Ale-Agha, Philipp Jakobs, Tim Spannbrucker, Olaf Eckermann.

Writing – original draft: Niloofar Ale-Agha, Christine Goy, Joachim Altschmied, Judith Haendeler.

Writing – review & editing: Niloofar Ale-Agha, Philipp Jakobs, Ioakim Spyridopoulos, Joachim Altschmied, Judith Haendeler.

References

1. Toyoshima H, Hunter T. p27, a novel inhibitor of G1 cyclin-Cdk protein kinase activity, is related to p21. Cell. 1994; 78:67–74. PMID: 8033213
2. Shin I, Yakes FM, Rojo F, Shin NY, Bakin AV, Baselga J, et al. PKB/Akt mediates cell-cycle progression by phosphorylation of p27(Kip1) at threonine 157 and modulation of its cellular localization. Nat Med. 2002; 8:1145–1152. https://doi.org/10.1038/nm759 PMID: 12244301
3. Viglietto G, Motti ML, Bruni P, Melillo RM, D'Alessio A, Califano D, et al. Cytoplasmic relocalization and inhibition of the cyclin-dependent kinase inhibitor p27(Kip1) by PKB/Akt-mediated phosphorylation in breast cancer. Nat Med. 2002; 8:1136–1144. https://doi.org/10.1038/nm762 PMID: 12244303
4. McAllister SS, Becker-Hapak M, Pintucci G, Pagano M, Dowdy SF. Novel p27(kip1) C-terminal scatter domain mediates Rac-dependent cell migration independent of cell cycle arrest functions. Mol Cell Biol. 2003; 23:216–228. https://doi.org/10.1128/MCB.23.1.216-228.2003 PMID: 12482975
5. Hauck L, Harms C, An J, Rohne J, Gertz K, Dietz R, et al. Protein kinase CK2 links extracellular growth factor signaling with the control of p27(Kip1) stability in the heart. Nat Med. 2008; 14:315–324. https://doi.org/10.1038/nm1729 PMID: 18311148
6. Konecny F, Zou J, Husain M, von Harsdorf R. Post-myocardial infarct p27 fusion protein intravenous delivery averts adverse remodelling and improves heart function and survival in rodents. Cardiovasc Res. 2012; 94:492–500. https://doi.org/10.1093/cvr/cvs138 PMID: 22492676
7. Quintero M, Colombo SL, Godfrey A, Moncada S. Mitochondria as signaling organelles in the vascular endothelium. Proc Natl Acad Sci U S A. 2006; 103:5379–5384. https://doi.org/10.1073/pnas.0601026103 PMID: 16565215
8. Spyridopoulos I, Fichtlscherer S, Popp R, Toennes SW, Fisslthaler B, Trepels T, et al. Caffeine enhances endothelial repair by an AMPK-dependent mechanism. Arterioscler Thromb Vasc Biol. 2008; 28:1967–1974. https://doi.org/10.1161/ATVBAHA.108.174060 PMID: 18757291
9. Negmadjanov U, Godic Z, Rizvi F, Emelyanova L, Ross G, Richards J, et al. TGF-beta1-mediated differentiation of fibroblasts is associated with increased mitochondrial content and cellular respiration. PLoS ONE. 2015; 10:e0123046. https://doi.org/10.1371/journal.pone.0123046 PMID: 25849590
10. van Dam RM, Feskens EJ. Coffee consumption and risk of type 2 diabetes mellitus. Lancet. 2002; 360:1477–1478. https://doi.org/10.1016/S0140-6736(02)11436-X PMID: 12433517
11. van Dam RM, Hu FB. Coffee consumption and risk of type 2 diabetes: a systematic review. Jama. 2005; 294:97–104. https://doi.org/10.1001/jama.294.1.97 PMID: 15998896

12. Freedman ND, Park Y, Abnet CC, Hollenbeck AR, Sinha R. Association of coffee drinking with total and cause-specific mortality. N Engl J Med. 2012; 366:1891–1904. https://doi.org/10.1056/NEJMoa1112010 PMID: 22591295

13. Gunter MJ, Murphy N, Cross AJ, Dossus L, Dartois L, Fagherazzi G, et al. Coffee Drinking and Mortality in 10 European Countries: A Multinational Cohort Study. Ann Intern Med. 2017; 167:236–247. https://doi.org/10.7326/M16-2945 PMID: 28693038

14. Greenberg JA, Dunbar CC, Schnoll R, Kokolis R, Kokolis S, Kassotis J. Caffeinated beverage intake and the risk of heart disease mortality in the elderly: a prospective analysis. Am J Clin Nutr. 2007; 85:392–398. https://doi.org/10.1093/ajcn/85.2.392 PMID: 17284734

15. Greenberg JA, Chow G, Ziegelstein RC. Caffeinated coffee consumption, cardiovascular disease, and heart valve disease in the elderly (from the Framingham Study). Am J Cardiol. 2008; 102:1502–1508. https://doi.org/10.1016/j.amjcard.2008.07.046 PMID: 19026304

16. Fisone G, Borgkvist A, Usiello A. Caffeine as a psychomotor stimulant: mechanism of action. Cell Mol Life Sci. 2004; 61:857–872. https://doi.org/10.1007/s00018-003-3269-3 PMID: 15095008

17. Banerjee P, Ali Z, Levine B, Fowler DR. Fatal caffeine intoxication: a series of eight cases from 1999 to 2009. J Forensic Sci. 2014; 59:865–868. https://doi.org/10.1111/1556-4029.12387 PMID: 24502704

18. Benowitz NL. Clinical pharmacology of caffeine. Annu Rev Med. 1990; 41:277–288. https://doi.org/10.1146/annurev.me.41.020190.001425 PMID: 2184730

19. Smellie FW, Davis CW, Daly JW, Wells JN. Alkylxanthines: inhibition of adenosine-elicited accumulation of cyclic AMP in brain slices and of brain phosphodiesterase activity. Life Sci. 1979; 24:2475–2482. PMID: 225626

20. Daly JW. Caffeine analogs: biomedical impact. Cell Mol Life Sci. 2007; 64:2153–2169. https://doi.org/10.1007/s00018-007-7051-9 PMID: 17514358

21. Lasley RD, Jahania MS, Mentzer RM Jr. Beneficial effects of adenosine A(2a) agonist CGS-21680 in infarcted and stunned porcine myocardium. Am J Physiol Heart Circ Physiol. 2001; 280:H1660–1666. https://doi.org/10.1152/ajpheart.2001.280.4.H1660 PMID: 11247777

22. Ribe D, Sawbridge D, Thakur S, Hussey M, Ledent C, Kitchen I, et al. Adenosine A2A receptor signaling regulation of cardiac NADPH oxidase activity. Free Radic Biol Med. 2008; 44:1433–1442. https://doi.org/10.1016/j.freeradbiomed.2007.12.035 PMID: 18206127

23. Mokranjac D, Neupert W. Protein import into mitochondria. Biochem Soc Trans. 2005; 33:1019–1023. https://doi.org/10.1042/BST20051019 PMID: 16246036

24. Larrea MD, Liang J, Da Silva T, Hong F, Shao SH, Han K, et al. Phosphorylation of p27Kip1 regulates assembly and activation of cyclin D1-Cdk4. Mol Cell Biol. 2008; 28:6462–6472. https://doi.org/10.1128/MCB.02300-07 PMID: 18710949

25. Fuster JJ, Gonzalez-Navarro H, Vinue A, Molina-Sanchez P, Andres-Manzano MJ, Nakayama KI, et al. Deficient p27 phosphorylation at serine 10 increases macrophage foam cell formation and aggravates atherosclerosis through a proliferation-independent mechanism. Arterioscler Thromb Vasc Biol. 2011; 31:2455–2463. https://doi.org/10.1161/ATVBAHA.111.235580 PMID: 21885849

26. Grimmler M, Wang Y, Mund T, Cilensek Z, Keidel EM, Waddell MB, et al. Cdk-inhibitory activity and stability of p27Kip1 are directly regulated by oncogenic tyrosine kinases. Cell. 2007; 128:269–280. https://doi.org/10.1016/j.cell.2006.11.047 PMID: 17254966

27. Sanz-Gonzalez SM, Melero-Fernandez de Mera R, Malek NP, Andres V. Atheroma development in apolipoprotein E-null mice is not regulated by phosphorylation of p27(Kip1) on threonine 187. J Cell Biochem. 2006; 97:735–743. https://doi.org/10.1002/jcb.20680 PMID: 16229012

28. Chiong M, Wang ZV, Pedrozo Z, Cao DJ, Troncoso R, Ibacache M, et al. Cardiomyocyte death: mechanisms and translational implications. Cell Death Dis. 2011; 2:e244. https://doi.org/10.1038/cddis.2011.130 PMID: 22190003

29. Abel ED. Obesity stresses cardiac mitochondria even when you are young. J Am Coll Cardiol. 2011; 57:586–589. https://doi.org/10.1016/j.jacc.2010.09.039 PMID: 21272750

30. Lowell BB, Shulman GI. Mitochondrial dysfunction and type 2 diabetes. Science. 2005; 307:384–387. https://doi.org/10.1126/science.1104343 PMID: 15662004

31. Wang S, Fusaro G, Padmanabhan J, Chellappan SP. Prohibitin co-localizes with Rb in the nucleus and recruits N-CoR and HDAC1 for transcriptional repression. Oncogene. 2002; 21:8388–8396. https://doi.org/10.1038/sj.onc.1205944 PMID: 12466959

32. Kurtev V, Margueron R, Kroboth K, Ogris E, Cavailles V, Seiser C. Transcriptional regulation by the repressor of estrogen receptor activity via recruitment of histone deacetylases. J Biol Chem. 2004; 279:24834–24843. https://doi.org/10.1074/jbc.M312300200 PMID: 15140878

33. Sun L, Liu L, Yang XJ, Wu Z. Akt binds prohibitin 2 and relieves its repression of MyoD and muscle differentiation. J Cell Sci. 2004; 117:3021–3029. https://doi.org/10.1242/jcs.01142 PMID: 15173318

34. Nijtmans LG, de Jong L, Artal Sanz M, Coates PJ, Berden JA, Back JW, et al. Prohibitins act as a membrane-bound chaperone for the stabilization of mitochondrial proteins. Embo J. 2000; 19:2444–2451. https://doi.org/10.1093/emboj/19.11.2444 PMID: 10835343

35. Bourges I, Ramus C, Mousson de Camaret B, Beugnot R, Remacle C, Cardol P, et al. Structural organization of mitochondrial human complex I: role of the ND4 and ND5 mitochondria-encoded subunits and interaction with prohibitin. Biochem J. 2004; 383:491–499. https://doi.org/10.1042/BJ20040256 PMID: 15250827

36. Rajalingam K, Wunder C, Brinkmann V, Churin Y, Hekman M, Sievers C, et al. Prohibitin is required for Ras-induced Raf-MEK-ERK activation and epithelial cell migration. Nat Cell Biol. 2005; 7:837–843. https://doi.org/10.1038/ncb1283 PMID: 16041367

37. Cheng M, Olivier P, Diehl JA, Fero M, Roussel MF, Roberts JM, et al. The p21(Cip1) and p27(Kip1) CDK 'inhibitors' are essential activators of cyclin D-dependent kinases in murine fibroblasts. EMBO J. 1999; 18:1571–1583. https://doi.org/10.1093/emboj/18.6.1571 PMID: 10075928

38. Mather K, Laakso M, Edelman S, Hook G, Baron A. Evidence for physiological coupling of insulin-mediated glucose metabolism and limb blood flow. Am J Physiol Endocrinol Metab. 2000; 279:E1264–1270. https://doi.org/10.1152/ajpendo.2000.279.6.E1264 PMID: 11093913

39. Yusuf S, Hawken S, Ounpuu S, Bautista L, Franzosi MG, Commerford P, et al. Obesity and the risk of myocardial infarction in 27,000 participants from 52 countries: a case-control study. Lancet. 2005; 366:1640–1649. https://doi.org/10.1016/S0140-6736(05)67663-5 PMID: 16271645

40. Laakso M. Hyperglycemia and cardiovascular disease in type 2 diabetes. Diabetes. 1999; 48:937–942. PMID: 10331395

41. Fero ML, Rivkin M, Tasch M, Porter P, Carow CE, Firpo E, et al. A syndrome of multiorgan hyperplasia with features of gigantism, tumorigenesis, and female sterility in p27(Kip1)-deficient mice. Cell. 1996; 85:733–744. PMID: 8646781

42. Claycomb WC, Lanson NA Jr., Stallworth BS, Egeland DB, Delcarpio JB, Bahinski A, et al. HL-1 cells: a cardiac muscle cell line that contracts and retains phenotypic characteristics of the adult cardiomyocyte. Proc Natl Acad Sci U S A. 1998; 95:2979–2984. PMID: 9501201

43. Uphoff CC, Drexler HG. Detection of mycoplasma contaminations. Methods Mol Biol. 2013; 946:1–13. https://doi.org/10.1007/978-1-62703-128-8_1 PMID: 23179822

44. Haendeler J, Hoffmann J, Tischler V, Berk BC, Zeiher AM, Dimmeler S. Redox regulatory and anti-apoptotic functions of thioredoxin depend on S-nitrosylation at cysteine 69. Nat Cell Biol. 2002; 4:743–749. https://doi.org/10.1038/ncb851 PMID: 12244325

45. Tamura M, Gu J, Matsumoto K, Aota S, Parson R, Yamada KM. Inhibition of cell migration, spreading and focal adhesions by tumor suppressor PTEN. Science. 1998; 280:1614–1617. PMID: 9616126

46. Abramoff MD, Magelhaes PJ, Ram SJ. Image Processing with ImageJ. Biophotonics International. 2004; 11:36–42.

47. Goy C, Czypiorski P, Altschmied J, Jakob S, Rabanter LL, Brewer AC, et al. The imbalanced redox status in senescent endothelial cells is due to dysregulated Thioredoxin-1 and NADPH oxidase 4. Exp Gerontol. 2014; 56:45–52. https://doi.org/10.1016/j.exger.2014.03.005 PMID: 24632182

48. Schroeder P, Popp R, Wiegand B, Altschmied J, Haendeler J. Nuclear redox-signaling is essential for apoptosis inhibition in endothelial cells—important role for nuclear thioredoxin-1. Arterioscler Thromb Vasc Biol. 2007; 27:2325–2331. https://doi.org/10.1161/ATVBAHA.107.149419 PMID: 17823364

49. Huang da W, Sherman BT, Lempicki RA. Systematic and integrative analysis of large gene lists using DAVID bioinformatics resources. Nat Protoc. 2009; 4:44–57. https://doi.org/10.1038/nprot.2008.211 PMID: 19131956

50. Huang da W, Sherman BT, Lempicki RA. Bioinformatics enrichment tools: paths toward the comprehensive functional analysis of large gene lists. Nucleic Acids Res. 2009; 37:1–13. https://doi.org/10.1093/nar/gkn923 PMID: 19033363

51. Binder JX, Pletscher-Frankild S, Tsafou K, Stolte C, O'Donoghue SI, Schneider R, et al. COMPARTMENTS: unification and visualization of protein subcellular localization evidence. Database (Oxford). 2014; 2014:bau012.

52. Drose S, Brandt U, Hanley PJ. K+-independent actions of diazoxide question the role of inner membrane KATP channels in mitochondrial cytoprotective signaling. J Biol Chem. 2006; 281:23733–23739. https://doi.org/10.1074/jbc.M602570200 PMID: 16709571

53. Haendeler J, Drose S, Buchner N, Jakob S, Altschmied J, Goy C, et al. Mitochondrial telomerase reverse transcriptase binds to and protects mitochondrial DNA and function from damage. Arterioscler Thromb Vasc Biol. 2009; 29:929–935. https://doi.org/10.1161/ATVBAHA.109.185546 PMID: 19265030

54. Faul F, Erdfelder E, Lang AG, Buchner A. G*Power 3: a flexible statistical power analysis program for the social, behavioral, and biomedical sciences. Behav Res Methods. 2007; 39:175–191. PMID: 17695343

Danksagung

Als erstes möchte ich mich bei Jojo Haendeler bedanken, die es mir ermöglicht hat, Teil ihrer Gruppe zu sein und somit viel Erfahrung sammeln zu können. Ich habe sehr von ihrem beeindruckenden Fachwissen profitiert.

Yogi Altschmied für seine Geduld bei der Durchsicht und Korrektur meiner zahlreichen Abbildungen.

Des Weiteren danke ich Prof. Dr. Axel Gödecke für die Übernahme des Zweitgutachtens. In diesem Zusammenhang bedanke ich mich auch beim internationalen Graduiertenkolleg 1902 für die zahlreichen Möglichkeiten der Weiterbildung.

Ich danke Klaus Unfried für das vorgestreckte Vertrauen und die Möglichkeit, an diesem interessanten und so aktuellen Thema arbeiten zu dürfen. Vielen Dank für Kritik, Hilfestellung und intellektuell anspruchsvolle Gespräche. Mein Kunstverständnis hat sich mit der Zeit erstaunlich weiterentwickelt.

Ich danke meinen Kollegen für die zahlreichen Vorlagen, die mir das Leben so einfach gemacht haben. Danke Nilo, Nadine, Fee, Florian, Olaf, Kirsten, Steffi, Nilo, Karin, Kathrin, Philipp, Mark und Tamara. Es ist mir eine Freude, mit diesem Team zusammenarbeiten zu dürfen.

Bedanken möchte ich mich auch bei all den Menschen, die mich auf meinem bisherigen Weg ein Stück begleitet haben. Ich möchte keinen von euch missen. Ich hoffe, einer von euch liest das hier!

Zuletzt möchte ich mich bei meiner Familie bedanken, die mich in allen Lebenslagen unterstützt hat. Es ist nach wie vor nicht immer einfach, aber euer Rückhalt macht vieles leichter und erträglich.